8-2018

A Study of Techniques and Mechanisms of Vagus Nerve Stimulation for Treatment of Inflammation

Jesse P. Somann
Purdue University

A STUDY OF TECHNIQUES AND MECHANISMS OF VAGUS NERVE STIMULATION FOR TREATMENT OF INFLAMMATION

by

Jesse P. Somann

A Dissertation

Submitted to the Faculty of Purdue University

In Partial Fulfillment of the Requirements for the degree of

Doctor of Philosophy

School of Electrical & Computer Engineering

West Lafayette, Indiana

August 2018

THE PURDUE UNIVERSITY GRADUATE SCHOOL
STATEMENT OF COMMITTEE APPROVAL

Dr. Pedro Irazoqui, Chair

Department of Electrical and Computer Engineering

Dr. Zhongming Liu

Department of Electrical and Computer Engineering

Dr. Terry L. Powley

Department of Psychology

Dr. Chi H. Lee

Department of Biomedical Engineering

Approved by:

Dr. Venkataramanan Balakrishnan

Head of the Graduate Program

Dedicated to my amazing wife, Brittany, and two wonderful children, Ruthi and Jesse.

Praise to my Lord and Savior

ACKNOWLEDGMENTS

I would like to formally acknowledge the many, many people that have helped me to accomplish my research aims here at Purdue.

- My committee members, Dr. Pedro Irazoqui, Dr. Terry Powley, Dr. Zhongming Liu, and Dr. Chi Hwan Lee.
- Dr. J. Paul Robinson, Jennifer Sturgis, and Kathy Rageb of the Purdue Cytometry Laboratories.
- Dr. Matthew Ward of the Weldon School of Biomedical Engineering.
- Dr. Robert Phillips, Elizabeth Baronowsky, Jennifer McAdams, and Diana Black of the Purdue Department of Psychological Sciences.
- Dr. John Jefferys of University of Oxford.
- Dr. Abigail Durkes of the Purdue Department of Comparative Pathobiology.
- Robyn McCain of the Purdue Translational Pharmacology Unit.
- Kun-Han Lu and Steven Oleson of the Purdue Laboratory of Integrated Brain Imaging.
- Bartek Rajwa of Purdue's Bindley Bioscience Center.
- Victor Bernal-Crespo of the Purdue Veterinary School Histology Laboratory.
- Bill Schoenlein and Susan Hardy of the Martin Jischke Hall of Biomedical Engineering.
- David Hankins, Dr. Eric Deitz, and all my fellow Airmen and servicemembers of the Purdue Military Research Initiative.
- And my many friends and lab-mates, past and present, in the Purdue Center for Implantable Devices: Gabriel Albors, Daniel Pederson, Chris Quinkert, Muhammad Arafat, Jack Williams, Kelsey Wasilczuk, Kaitlyn Neihouser, Kelsey Bayer, Jay Shah, Curtis Slaubaugh, Ryan Budde, Vivek Ganesh, Grant Wang, Quan Yuan, Mark Bevilacqua, Shelby Olson, Jui-Wei Tsai, Ethan Biggs, Songjingwei Li, Henry Mei, Kyle Thackston, Rebecca Bercich, Hansraj Singh, Young-Joon Kim, Yu-Wen Huang, Hans Ajieren, and the many others not listed here that helped contribute.

TABLE OF CONTENTS

LIST OF TABLES

LIST OF FIGURES

LIST OF ACRONYMS

ACB	Accessory Celiac Branch of Vagus Nerve
ACBes	Accessory Celiac Branch Stimulation of Intact Nerve
ACBvx	Accessory Celiac Branch Stimulation with Efferent Vagotomy
AFE	Analog Front End
AGB	Anterior Gastric Branch of Vagus Nerve
AGBes	Accessory Celiac Branch Stimulation of Intact Nerve
AGBvx	Accessory Celiac Branch Stimulation with Efferent Vagotomy
ANC	Autonomous Neural Control
ANOVA	Analysis of Variance
AP	Area Postrema
ARL	Army Research Labs
ASIC	Application Specific Integrated Circuit
CID	Center for Implantable Devices
CNAP	Compound Nerve Action Potential
COTS	Commercial Off-the-Shelf
CSC_C	Cathodal Charge Storage Capacity
CV	Cyclic Voltammetry
CVes	Cervical Vagus Nerve (Left) Stimulation with Intact Nerve
CVns	Cervical Vagus Nerve (Left) Sham Stimulation Subgroup
DAC	Digital to Analog Converter
DC	Direct Current
DMN	Dorsal Motor Nucleus
EIS	Electrochemical Impedance Spectroscopy
FG	Fluorogold
GI	Gastrointestinal
GM-CSF	Granulocyte-Macrophage Colony-Stimulating Factor
H&E	Hematoxylin and Eosin
HB	Hepatic Branch of Vagus Nerve
HBes	Accessory Celiac Branch Stimulation of Intact Nerve
HBvx	Accessory Celiac Branch Stimulation with Efferent Vagotomy
HCS	Howland Current Source
INF	Interferon
IL	Interleukin
IP	Intraperitoneal
IV	Intravenous
LPS	Lipopolysaccharides
MRI	Magnetic Resonance Imaging
NIH	National Institutes of Health
NTS	Nucleus of the Solitary Tract
PCBA	Printed Circuit Board Assembly
PtIr (Pt/Ir)	Platinum Iridium
SubD Sham	Subdiaphragmatic Sham Subgroup
TNF	Tumor Necrosis Factor
UTD	University of Texas – Dallas
VNS	Vagus Nerve Stimulation
WPT	Wireless Powering Transfer

ABSTRACT

Author: Somann, Jesse, P. PhD
Institution: Purdue University
Degree Received: August 2018
Title: A Study of Techniques and Mechanisms of Vagus Nerve Stimulation for Treatment of Inflammation.
Major Professor: Pedro Irazoqui

Vagus nerve stimulation (VNS) has been on the forefront of inflammatory disorder research for the better part of the last three decades and has yielded many promising results. There remains, however, much debate about the actual biological mechanisms of such treatments, as well as, questions about inconsistencies in methods used in many research efforts.

In this work, I identify shortcomings in past VNS methods and submit new developments and findings that can progress the research community towards more selective and relevant VNS research and treatments. In Aim 1, I present the most recent advancements in the capabilities of our fully implantable Bionode stimulation device platform for use in VNS studies to include stimulation circuitry, device packaging, and stimulation cuff design. In Aim 2, I characterize the inflammatory cytokine response of rats to intraperitoneally injected endotoxin utilizing new data analysis methods and demonstrate the modulatory effects of VNS applied by the Bionode stimulator to subdiaphragmatic branches of the left vagus nerve in an acute study. In Aim 3, using fully implanted Bionode devices, I expose a previously unidentified effect of chronically cuffing the left cervical vagus nerve to suppress efferent Fluorogold transport and cause unintended attenuation to physiological effects of VNS. Finally, in accordance with our findings from Aims 1, 2, and 3, I present results from new and promising techniques we have explored for future use of VNS in inflammation studies.

1. INTRODUCTION

1.1 Background and Motivation

1.1.1 The vagus nerve

The vagus nerve, often referred to as the wandering nerve due to the Latin definition of "vagus" and the fact that it is the longest nerve and reaches parts of virtually every part of the body (see Figure 1.1), could be the key to treating countless ailments, diseases, and syndromes [1]. The vagus nerve has been connected to cough reflexes in the respiratory tract, seizures in epilepsy patients, cardiac function and heart failure, hearing issues such as tinnitus, and many others such as Alzheimer's, migraines, stroke, obesity, and even hiccups [1].

Of specific interest to our research aims, however, is the connection of the vagus nerve to the gastrointestinal (GI) region of the body and its effect on the systemic inflammation originating in that region. The left cervical vagus nerve trunk separates into three primary branches below the diaphragm, which are most commonly associated with inflammatory controls. These subdiaphragmatic branches are the anterior gastric, accessory celiac, and hepatic branches, and have their routes outlined well in Figure 1.2. The anterior gastric branch terminals lead mainly to the stomach, while the accessory celiac branch reaches multiple locations including the spleen, intestines, and pancreas. The hepatic branch primarily innervates the liver, while also reaching to the pancreas.

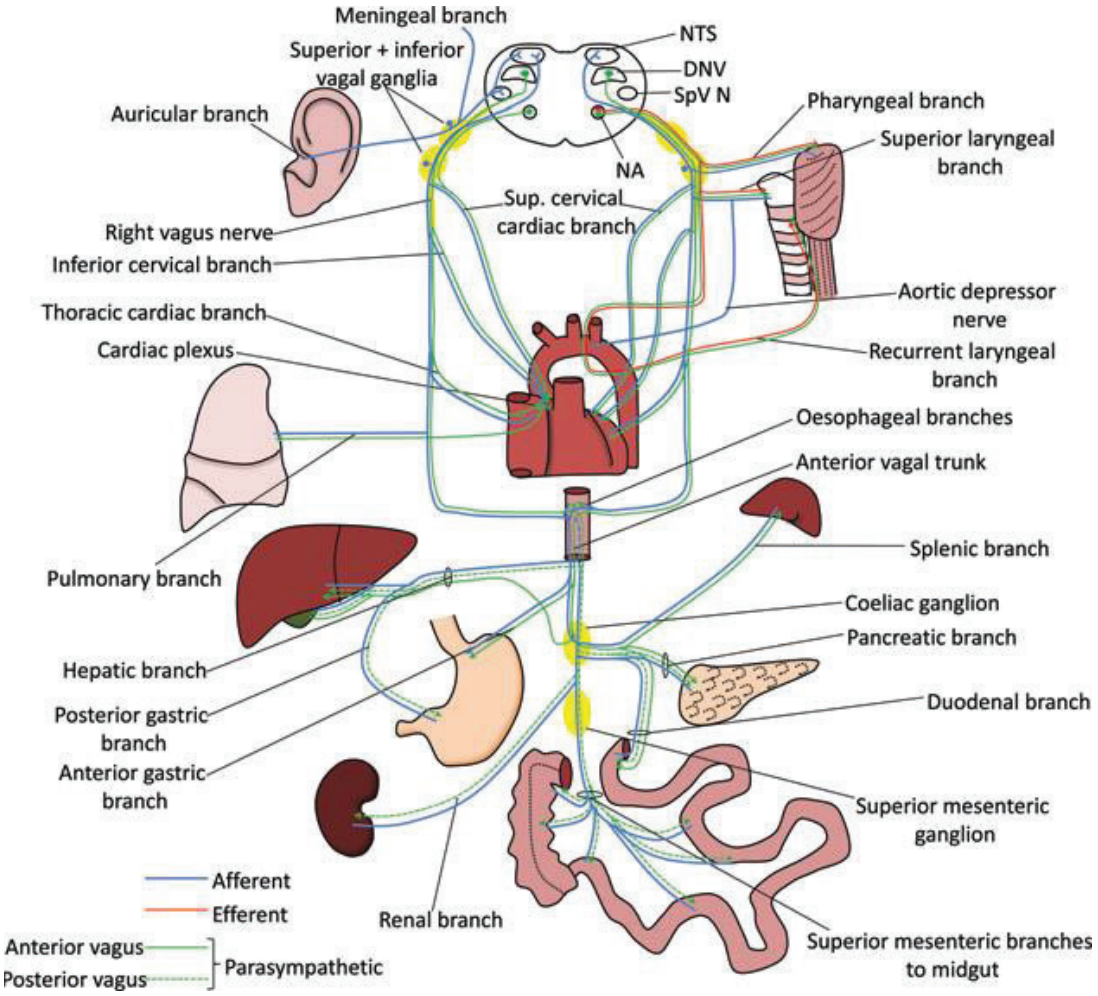

Figure 1.1 Representation of the distribution and central connections of the vagus nerve. All cervical and thoracic branches are bilateral and may have been omitted for clarity. The right recurrent laryngeal nerve (not shown) passes round the right subclavian artery instead of the arch of the aorta. Left and right vagus nerves form the oesophageal plexus and then become anterior and posterior trunks as they pass through the diaphragm to supply the abdominal viscera up to two-thirds along the transverse colon. Abbreviations: DNV, dorsal nucleus of the vagus; NA, nucleus ambiguus; NTS, nucleus tractus solitarii; and SpV N, spinal trigeminal nucleus [1]. Note that the Splenic branch is a synonymous part of the Accessory Celiac branch.

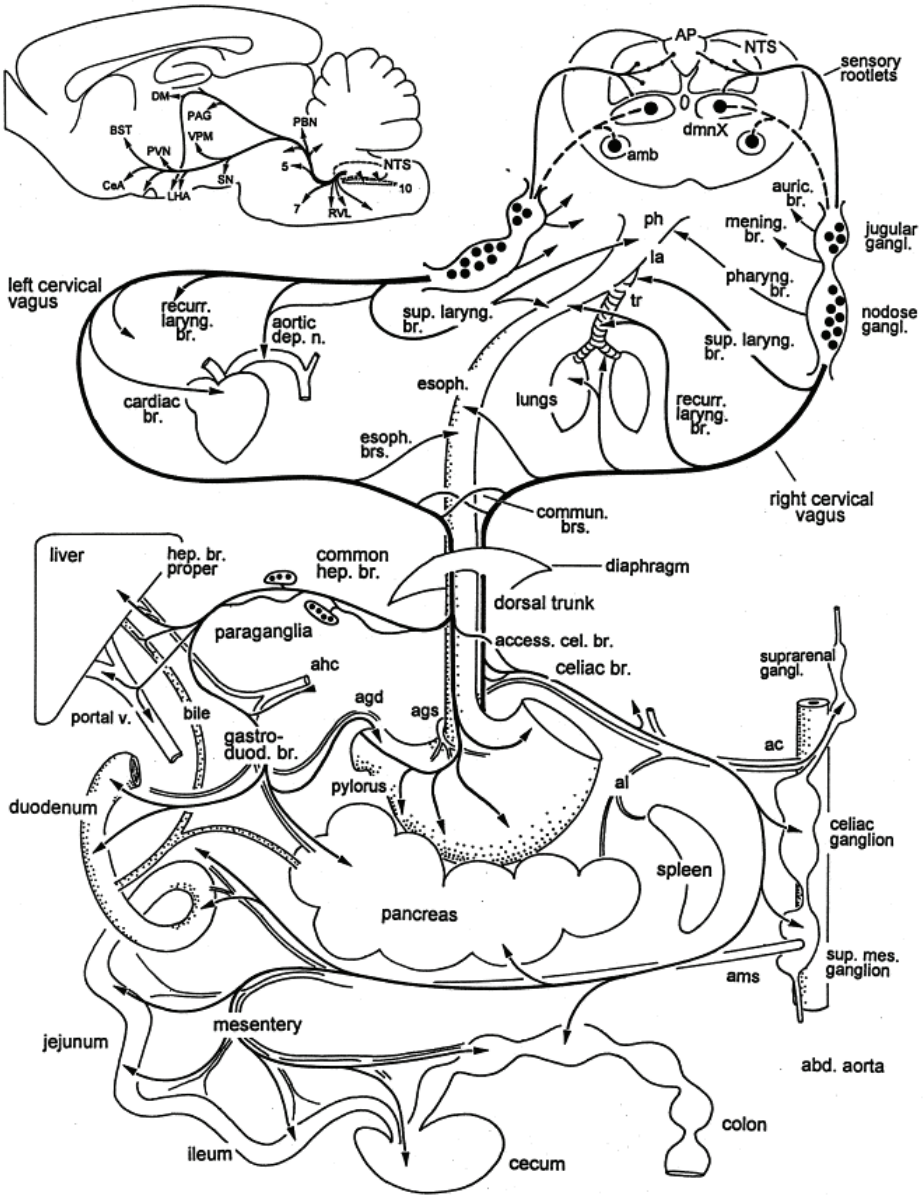

Figure 1.2 Distribution of the vagus nerve and central distribution of vagal afferents from NTS. Abbreviations for periphery: ac, celiac artery; agd, right gastric artery; ags, left gastric artery; ahc, common hepatic artery; al, splenic artery; ams, superior mesenteric artery; la, larynx; ph, pharynx; tr, trachea. Abbreviations for brain areas: Amb, nucleus ambiguus; AP, area postrema; BST, bed nucleus of stria terminalis; DM, dorsomedial nucleus of thalamus; CeA, central nucleus of amygdala; LHA, lateral hypothalamic area; NTS, nucleus tractus solitarius; PAG, periaqueductal gray; PVN, paraventricular nucleus of hypothalamus; PBN, parabrachial nucleus; RVL, rostroventrolateral medulla; SN, substantia nigra; VPM, ventral posteriomedial nucleus of thalamus; 5, trigeminal nucleus; 7, facial nucleus; 10 (dmnX), dorsal motor nucleus of vagus [2].

The presumed key to controlling inflammatory ailments in the body is the modulation of inflammation, specifically the inflammatory cytokines produced in the subdiaphragmatic region. It was hypothesized by Tracey in 2002 [3] that vagal efferent fibers to the spleen modulated cytokine release through an "inflammatory reflex" that could produce a therapeutic anti-inflammatory effect (see Figure 1.3). Since then, there has been ample research conducted to explore and dispute details of this inflammatory reflex [4-8], but much of the specific mechanisms for cytokine modulation remain undefined.

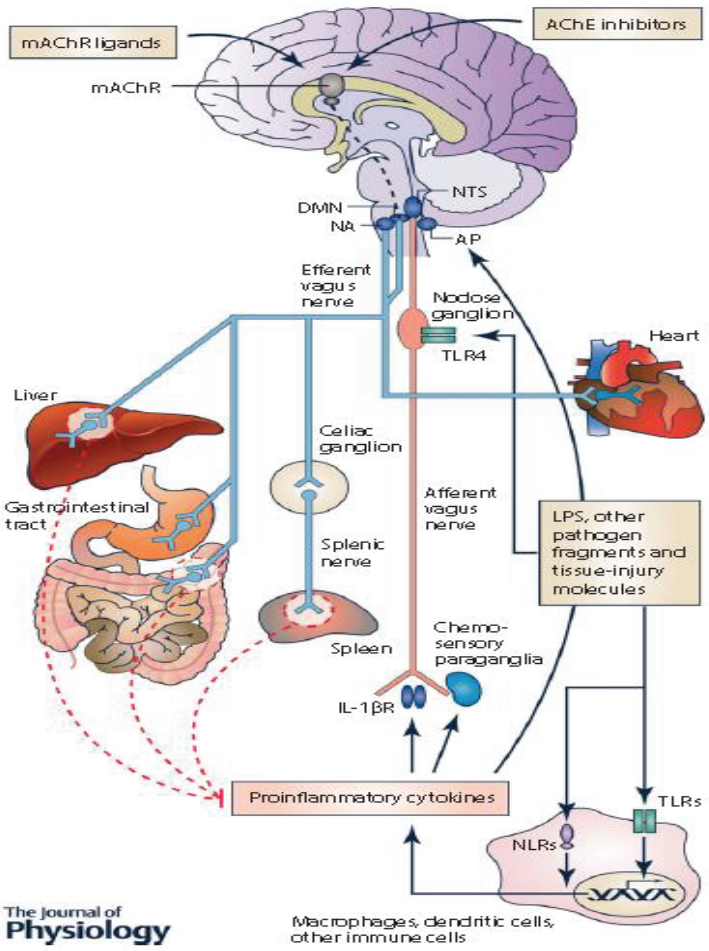

Figure 1.3 The functional anatomy of the inflammatory reflex (according to Pavlov & Tracey, 2015) AChE, acetylcholinesterase; AP, area postrema; DMN, dorsal motor nucleus of the vagus nerve; LPS, lipopolysaccharide (endotoxin); mAChR, muscarinic acetylcholine receptor; NA, nucleus ambiguus; NLRs, nucleotide-binding oligomerization domain-like receptors; NTS, nucleus tractus solitarii; TLR4, Toll-like receptor 4 [9].

1.1.2 Vagus nerve stimulation

Vagal nerve stimulation (VNS) therapy has become a prominent fixture in treatment research and has been proposed as a therapy for ailments such as depression [10], rheumatoid arthritis [11], obesity [12], and many others. While the U.S. Food and Drug Administration (FDA) has approved VNS for seizure prevention in epilepsy and as an alternative for drug-resistant depression [13, 14], the exact mechanics of much of the body's response to VNS has yet to be characterized. This is also true for anti-inflammatory treatments for ailments stemming from the GI tract and other subdiaphragmatic regions.

There are two major aspects to consider when studying effects of VNS. The first is that the cervical vagus is populated with both sensory afferent fibers (~80%) and efferent motor fibers (~20%). Afferent fibers collect in the nodose ganglia of the vagus nerve before reaching to the nucleus of the solitary tract (NTS) in the medulla oblongata, while efferent motor fibers originate from the dorsal motor nucleus (DMN) of the medulla, as is represented in Figure 1.4. These fibers serve many separate and distinct functions of the nervous system, but are also connected within a parasympathetic system that contributes to the inflammatory reflex [9] and could cause possible conflicting effects between the two fiber types with VNS. Some studies have circumvented this potential offset by chemically or electrically attenuating the functionality of a specific fiber type [15-17].

The second major aspect to consider is whether to attempt a chronic or acute study. There are ample acute studies that have been performed on the topic of anti-inflammatory pathways using rodent models [5, 15, 18-20]. Nonrecovery studies give researchers the ability to evaluate the physiological effects of rats in a controlled environment, allowing idealized set-ups for surgical processes, precise stimulation electrode placement with reduced noise (due to shorter electrical leads), and easier use of faradaic cages. Long term effects of treatment over days, weeks, and even years cannot be accurately studied acutely. Also, due to the nature of the anesthetic used in acute surgical procedures, potential unintended and detrimental physiological effects on the body's normal state can be caused [21]. As was explored by Picq et al [22], the immunoregulatory effects of isoflurane can influence the results of studies aimed at anti-inflammatory effects of VNS.

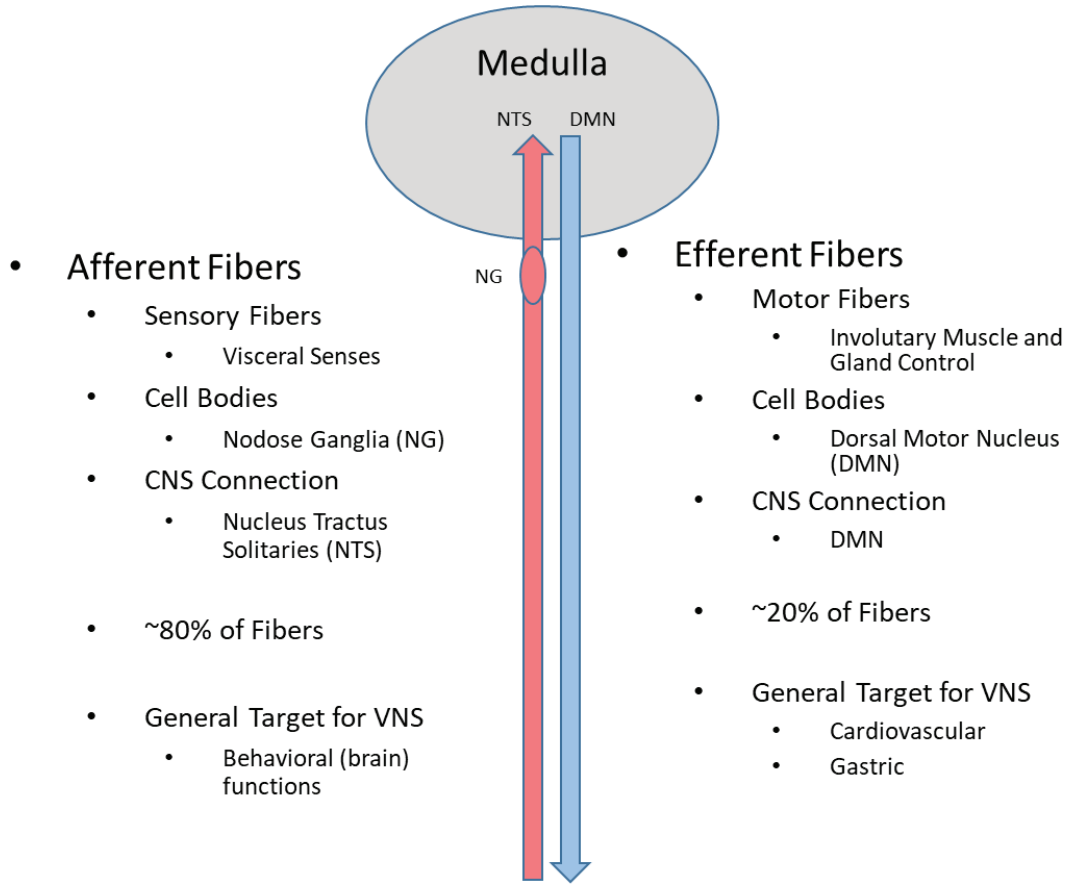

Figure 1.4 Comparison of afferent versus efferent fibers in the cervical vagus nerve.

We resolve that the best option for studying the true effects of VNS for the treatment of inflammation and many other physiological effects remains a reliable long-term chronic study on an awake and freely moving subject. However, such a study adds many complexities including implantable device design considerations such as powering and noise, surgical implantation factors of device migration and leaks, and biological ramifications such as potential infections.

In addition, the research community is plagued by inconsistency in experimental methods in both the acute and chronic realms. Devices and protocols used vary greatly between labs and research projects. This makes it difficult to replicate results and translate them into future research and treatments.

1.2 Aims

There are three primary aims demonstrated by my research:

1. Developing and improving devices and equipment for VNS studies. A significant effort was made by myself and the Center for Implantable Devices (CID) to build a fully implantable Bionode device and that could be used reliably for multiple experiments. I played a vital role in the development of the Bionode stimulator, as well as the manufacturing and packaging techniques. In addition, I was the primary developer and tester of stimulation electrodes in the CID.

2. Exploring underlying biology behind endotoxin induced inflammation and subsequent VNS treatment. I, in conjunction with Kelsey Wasilczuk, performed an in-depth acute study of the effects on cytokine levels in the plasma of rats following an intraperitoneally (IP) injected dose of endotoxin, and a subsequent VNS treatment of the individual subdiaphragmatic nerve branches. New analysis methods were developed by myself to deal with high temporal variations in our data.

3. Exploring the challenges of chronic applications of VNS. In an attempt to complete a chronic study on the effects of cervical VNS, we discovered an unexplored issue of attenuated efferent transport of a retrograde tracer in chronically cuffed nerves. This signaled a potentially larger issue of underlying damage to the cuffed nerves. I defined this new discovery and addressed the larger potential issues it presents to the VNS community.

In addition to the primary aims, I also spent a portion of time dedicated to looking at alternate methods of VNS research and applications for potential future research. Those are presented in a separate “Future Work” section.

Together, the works presented in this thesis tell a story of progress towards more consistent and reliable studies of VNS for treatment of inflammation in the future.

2. AIM 1: VNS DEVICE DEVELOPMENT

2.1 Motivation

As with any research effort, having the appropriate tools, materials, and facilities to properly accomplish the research task is vital to obtaining reliable results. In the case of VNS research, those tools include devices to stimulate the appropriate biological target, and to record, if desired, the physiological outcomes of the stimulation therapy. There are plenty of options for stimulation devices that can be found commercially for these uses, however, as is explained in the following subsections, many of those options are made for specific applications or interfaces, with specific software, and are not easily adjustable for custom research applications.

Along with the electronics to do said stimulation and recording, an appropriate package is needed if desiring to test the device chronically in an animal, as well as an effective set of electrodes to interface with the biology being studied.

Our Aim 1 addresses these issues with respect to our specific studies by outlining the development of critical portions of the Bionode's development in our lab. I was intricately involved in many pivotal junctures of the Bionode's evolution over the past three years. Those research efforts are documented here. In addition, I was our lab's lead researcher in development and characterization of stimulation cuffs for effective VNS and other stimulation studies. Those efforts are outlined in section 2.3.

Material in section 2.2 (except for 2.2.2.4, 2.2.2.5, and 2.2.4) come directly from our lab's paper titled "The Bionode: A Closed-Loop Neuromodulation Implant," lead authored by Dan Pederson and submitted to Association for Computing Machinery (ACM) Transactions on Embedded Computing Systems in January of 2018 [23]. Used sections include portions of the paper either directly authored by myself, or that I played an integral part in developing. Formatting changes have been made as were appropriate and some updates and additions were made to section 2.2.3.4. Additional sections have been added to clarify more recent developments that have been

made to our devices. Many figures for section 2.2.2.4 were made in conjunction with Gang Seo for his thesis and are used here also. They are referenced as such.

2.2 Bionode Introduction

Wireless implantable devices with the ability to record biopotential signals and electrically stimulate the nervous system have been used to study and treat a wide variety of neurological and neuropsychiatric disorders in humans including epilepsy, Parkinson's disease, depression, and drug addiction [24-28]. To further research these disorders in rodent models, various miniature wireless implantable devices have been developed [29-33]. To achieve a small size and reduce power requirements, many of these devices rely on application specific integrated circuits (ASICs), specifically designed packaging methods, and/or proprietary technologies. While these techniques can provide for sufficiently small and power efficient implantable devices, reliability is low and the ability to reproduce them in a typical laboratory setting is often prohibitively difficult and expensive. Additionally, the application-specific nature of such devices introduces problems when adapting them to alternative applications. This paper documents the design, fabrication, and deployment of a miniature wireless implantable device for rodent through clinical models called the Bionode. The Bionode features fully customizable recording and stimulation channels in a flexible, modifiable, and re-useable package to accommodate a wide variety of use cases.

The Bionode was developed over the course of four years at the CID at Purdue University. With the ability to record up to four differential biopotential signals and provide up to 10 mA (limited by 10 V headroom) of biphasic constant current electric stimulation, its capabilities and performance exceeds that of currently available implantable devices for rodent models [29, 31, 32, 34]. Each input channel contains multiple gain and filtering stages that can be modified to accommodate a variety of input signal types. Bi- directional communication between the implant and external systems allows for the real-time specification of stimulation wave-forms, providing a platform for closed-loop recording and stimulation studies. Furthermore, all components used to construct the Bionode are available as commercial off-the-shelf (COTS) components with the intent that any and all aspects of the Bionode's design can be readily reproduced and used by a typical university laboratory or small medical device company.

Over the past four years, the Bionode has been used by researchers at Purdue University to study epilepsy, Parkinson's disease, glaucoma, urinary incontinence, and vagus nerve stimulation for modulation of the inflammatory reflex and gastroparesis. Throughout the course of these studies, 76 Bionode implants have been successfully performed. The methods used to encapsulate the Bionode for implantation have been refined to increase its ease of use and re-use.

2.2.1 Implant system overview

The Bionode implant consists of three printed circuit board assemblies (PCBAs): The Bionode mainboard, the Powernode, and the Feedthrough board. The Bionode mainboard contains all circuitry for the recording and stimulating channels as well as a microcontroller, radio, and antenna for data transmission and reception. The Powernode provides power rails to the Bionode mainboard. Electrodes are connected to the Bionode mainboard via the Feedthrough board. Fully assembled and fully packaged Bionodes are pictured in Figure 2.1.

Figure 2.1 Bionode implant assembly (left) and Bionode inside glass packaging (right).

The Bionode is supported by various external systems as seen in Figure 2.2. A Wireless Powering Transfer (WPT) chamber provides both power to the Bionode and a living space for the implanted rodent (WPT details are not covered in this thesis). All data wirelessly transmitted to and from the Bionode passes through an external Base Station that provides a communication interface between the Bionode and a PC via a Wi-Fi link. A custom-designed cross-platform application provides a graphical user interface allowing users to view and save data transmitted

by the Bionode as well as specify various settings (i.e. stimulation waveform parameters) on the Bionode.

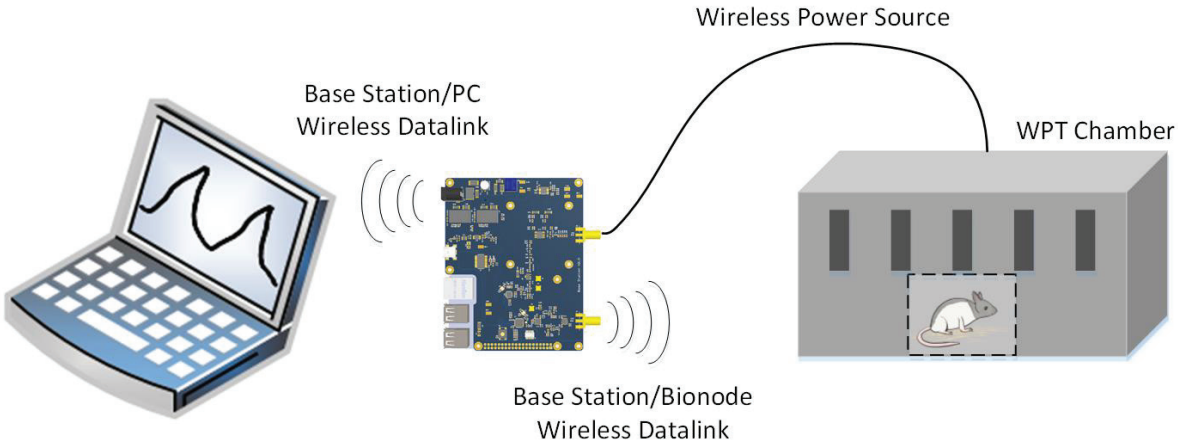

Figure 2.2 Bionode settings are updated and acquired data is displayed via a custom designed cross-platform application. Bi-directional communication is facilitated via the Base Station which also provides the wireless power source that drives the WPT chamber. The WPT chamber houses the implanted rodent and carries the circulating magnetic field that powers the device.

2.2.2 Stimulation

Many open loop implantable systems have been designed to either record biological signals [35] or to produce a physiological response by means of electrical, mechanical, or optical excitations [36, 37]. For a closed-loop study, however, both capabilities are required. Therefore, the Bionode is designed with a flexible single electrical stimulation channel to supplement its recording capabilities. Alternatively, the stimulation channel is able to drive an LED for optogenetic stimulation if desired [38].

2.2.2.1 Stimulation circuit design considerations

When designing an electrical stimulator, the specific type of stimulation that is needed must be considered. Constant voltage stimulation between a reference and counter electrode is relatively easy to implement but suffers from the drawback of variable charge injection due to the capacitive nature of the electrode/body interface, leading to variable and therefore unreliable stimulation efficacy. Constant current (galvanostatic) stimulation is more difficult to implement,

but has the advantage of attaining a consistent and knowable charge injection throughout a stimulation pulse [39]. We implement a constant current stimulator on the Bionode using a Howland current source to ensure stimulation consistency and efficacy.

Another consideration in electrical stimulation is the flexibility of the stimulation waveform generated. Stimulation parameters such as amplitude, pulse width, frequency, and charge balancing are adjusted to meet the safety and efficacy needs of a given study. For example, while using a monophasic pulse train stimulus will likely result in an increased amount of action potential responses in nerves, this stimulus waveform will also likely cause tissue damage and electrode erosion over time. This might be sufficient for short-term acute studies, but for long-term chronic experiments, a charge-balanced biphasic pulse train is more appropriate to prevent future tissue and electrode damage in the subject. The tradeoffs of efficacy and safety in stimulation protocols are studied at length in the literature [40]. The Bionode allows the stimulation amplitude, pulse width, and frequency to be defined by an outside user in real time using its bidirectional communication capabilities. For the long-term safety reasons mentioned previously these parameter choices force the stimulation to be biphasic and charge balanced, although a simple firmware change will allow for non-balanced and/or monophasic stimulation if needed or desired.

A final important consideration in electrical stimulation is the accuracy and precision of the output of the stimulation circuit. Safe stimulation requires an accurate delivery of the desired stimulation waveforms. Unbalanced pulses, inconsistent pulse delivery times, and direct current (DC) offsets on the stimulation waveform can cause unintended damage to the nerve and compromise electrode integrity. The Bionode is measured to have an acceptable charge balance (<0.5% error), and has the added safety of a stimulation glitch switch built in to prevent unintended charge release during device startup.

2.2.2.2 Stimulation circuit design

We construct the constant current stimulation waveform using a current source (LT6375) driven by a DAC7551 digital to analog converter (DAC) as seen in Figure 2.3.

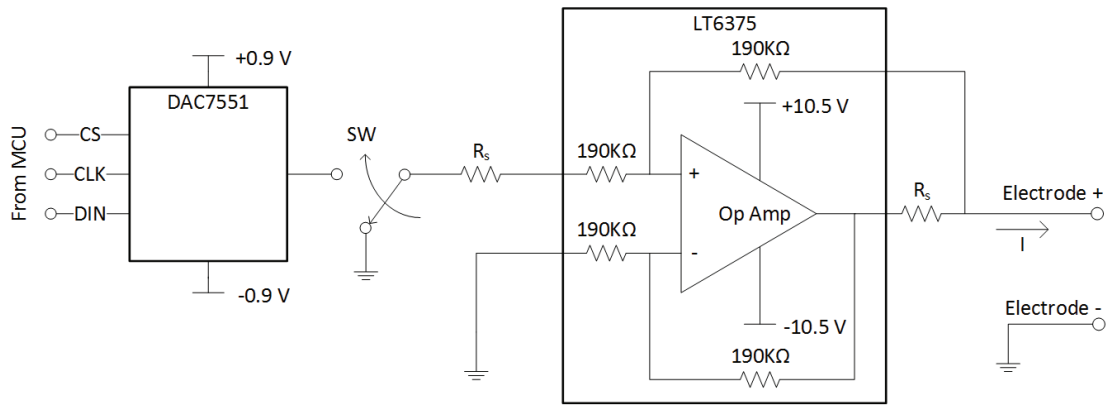

Figure 2.3 Constant current stimulation is generated via an LT6375 Howland current source. The output of the Howland current source is set by the microcontroller on the Bionode via a 12-bit digital to analog converter (DAC7551). A normally grounded control switch is used to ensure that unwanted stimulation does not occur during the Bionode power-on sequence. To ensure true bi-phasic stimulation, the positive stimulation electrode swings around the negative stimulation electrode which is directly tied to the Bionode's ground.

The LT6375 improved Howland current source (HCS) converts a control voltage provided by the DAC into a current waveform to achieve constant current stimulation [41]. We prefer the HCS topology over other topologies like current mirroring or electrode polarity switching (where the positive and negative electrodes are physically switched) because the HCS can generate reliable symmetric bipolar current pulses. It is difficult to achieve symmetric pulses using current mirroring topologies due to part tolerances, and electrode polarity switching can sometimes create asymmetric responses in stimulated nerves due to the physical change in anodic and cathodic electrode placement.

In the LT6375, the output current I is related to the control voltage V_{CTRL} by the equation (2.1):

$$I = \frac{V_{CTR}}{} \tag{2.1}$$

Here, 0 is a current limiting resistor which we choose while populating the Bionode PCB such that the specified stimulation current amplitude and precision are met. For example: let's say the

Bionode is designed to provide a maximum stimulation current of 1 mA through a 10 kΩ electrode impedance. Because the output voltage range for the DAC which provides V_{CTRL} is -0.9V to 0.9V, $_S$ is set to 800 Ω; allowing the HCS to provide current outputs ranging from -1.125 mA to 1.125 mA. To drive this current across a 10 kΩ electrode impedance, the HCS is powered by a ± 10.5 V supply allowing a maximum voltage of 10.5 V to appear at the output terminal.

Stimulation waveforms are created by the 12-bit DAC7551 DAC which is controlled by the Bionode's onboard NRF51822 microcontroller via a serial peripheral interface (SPI). These stimulation waveforms are biphasic rectangular pulses defined by the user in terms of amplitude, pulse width (T_{PW}), and pulse repeat time (T_{PRT}) (See Figure 2.4).

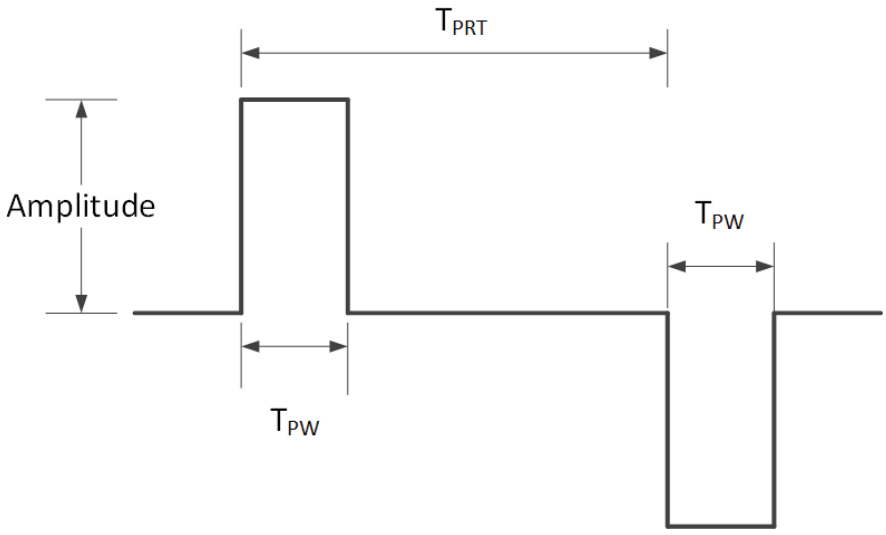

Figure 2.4 The biphasic stimulation waveform is defined in real time by the user via the Bionode's bi-directional communication interface. The aspects of the stimulation waveform that are settable by the user are its amplitude, pulse width (T_{PW}), and pulse repeat time (T_{PRT}).

The user defines these parameters using the Bionode Dataview application which subsequently instructs the Bionode to set interrupt registers in its onboard NRF51822 microcontroller. These interrupt registers define the stimulation waveform by specifying when DAC output voltage updates must occur. To further increase the accuracy of the DAC output, calibration registers may also be defined by the user and used by the NRF51822 to automatically compensate for any

static DC offset voltages that may be present on the output of the DAC. The range of these DC offset voltages is documented in the DAC7551 datasheet, and calibration values to compensate for these offsets can be obtained experimentally during the fabrication of each Bionode.

A single-pull double-throw (SPDT) switch between the DAC output and the HCS input avoids a documented start-up glitch on the output of the DAC that appears when the DAC is first powered on. If not avoided, this glitch will cause the stimulator circuit to output an unwanted stimulus pulse every time the Bionode is powered on. This switch is controlled by the onboard NRF51822 microcontroller and has a pull-down resistor attached to the control line which ensures that the switch is in position 0 even when the microcontroller is powering on and not yet driving its control voltage level. When at position 0, the switch connects the V_{CTRL} line of the HCS to ground, causing the stimulator to not output any current. When at position 1, the switch connects the output of the DAC to V_{CTRL}, allowing the DAC to control the current output of the stimulator circuit. For safety reasons, the switch is only set to position 1 when the user has specified that stimulation should occur. **Error! Reference source not found.** shows a list of key performance specifications for the stimulator.

Table 2.1. Performance characteristics of the Bionode stimulator.

	Value	**Units**
Voltage headroom	10.5	V
Current amplitude[1]	0.005 - 1.050	mA
Current amplitude resolution	4.4	µA
Pulse width (T_{PW})	50 - 8.36e6	µs
Pulse width resolution	1	µs
Pulse rate	1e-5 - 20	kHz
Charge balance error[2]	<0.5	%

[1]Over a 10 kΩ load
[2]PW = 100 µs, amplitude = 1 mA

2.2.2.3 In-vivo results

The Bionode's ability to concurrently stimulate and record from the nervous system, canceling stimulus artifacts in either software or hardware, is demonstrated by using a pair of cuff electrodes to stimulate the vagus nerve of a rat and record the resulting compound nerve action potentials (See Figure 2.5). Observed nerve fiber activations can be categorized by fiber type (e.g. A, B, and C fibers) by using the distance between the stimulating and recording cuff electrodes to calculate propagation velocities. The recorded activation of various nerve fibers within a larger nerve indicates successful stimulation of the whole nerve, and allows selective stimulation of specific fiber types within the nerve using our prior work implemented in this device [42].

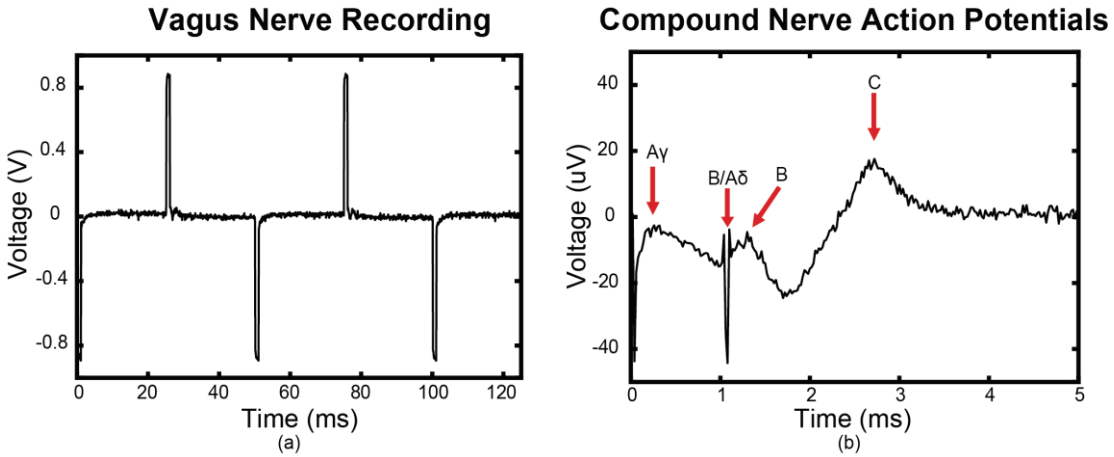

Figure 2.5 In-vivo vagus nerve stimulation using a 1 mA bi-phasic current pulse with a 1 ms pulse width and a 25 ms pulse repeat time. The stimulation waveform was delivered to the vagus nerve of a rat using a cuff electrode. (a) Voltage on the vagus nerve is recorded during stimulation by a recording cuff electrode located 6.2 mm away from the stimulation cuff electrode. (b) Compound nerve action potentials can be observed by averaging the vagus nerve recordings in (a) over multiple stimulation pulses. The annotated nerve fiber activations are consistent with known nerve fiber action potential propagation velocities.

2.2.2.4 Recent stimulation circuit improvements

The previous subsections covered in detail the implementation of the Bionode version 4.1 that was used in experiments up until this year. I have since spent a great deal of effort to resolve persisting issues that were found with that simulator implementation for the recently fabricated

Bionode version 5.0. These issues prevented a robust use of the Bionode 4.1 for some stimulation applications and prevented critical components needed for transition to a clinical use, such as a DC blocking capacitor to be used. New improvements implemented by myself, with the help of Dan Pederson and Grant Wang, to alleviate these issues have added various new components to the stimulation circuitry, as are illustrated in Figure 2.6. Each problem is described in detail below, along with the implemented solution.

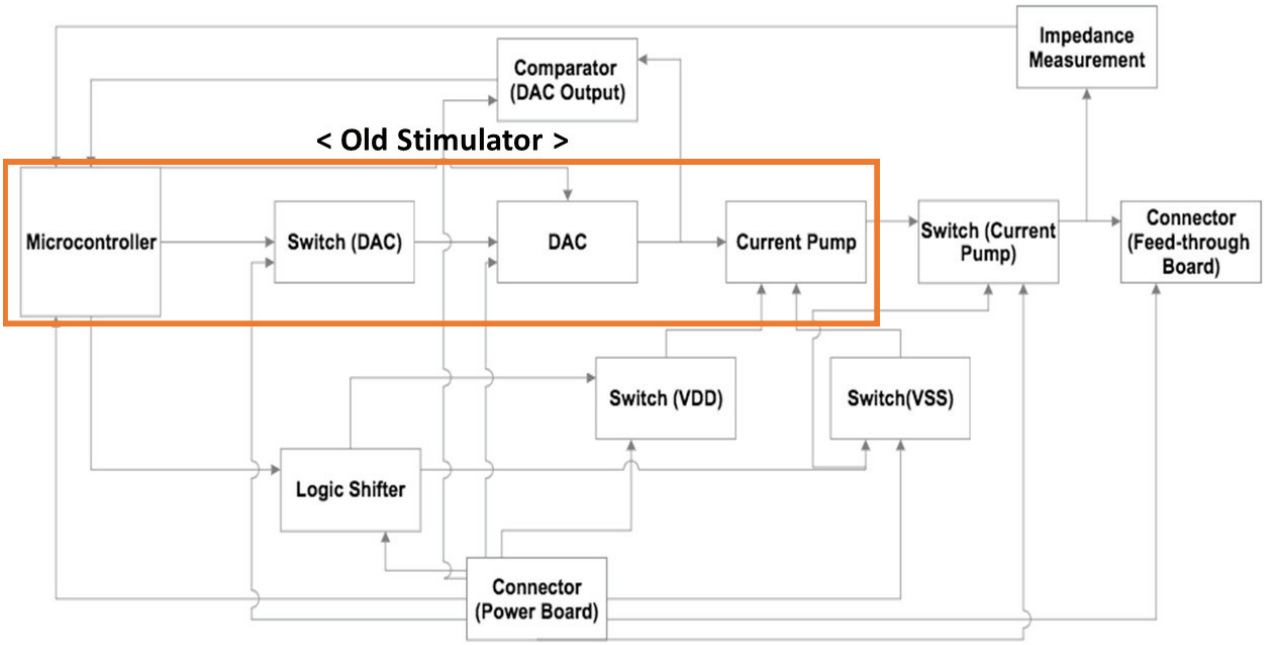

Figure 2.6 Block diagram of the new stimulator circuitry for Bionode 5.0 [43].

2.2.2.4.1 Stimulation channel DC offset

The first issue addressed with the stimulation circuitry of the Bionode 4.1 was that of a DC offset occurring in the stimulation channel when the stimulator was turned on. The cause of this DC offset related back to the singular DAC that was used to create the voltage reference for the HCS that produced the stimulation signals. When not turned on, the reference for the HCS was the circuit's ground, but when stimulation was initiated the reference changed to that of the DAC's virtual ground reference. The digital nature of a DAC meant that there was not a dedicated "ground" reference for the DAC to create stimulation pulses around. Therefore, we set a digital value of '2048', which is the middle value to our DAC's precision of 0 – 4096 digital steps, to be

the “ground” reference during stimulations. Due to inherent limits of digital precision and part variances, however, this artificial ground did not match the exact ground of the HCS and stimulation circuity. Therefore, it created varying amounts of DC offset in the stimulation channel, as shown in Figure 2.7.

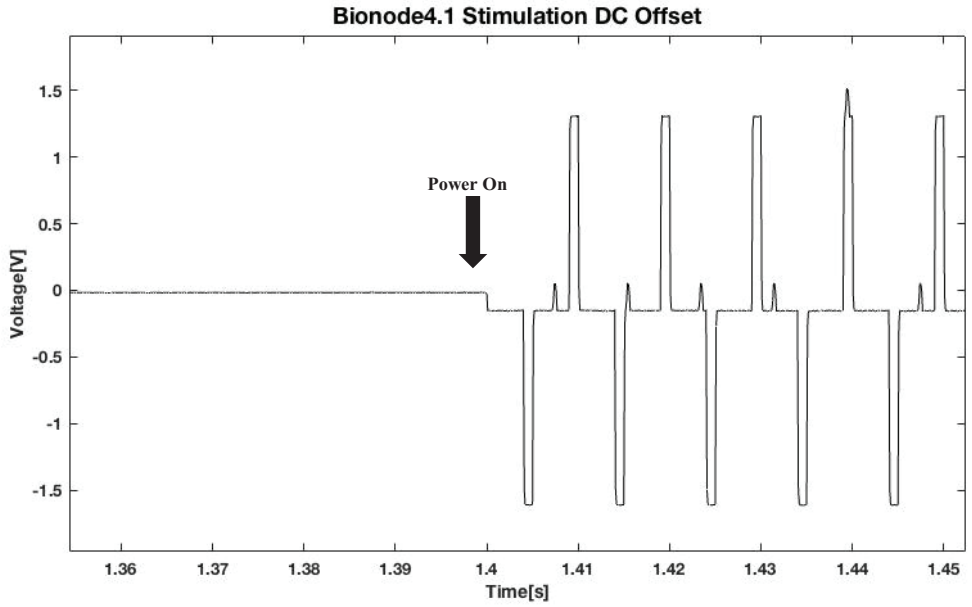

Figure 2.7 Stimulator output showing a shift in the DC level when stimulation is turned on [43].

These DC offsets could be minimized by calibrating the DC midpoint utilized by the Bionode on our Dataview software. However, this required testing by the user with an oscilloscope before use of the device. In addition, the DC offset often shifted when aspects of the experimental setup were changed, such as the load or stimulation parameters. Therefore, the user needed to test and verify the stimulation each time the stimulator was used to ensure a minimized DC offset.

To mitigate this issue, I added a voltage comparator on the DAC output to compare its output to the actual ground reference of the HCS circuitry. This comparator communicated directly with the microcontroller to adjust the DAC’s digital ground level to fluctuate around that of the HCS ground. This caused a constantly fluctuating DAC reference level that better approximated the actual ground reference and could automatically adjust to new experimental setups without requiring user involvement.

We made a final firmware adjustment to account for the hysteresis levels of the voltage comparator we used. The DAC reference level was constantly fluctuating to levels between the upper and lower hysteresis limits. We saw that when the stimulator was turned on that the stimulation was centered around whichever point the DAC was currently referenced at, which could be multiple digital levels above or below the optimal "ground." To alleviate this, we programmed the Bionode to average the peaks of the reference fluctuation and use that value instead when the stimulator was started. This effectively gave us an optimal, though still not exact, digital approximation of the actual ground reference as can be seen in Figure 2.8.

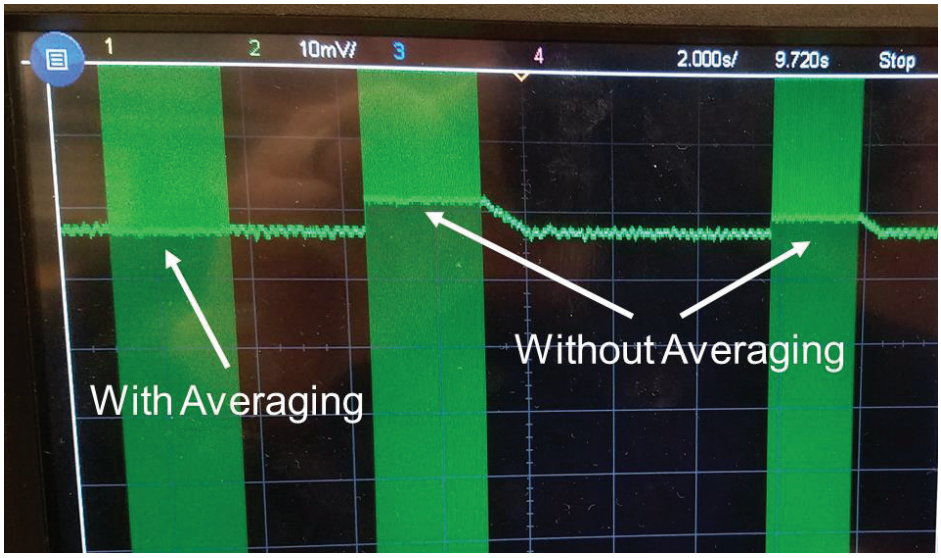

Figure 2.8 Oscilloscope image of DAC stimulation outputs (which appear as solid green sections) with and without hysteresis averaging.

2.2.2.4.2 Charge build-up on DC blocking capacitor

When transitioning a stimulation circuit to be used in animal studies or to clinical human trials, it is extremely important to prevent any unintended electrical currents from reaching the subject. Such stray currents can attenuate the physiology of the tissue you are trying to stimulate or even damage it. To prevent stray DC charges from reaching the tissue, it is advantageous to utilize a blocking capacitor in series with the stimulator load to absorb any DC currents that may be present.

In the Bionode 4.1, there were multiple sources that caused stray DC currents to pass through to the stimulation line. The primary source was the previously described DC offset in the DAC reference signals. While our voltage comparator feedback minimized this effect, there were still small amounts of offset that would allow DC current to pass through during stimulation. In addition, the HCS circuity allowed small amounts of stray current into the line even when the stimulator was turned off. We could prevent these currents from reaching the load by inserting a DC blocking capacitor into the stimulation circuit, but that capacitor would continually charge until saturated. Once saturated, the capacitor would cause stimulation pulses to become charge saturated and imbalanced, as can be seen in Figure 2.9. The result was that a DC blocking capacitor could not effectively be used with the Bionode 4.1.

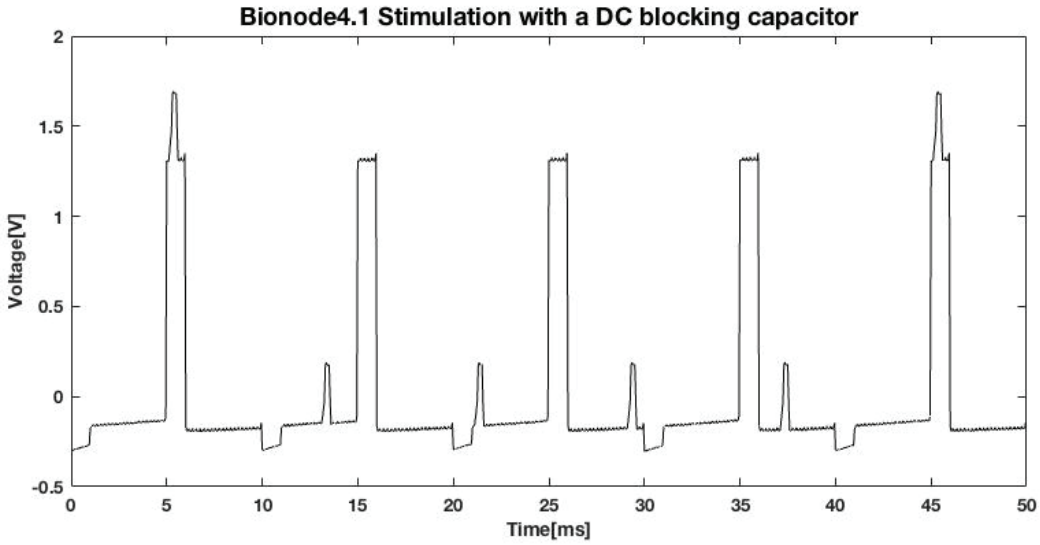

Figure 2.9 Stimulator output showing the effects of charge saturation of a DC blocking capacitor in series with the stimulation line [43].

To alleviate this issue, we placed a normally closed and digitally controlled switch in the stimulation output line parallel to the blocking capacitor and load. We programmed the switch to open only at times when the stimulator was sending out a pulse. This effectively routed any stray currents straight to the ground when stimulation was not occurring, both when the stimulation was deactivated and between stimulation pulses when stimulation was activated. Additionally,

any charge that would be built up on the capacitor during actual stimulation pulses was discharged through this same route once the pulse was finished.

I must note that the capacitor discharge switch required a larger voltage to control than that of the microcontroller output. We therefore added level shifters to the circuit to increase our switch control signal from 1.8 V to 2.7 V, which was an already available power rail in our Bionode circuit.

2.2.2.4.3 Transmission noise on stimulation channel

A third issue noted during testing and use of Bionode 4.1 was that of noise spikes appearing on the stimulation channel. These spikes were traced back to transmission signals from the microcontroller. Due to high levels of power needed for the microcontroller to transmit a data packet, each time it transmitted, the power rails connected to the microcontroller would experience an instantaneous fluctuation in the form of a power spike. Since the stimulator's DAC shared these power lines, specifically the low power rail (-0.9 V), these power spikes were induced onto the DAC output and, subsequently, the HCS output as well. These spikes were present at all times in various capacities, but when high impedance routes were introduced to the power rails (such as with loose solder connections), the spikes increased greatly and interfered with intended stimulation protocols. The issue was accentuated because these power spikes were present even when the stimulator was not enabled. This effect can be seen in Figure 2.10.

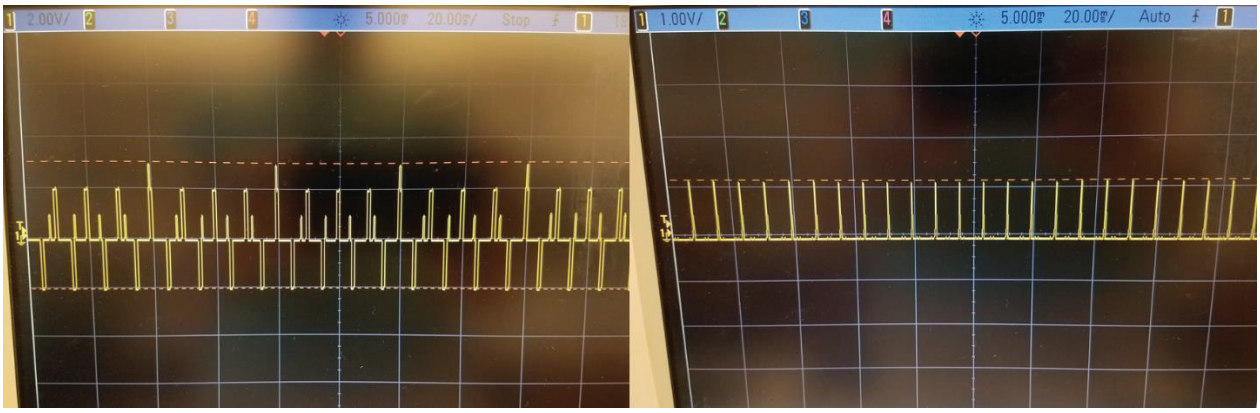

Figure 2.10 Oscilloscope images of waveforms with severe transmission noise spikes during stimulation (left) and while stimulation is off (right).

This issue was mitigated in two ways. First, the previously added DC blocking capacitor discharge switch forced any power spikes to be grounded whenever the switch was closed. Thereby, the spikes were only present during actual stimulation pulses. Second, the remaining pluses have been minimized by adjustments we have made in the power rails. We have changed the DAC powering scheme from using -0.9 V to 0.9 V rails, to using 0 V (ground) to 1.8 V rails. This shift has allowed the low reference of the DAC (the one most vulnerable to transmission power spikes) to be on a more robust ground plane. In addition, we isolated all microcontroller rails from those used in the recording and stimulating circuit.

While transmission spikes are still present in a very minimal amplitude on the Bionode 5.0, they are no longer seen at significant levels on the stimulation channel.

2.2.2.4.4 Turn-on glitches

The final issue address in the stimulator circuit for Bionode 5.0 was that of turn-on glitches. During initial power-up of the Bionode circuitry, we noted very large surges of charge delivered to the load of the stimulation output, as can be seen in Figure 2.11. This glitch was present despite the grounded control switch illustrated in Figure 2.3 and the normally closed DC blocking capacitor discharge switch.

We traced the problem back to the power-up sequences of various component and the HCS circuit itself. The DC blocking capacitor discharge switch required sufficient voltage to properly “close” the switch. When not sufficiently powered, the switch would show a significant nominal resistance in the channel. Therefore, upon device turn-on, stray currents in the HCS rails allowed a quick and significant build-up of charge onto the stimulator’s DC blocking capacitor before the discharge switch was able to activate and ground the connection.

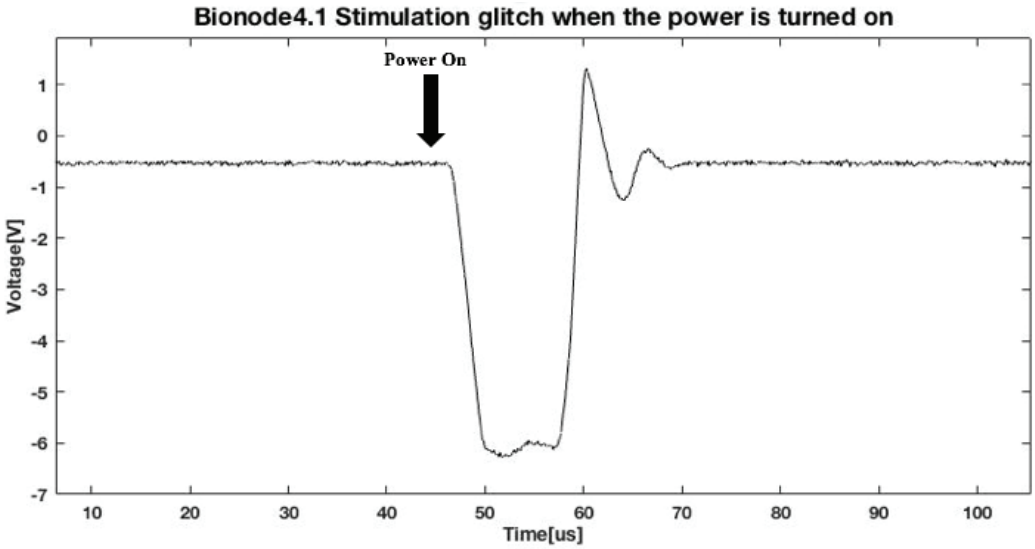

Figure 2.11 Stimulator output showing a large surge of current applied to the stimulation channel when the Bionode circuit is turned on [43].

We mitigated this issue by adding normally open and digitally controlled switches to the power rails of the HCS. Unlike the normally closed switches, the normally open switches did not require power to act as open circuits. Therefore, we effectively created a separate power control for the HCS that prevented it from diverting stray current during powering sequences to the stimulation channel. The HCS can instead remain powered down until needed. This serves as a solution to the turn-on glitch and provides a small overall power savings to the Bionode 5.0 device.

2.2.2.4.5 Stimulation circuit improvement results

Due to the multiple changes made to the stimulation circuit for the Bionode 5.0, the stimulator has become much more robust. As can be seen in Figure 2.12, all issues are no longer present, and a DC blocking capacitor can now be effectively used.

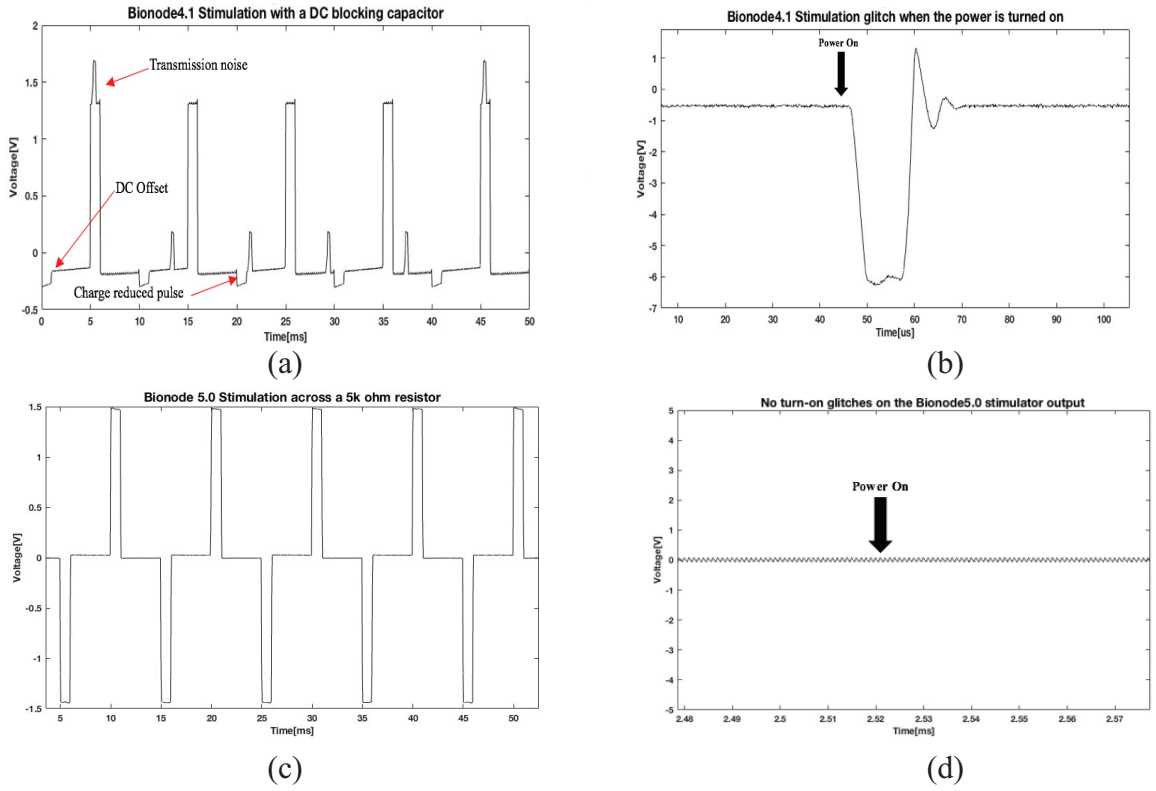

Figure 2.12 Stimulator performance comparison between Bionode 4.1 and Bionode 5.0: (a,c) results of stimulation with DC blocking cap, (b,d) Turn-on glitch test results [43].

2.2.2.5 Impedance measurement

In addition to making the multiple improvements to the stimulation circuit itself as previously described, I also created a relative impedance measurement system to the stimulation output. I worked Jay Shah to build and test the circuit and it has now been integrated into the Bionode. This circuit consisted of separate current and voltage sensing circuits that utilized simple operational amplifiers to accurately measure the instantaneous current flowing through the stimulation output channels, as well as measure the instantaneous voltage being applied to the stimulation load. A diagram of the circuit can be seen in Figure 2.13.

While this circuit does not provide a true potentiostatic impedance measurement that you would get with a commercial system such as made by Gamry, it does give the user an instantaneous and accurate estimate of the actual electrical waveforms that are passing through the load. Using the

voltage and current measures, the user can easily estimate the resistance of the load by using Ohm's law. This provides the user a quick verification of correct operation of the device, as well as, how the load may change throughout the use of the device.

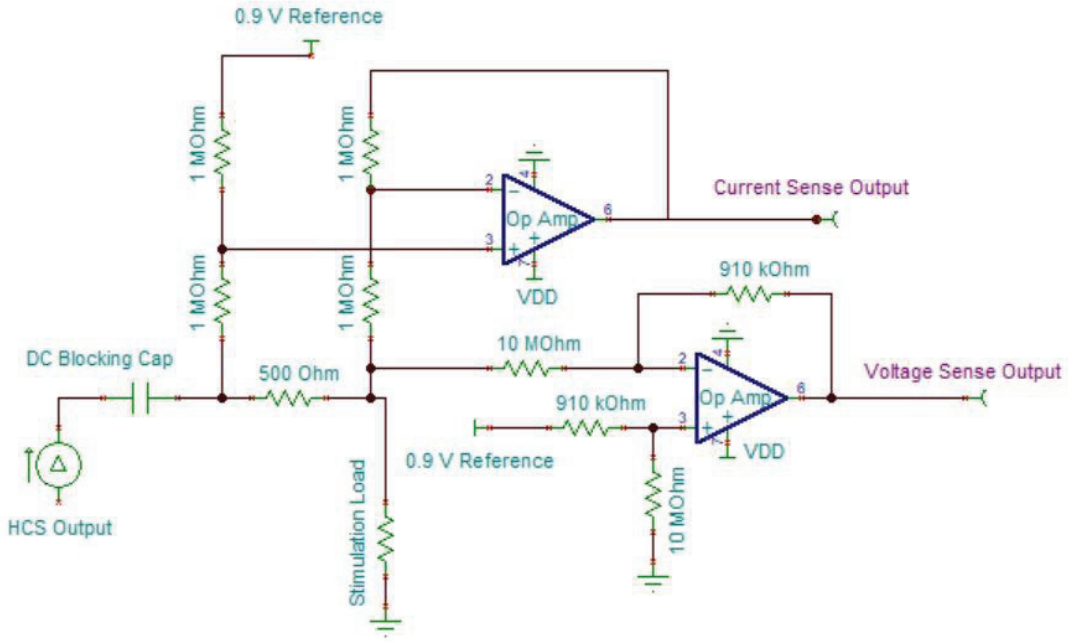

Figure 2.13 Schematic of relative impedance measurement system added to Bionode 5.0. Circuit consists of two operational amplifiers and nine resistors configured to accurately measure the current and voltage being applied to the stimulation load.

Resistors values were determined by initial testing. A 500 Ω sense resistor was used to give an increased accuracy on the current measurement. A smaller resistor could be substituted to improve power consumption at the risk of losing some accuracy. Similarly, the voltage dividing resistors of the current and voltage sense circuits were chosen at the mega-ohm or near mega-ohm levels to reduce the power consumption of the circuit. Lower values can be used but will result in less stimulation charge being delivered to the load, which would then reduce the accuracy of the intended stimulation command to the Bionode and require the software to be re-calibrated. Alternately, the resistors could be increased further in value, but this will result in more noise in the signal received by the user.

The outputs of the current and voltage sense circuits were connected directly to input pins of the integrated Bionode 5.0 microcontroller and can be seen in real-time using the Dataview software GUI. Sample outputs from a stimulation pulse over a 5 kΩ load in Dataview can be seen in Figure 2.14. It should be noted that the voltage spike is inverted from the current spike. This is simply a factor of the circuit's amplifier orientation and could be corrected with a simple firmware change if desired. The amplitudes of the recorded spikes however give a good estimate of the actual resistive load.

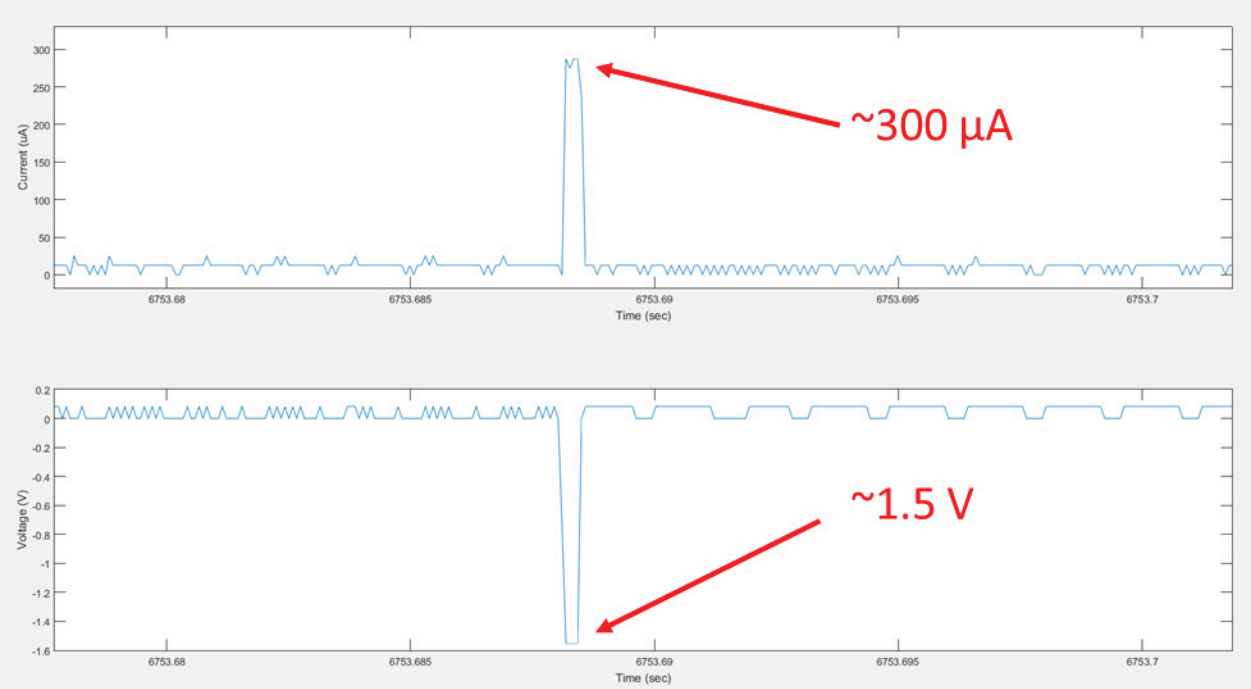

Figure 2.14 Bionode Dataview output of our current and voltage sensing circuits. The Bionode was directed to apply a 300 µA stimulation pulse with a duration of 360 µs across a 5 kΩ resistive load.

I have successfully estimated resistive loads in the range of 500 Ω to 40 kΩ to within 7% accuracy, or better, using stimulation pulses ranging from 200 µA to 1 mA using this circuit.

2.2.3 Manufacturing/Packaging

Successfully fabricating and packaging a device for chronic implantable applications depends greatly on miniaturized form factors and robust device encapsulation. All physical aspects of

the Bionode implant are designed with the goal of creating an adaptable, inexpensive, robust, and fully implantable device with a form factor allowing for long-term chronic implantation in rodents or minimally invasive implantation in humans. These design considerations were further constrained by the desire to use only COTS components as well as a need to maximize manufacturing yield. The components of the Bionode that most define its form factor and manufacturability are its printed circuit board assemblies (PCBAs), electrodes, wireless powering coils, and packaging used to encapsulate the implant.

2.2.3.1 PCBA considerations

The Bionode implant contains two PCBAs: The Bionode motherboard, and the Powernode. The motherboard contains the analog front end (AFE), stimulator, microcontroller, radio, and antenna. The Powernode contains all circuitry necessary to provide power rails to the Bionode mainboard and wirelessly recharge battery if used. Because these two boards were developed in a modular fashion, each board could be designed, optimized, fabricated, and tested independently. The ability to fabricate and test the two Bionode PCBAs separately made manufacturing defects easier to find and repair, which increased device manufacturing yield. This approach also allowed a modular design where different Powernodes (e.g. with and without rechargeable batteries) could be used in different applications.

Both PCBAs were optimized for size by selecting small component packages and laying out all pads and traces on the PCB using a minimum spacing and width of 0.127 mm wherever possible. The Bionode mainboard is a 6-layer board, while the Powernode is a 2-layer board. Both PCBs were fabricated by Advanced Circuits and hand populated by researchers and technicians at the CID at Purdue University.

2.2.3.2 Electrode considerations

A variety of electrodes and leads can be successfully used with the Bionode for both recording and stimulating including nerve cuffs, helical leads, pressure sensors, thermocouples, deep brain

electrodes, and bone screws. All of these electrodes connect to the Bionode by means of low-impedance commercial pins. This interface allows virtually any electrode to be terminated with a 0.46 mm – 0.51 mm diameter mating pin and connected to the Bionode.

2.2.3.3 Coil considerations

Wireless powering coils were hand-wound by the authors at the CID using 22-gauge wire. The front-coil has a 7 mm inner diameter and the top-coil has a 5 mm inner diameter. These dimensions were constrained so that the coils could fit inside the cylindrical package described next.

2.2.3.4 Packaging considerations

To chronically implant the Bionode in a rodent model for any length of time, it must be encapsulated in a package that insulates it from tissue. Many materials including polymers, metals, ceramics, and glasses have been used in recent years for hermetic and non-hermetic implantable device packaging [44-47]. While metal packages with glass or ceramic feedthroughs have become popular for long term medical implants, the sealing processes often require highly controlled environments and expensive precision equipment (i.e. infrared lasers to melt glass or laser-beam welders to fusion weld metals). Metal packaging also may require powering coils and communication antennas to be placed outside of the metal packaging to avoid power and communication losses; further complicating the packaging process [44].

With these considerations in mind, the inexpensive and flexible option of using medical grade epoxy to encapsulate the Bionode was chosen, which has been successfully verified as a legitimate option in other research [45, 48]. Fully encapsulating the Bionode in medical grade (Hysol Loctite M-31CL) epoxy was achieved using a multi-step process illustrated in Figure 2.15. Prior to encapsulation, a custom designed 3D printed case is created to shield the Bionode electronics from the epoxy. All electrode connections are made via a feedthrough board which electrically connects the electrode pin receptacles to the Bionode AFE inputs or stimulator outputs. While this feedthrough board provides an easy way to attach various electrodes to the

Bionode, its main function is to prevent leakage into the implant body via a faulty lead. Lead breakages are often a cause for implant device failure [49]. The feedthrough board isolates the leads from the inside of the implant case, which ensures that broken leads do not provide a path for fluid to enter the implant.

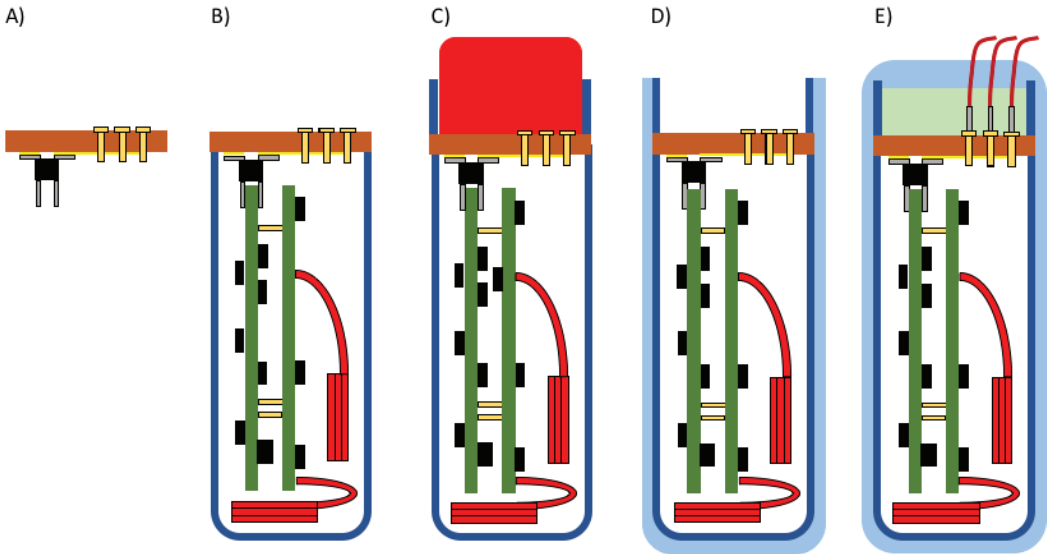

Figure 2.15 This figure illustrates the packaging process of the Bionode via a cross-sectional view. (A) A feedthrough cap containing receptacles for electrodes as well as a connector for the Bionode Mainboard is constructed. (B) The fully assembled Bionode and Powernode are connected to the feedthrough cap, and a 3D printed case is glued directly to the feedthrough cap. (C) A plug is connected to the outside of the feedthrough cap to insulate the electrode receptacles from epoxy, which is used to create a well above the feedthrough cap. (D) A second coating of epoxy is applied around the entire 3D printed case and then the plug is removed. (E) Electrodes are connected to the electrode receptacles, and the well above the feedthrough cap is insulated with a layer of silicone. Once the silicone is cured, the entire implant is coated once again in epoxy which fully encapsulates the implant.

The encapsulated Bionode package is 3.5 cm long with a diameter of 1.5 cm and weighs 9 grams, which is comparable to other non-application specific integrated circuit (ASIC) systems [50, 51]. This packaging method has demonstrated excellent reliability for short to medium term chronic animal testing. To date, using this packaging method, 76 Bionodes have been successfully implanted for chronic studies lasting up to 71 days. No packaging failures have been observed during the course of these studies.

This packaging approach optimizes for customization and flexibility in the design and test cycle of the implantable device. Changes in the board shape, size, and architecture can be accommodated by quick changes to device casing and feedthrough board layout, providing fast turn-around and implementation. In addition, the interconnects utilized by the feedthrough board can be modified to meet the ever evolving attributes of future devices [52] such as capacitive feed-through systems [53, 54]. Unlike other hermetic sealing examples [29, 46, 55] have used alternative materials and methods, the materials and tools used in this method are relatively inexpensive and easy to obtain and adopt.

In a recent study involving the long-term chronic implantation of the Bionode in rats, the 3D printed case was replaced with a glass cylinder. This reduced the amount of medical grade epoxy needed to seal the device because the glass case does not need to be fully encapsulated in epoxy. One of these devices is pictured in Figure 2.1.

Explanted Bionodes can be recycled using various methods depending on the type of adjustments needed between implantations. For devices that do not require any adjustments to the Bionode hardware, the top layer of epoxy surrounding the feedthrough well can be removed using a band-saw or rotary tool. Once the epoxy is removed, the silicon and leads can be removed by hand, as in Figure 2.16. New leads can then be inserted, the well can be refilled with silicon, and the device can be re-encapsulated in epoxy. For devices needing adjustments to the Bionode hardware (i.e. devices needing different AFE passband values), the casing can be cut below the feedthrough board, and the device can be removed, adjusted, and mounted to a new feedthrough board for repackaging. To date, fifteen Bionodes have been successfully recycled using this process, with some being successfully recycled multiple times.

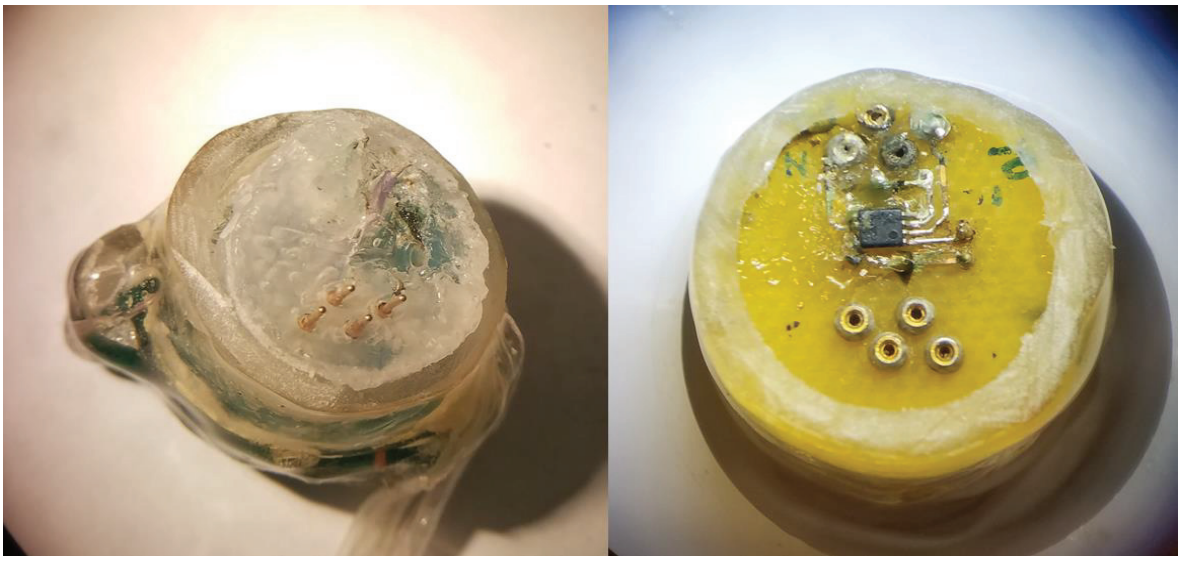

Figure 2.16 Explanted and dissasembled Bionode device. Top (left) has been removed with silicon and pins in place. Bottom (right) contains working device and can be repopulated with new electrodes, re-sealed, and re-implanted.

In addition to durability during implantation, I tested tether-powered versions of the Bionode device packaged in medical grade epoxy for its ability to be sterilized using an autoclave (see Figure 2.17). While it is unlikely that this technique could be used to prepare our new battery powered devices, the non-battery powered implementation tests withstood ten separate cycles of standard autoclave sterilization and still operated with no decreased ability.

2.2.4 Comparable Devices

As referenced earlier, there have been many stimulation and recording devices developed in recent years for various applications. While many of them are well suited for the specific applications that they were designed for, most do not share the capabilities of the Bionode to serve diverse uses in animals studies.

We compared published literature on eight such devices [29-34, 56, 57] (presented in Appendix A) and found that none of the reviewed devices could match the Bionode for inexpensive, flexible, adaptable, configurable, implantable, recording and stimulating capabilities.

Only three of the other reviewed devices provided both recording (only one provided more than two recording channels) and stimulation capabilities and only one provided an impedance measurement option. Those with better stimulation capability were only deemed so due to having more than one stimulation channel available.

Virtually all reviewed devices had passive or pre-programmed controls versus the active recording and stimulation control of the Bionode system. In addition, none of them offered both battery and inductive powering options like the Bionode does. Those that were smaller in size were so because they used ASIC electronics, making them less easily manufactured and configured in a small laboratory setting at a low cost. Finally, not all the devices reviewed were shown to be fully implantable or tested in-vivo on small animals as we require.

2.3 Nerve Cuffs

Possibly of equal importance to the stimulation circuitry are the electrodes used to deliver the electrical charge to the intended load. There have been countless research efforts dedicated to the design and development of stimulation electrodes [58-60]. For stimulation of peripheral nerves, the most common electrode types are cuffs, flat interfaces, and intrafascicular electrodes.

In our studies, we have concentrated on the development and use of cuff electrodes. Cuff electrodes are essentially a layer of flexible and biocompatible material that forms a “cuff” that can be wrapped around the circumference of the intended nerve to be stimulated. Within that cuff is one or more electrodes made of a conductive and biocompatible material. The electrode may

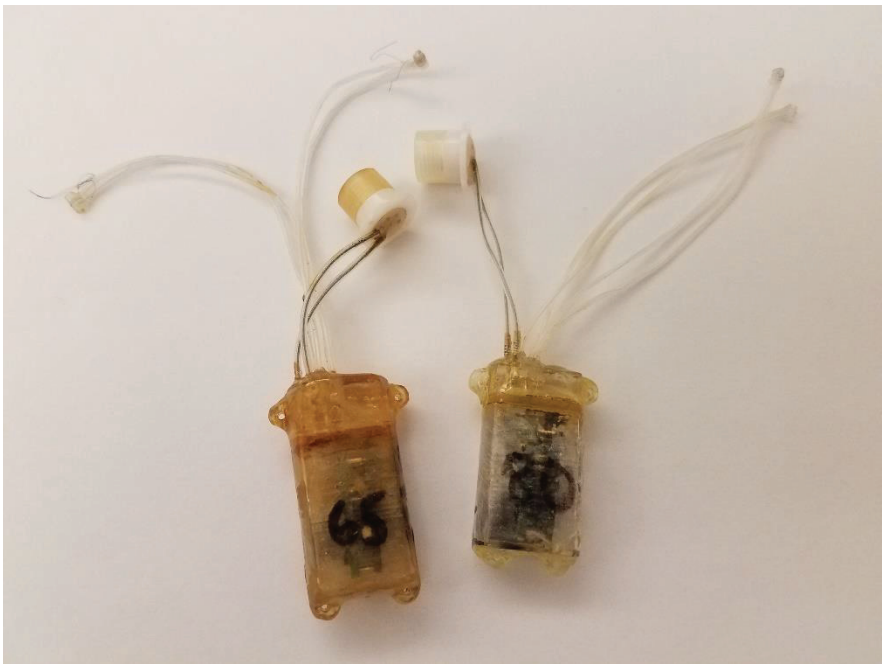

Figure 2.17 Bionode devices after sterilization cycles in an autoclave. Device on the left remained fully functional after ten standard cycles (20 psi, 250˚ F, 20 minutes). Device on the right remained fully functional after one increased intensity cycle (30 psi, 270˚ F, 20 minutes).

be in the form of a wire, flat foil, or deposited thin film. Common conducting materials used for stimulation and recording electrodes are platinum and platinum iridium, iridium oxide, tantalum, titanium nitride, and PEDOT [59, 60]. In addition, the electrodes need a conductive lead that can reach and connect to the stimulator device. These leads must be insulated, flexible, and can either be welded to the cuff electrodes, or an extension of the electrode if made of wire. Literature on aspects of cuff and other electrodes is extensive [59, 60].

In addition to mechanical and biocompatibility factors, electrical factors of the cuff electrodes must be taken into consideration when designing them for experimental use. The most commonly tested performance factors for stimulation electrode characterization are that of electrochemical impedance spectroscopy (EIS) and cyclic voltammetry (CV). These factors are explained in detail by Stuart Cogan [59]. EIS is basically a measure of the electrical impedance made over a broad frequency range of stimulation. Though even more important for recording electrodes, it is also an important measure for stimulation electrodes as it helps to determine how much charge must be applied by the stimulator to produce an intended stimulation charge to the

load. A preliminary EIS measurement can be made in phosphate buffered saline (PBS) and the standard characterization is done for the impedance measured at 1 kHz frequency. An in-vivo measurement can also be done to determine the resistive contributions of the tissue the electrode is attempting to stimulate. The CV measurement produces what amounts to a measure of charge-injection capacity for neural stimulation. In essence, CV sweeps the potential of an electrode within the water electrolysis window. The standard characterization measure is made by calculating the area under the negative curve of the sweep that represents the cathodal charge storage capacity (CSC_C). This total value can be divided by the effective exposed surface area of the electrode to give the CSC_C per unit area of the electrode material.

2.3.1 Types of cuffs and electrodes tested

During the process of developing an implantable Bionode device for animal studies and performing Defense Advanced Research Projects Agency (DARPA) testing for Aim 3 of this study, I tested multiple variations of cuff electrodes made both in our lab and by outside industry manufacturers and university labs. Many of those tested are pictured in Figure 2.18 and their EIS and CV data can be seen in Table 2.2. I tested the following cuffs:

- CorTec tunnel cuff with Platinum Iridium (PtIr) foil electrodes imbedded in silicon. Cuff was 3 mm in length with a 0.6 mm inner diameter.
- Shape memory polymer cuff fabricated by University of Texas – Dallas (UTD) as presented in Figure 2g of Ware et al [61]. Shape memory makes the effective cuff diameter variable depending on implementation factors.
- Army Research Labs (ARL) conductive carbon nanofiber polymer "cuff." The material was obtained from ARL and was presented by Slipher et al [62]. An actual cuff was not made, but a reasonable sized section of the material was formed to be tested for electro-chemical properties. Both 4% and 7% carbon nanofiber makeups were tested.
- Our own experimental thin film cuff electrodes were developed and tested in the CID here at Purdue. The electrodes were created by Quan Yuan in our cleanroom by depositing either gold or platinum electrode material onto 12 μm think parylene substrate cuff material. These cuff electrodes were designed to be wrapped around the nerve to

create ~1.5 mm diameter cuffs with a separate 11 mm tab to wrap around the nerve and anchor to the carotid artery (for cervical implantation). A zip design originally presented by Yu et al [63] was utilized to keep the cuff wrapped during implant, and quick curing medical silicone material was used to seal the cuff in place.

- Microprobe platinum wire cuff electrodes that were utilized for the acute Magnetic Resonance Imaging (MRI) stimulation testing shown in Aim 3. These cuffs are very similar in shape and form (~0.5 mm inner diameter) to our own CID wire cuffs but utilize a single solid strand of 100 µm wire and have embedded suture materials to for closing the cuff.
- CID wire cuff electrodes. We tested multiple different variations of wire cuff electrodes as are presented sections 2.3.2, 2.3.3, and 4.4.4.1.

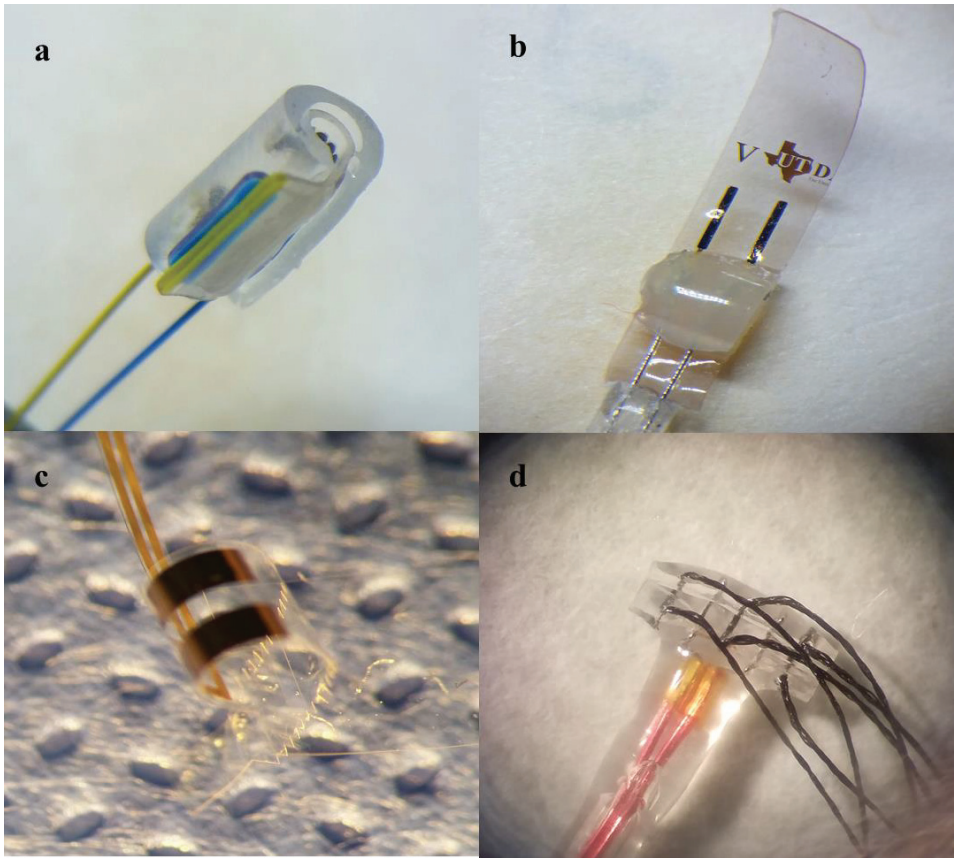

Figure 2.18 Cuff electrode variants tested and used in this study. a) CorTec tunnel cuff with PtIr foil electrode. b) UTD shape memory polymer cuff with thin film electrode. c) CID custom zipping parylene cuff with thin film electrode. d) Microprobe silicon cuff with Pt wire electrode and copper leads for use in MRI.

Table 2.2. Electrochemical characterizations of cervical vagus nerve cuffs variants tested for use in our studies. Averaged values of tested cuffs are presented.

Cuff Variant	Electrode Material and Form	Measured CSC_C Total (µC)	Exposed Surface Area (mm^2)	CSC_C Per Area ($\mu C/mm^2$)	Impedance at 1 kHz (Ω)
CorTec	Platinum Foil on silicone cuff	9.05	0.3	30.18	3.66 k
UTD Thin-Film	Gold layer on shape memory polymer	0.97	0.7	1.39	1.21 k
ARL 4%	Conductive carbon nanotube polymer cuff	26.2	36	0.72	2.32 k
ARL 7%		7.69	36	0.21	1.15 k
CID Thin-Film	Gold layer on Parylene	9.58	1.48	6.47	476
	Platinum Film on Parylene	15.46	1.13	13.65	1.77 k
MRI	Platinum wire in silicone cuff	5.35	0.49	10.87	2.11 k
CID Wire	Platinum Iridium wire (1x7 strand) in silicone cuff	9.33	0.5	18.62	1.52 k

Despite the multiple options available and tested, we primarily used, and continue to use, our CID wire cuff electrodes. As can be seen above, they show comparable or superior electro-chemical properties to the other available options we have tested. Their EIS impedance of 1.52 kΩ is better than other wire or foil options tested. The CID wire cuffs also have superior CSC_C to all but the CorTec electrodes, but the CorTec variant are also smaller and less suited for multiple applications. In addition, the CID cuff electrodes can be made in-lab with no special equipment requirements. This saves a lot of lab resources as custom industry electrodes are expensive and follows the theme of the making the Bionode highly adaptable to many research needs.

2.3.2 Wire considerations

With respect to our in-house wire cuff electrodes, there have been multiple variations made in the past 5 years. One of the many consideration in these electrodes are the type of wire used to

form the electrodes themselves. We have had the luxury of a good working relationship with Fort Wayne Metals of Fort Wayne, IN. They have supplied us with various samples to try and a reliable supply of the actual 1x7 braided wire that we now most commonly use. When running low on supplies, I worked with Fort Wayne Metals to acquire multiple wire samples, and tested each for electro-chemical properties, as well and mechanical properties to determine the best option for our cuffs going forward. Relative size comparisons can be seen in Figure 2.19 and electrochemical test results can be found in Table 2.3. I tested the following wire variants (all made from Platinum (90%) Iridium (10%)) in our cuffs:

- 1x1 solid strand wire showed sufficient size and EIS and CV characteristics to be used as a stimulation electrode. It was also very flexible, but a bit too pliable to effectively hold a cuff shape during the rigors of implantation. It often was manipulated and lost the ideal cuff contours we desired.
- 1x7 braided wire showed very similar electro-chemical characteristics to the 1x1 solid strand and proved to be a much better option as it was very flexible and pliable, but also showed enough “bounce back” when manipulated so that it could keep its cuff contours during implementation. This is the wire variant we have moved forward with for in-vivo experiments.
- 1x19 braided wire was used in some early CID cuff electrodes as we had obtained a sample spool of it. Successful in-vivo and chronic tests were performed with this variant on the cervical vagus nerve (data now shown here). It showed superior EIS and CV measures to the 1x1 and 1x7 variants as would be expected by its larger size, but also proved to be harder to manipulate and form into cuffs. It would have been difficult to form this variant into smaller cuffs such as those we used for subdiaphragmatic stimulations in Aim 2. It was also not commonly made by Fort Wayne Metals and would have been prohibitively expensive to obtain more of.
- 7x7 braided wire cable was basically 7 separate 1x7 wires braided together and was very large for our purposes. A sample was sent and tested and, as expected, showed very good electrochemical properties. However, it was much too large for any practical nerve cuff purpose in rodent studies as it could not be bent into the appropriate cuff size even for cervical uses.

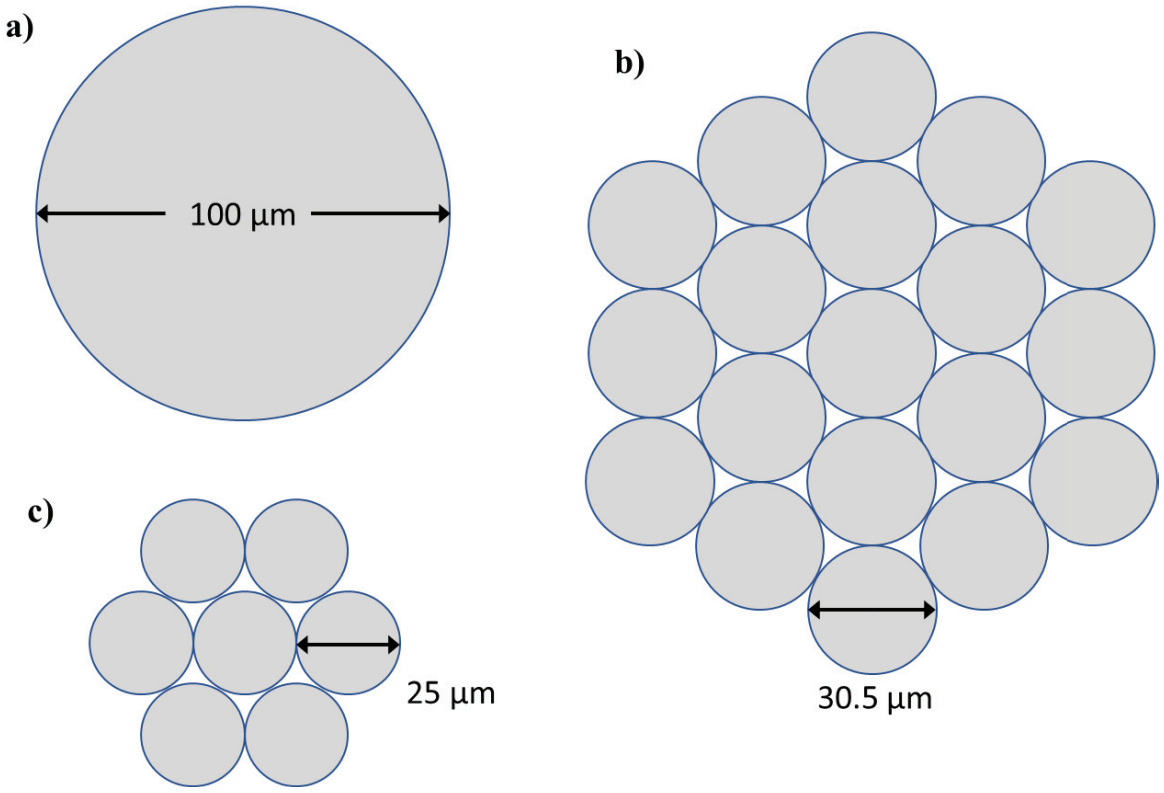

Figure 2.19 Relative size comparison of cross sections of wire variants tested for use in our cuff electrodes. a) 1x1 solid strand PtIr wire. b) 1x19 braided PtIr wire bundle. c) 1x7 braided PtIr wire bundle.

For surface area estimates of wire, we utilized equation (2.2) for the solid single strand as it is the standard surface area equation of a cylinder minus the ends. Braided wire is more difficult to estimate the surface area of, but we utilized equation (2.3) supplied to us by Fort Wayne Metals. Equations contain variables of *d* as the diameter of a single wire fiber, *L* is the length of wire exposure, and *N* is the number of peripheral strands of wire (if a braided variant).

$$A_{solid} = \pi dL \tag{2.2}$$

$$A_{braided} = \left(\frac{2}{3}\right)\pi dLN \tag{2.3}$$

Table 2.3. Electrochemical characterizations of cervical vagus nerve cuffs made with wire threaded to cover a length of ~70% of the inner circumference (0.76 mm) of silicone tubing with a single strand. Averaged values of tested cuffs are presented.

Wire Variant (Platinum Iridium)	Measured CSC_C Total (µC)	Exposed Surface Area (mm^2)	CSC_C Per Area ($\mu C/mm^2$)	Impedance at 1 kHz (Ω)
1x1 Wire – Single Strand	8.70	0.49	17.69	1.48 k
1x7 Wire – Single Strand	9.33	0.5	18.62	1.52 k
1x19 Wire – Single Strand	31.42	1.16	27.15	630
7x(1x7) Wire Cable – Single Strand	177	2.2	51.94	615

2.3.3 Wire threading

During our studies utilizing cuff electrodes, it became known that the basic cuff design we were utilizing was not sufficient for all applications we wished to use it on. For example, although a single length of the 1x7 braided wire showed good properties for the majority of applications, we found certain circumstances in while a greater exposed surface area and consequently, a lower impedance were necessary.

One such instance was in applications where a higher amplitude of current was required to be delivered to the biological interface. If the interface itself was of a high impedance such as a relatively dry surface, then the ability of the Bionode to supply the required charge was limited due to its voltage supply limits. Since the voltage limits were not easily adjustable in our Bionode setup, we were required to find a way to lower the impedance of our electrodes.

Another instance of needing lower impedance and higher surface area was when we tried to stimulate and record from the same nerve in the body of the animal, such as with the Autonomous Neural Control (ANC) algorithm that is presented in more detail in sections 4.2.6.2 and 5.5. We found that the recordings in these instances were very noisy and that it was greatly improved when an extra ground connection to the body of the animal was applied. We theorized that since the ground for the entire system was based on the stimulator's connection to the body of the animal, then the exposed ground plane being supplied by the electrode was not sufficient.

To solve this issue, I developed the strategy of using multiple wire thread lengths in our electrodes. This was done by threading the wire through the inside and then outside of the cuff electrode multiple times. Images of the threaded cuffs can be seen in Figure 2.20. We began by testing and utilizing vertical threading patterns in the cuffs. This was very effective at increasing the exposed surface area and reducing the cuff impedance, as can be seen in Table 2.4. The external threading lengths were the most effective as they added the most length of exposed wire, and we theorized the potential shunting of current to the outside of the cuff to be minimal if the cuff was small and sealed shut. However, we also developed cuffs with no exposed external thread lengths by either adjusting the threading pattern or by simply covering the external lengths with fast curing silicone adhesive.

The downsides to vertical threading was that the lengths of wire were difficult to thread parallel to each other and tended overlap each other which could potentially cause pinching of the nerve fibers being cuffed. They also made it difficult to close and seal the cuffs due to multiple wire strands holding the cuff opening open. Finally, the long lengths tended to be unintentionally manipulated and damaged at times while trying to surgically attach the cuff.

Due to the issues mentioned, I came up with a strategy to utilize horizontal threading of the wire in the cuff instead. While horizontal threading is more difficult to perform consistently, it showed some significant advantages over that of vertical threading as well as showing similar levels of impedance. Horizontally threaded cuffs were much easier to manipulate during surgery and less apt to wire breakage. The largest disadvantages to threading horizontally were an increased effort and time to manufacture as well as incomplete coverage of the wire around the nerve. However, it can be argued that the overall coverage is better due to the ability to thread the wire closer to the edges of the cuff opening. In addition, if a slight angle was added to the threading, an overlap of nerve length could be covered, and, in essence, could create close to a full coverage of nerve fibers. These advantages were critical when developing larger cuffs for use in a pig model that will be covered in section 5.2.

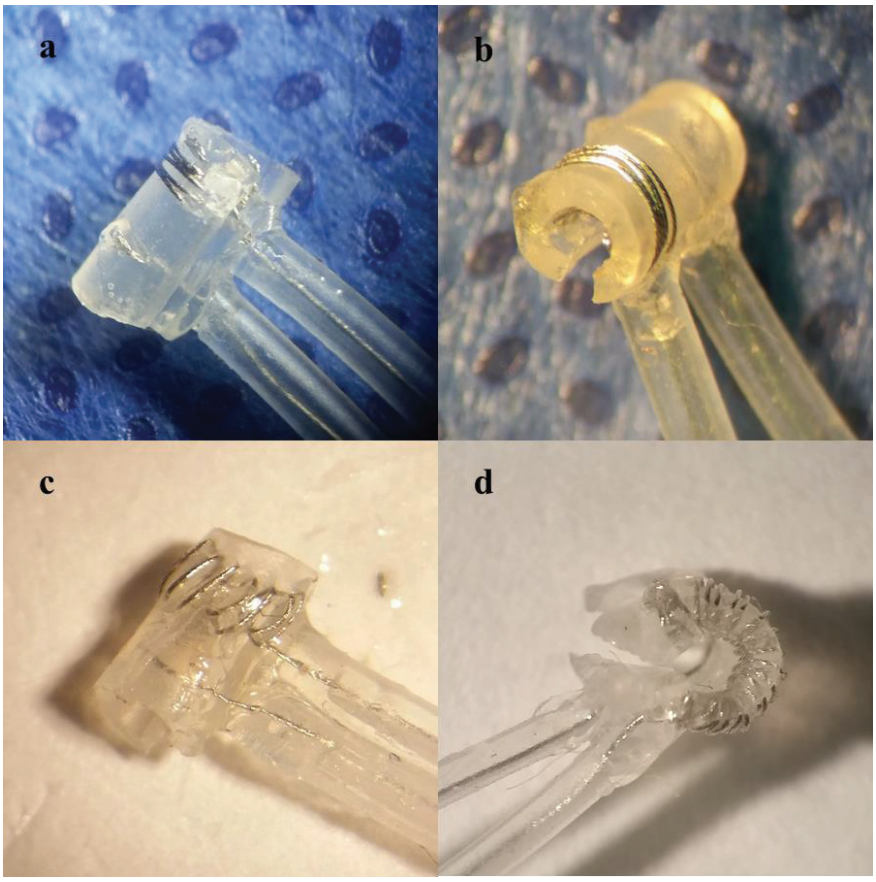

Figure 2.20 Threaded wire cuff variants used in cervical VNS on rats. a,b) Vertical threading of 1x7 PtIr wire into silicone cuffs. c,d) Horizontal threading of 1x7 PtIr wire into silicone cuffs.

Table 2.4. Measured impedance values for threaded 1x7 PtIr wire patterns in silicone tube cuffs. Averaged values of tested cuffs are presented.

Wire Threading Pattern	Inside Wire Lengths	Outer Wire Lengths	Impedance at 1 kHz (Ω)
Vertical	1	0	1.55 k
Vertical	2	0	1.00 k
Vertical	3	0	983
Vertical	4	0	896
Vertical	5	0	590
Vertical	2	1	428
Vertical	3	2	277
Vertical	4	3	211
Vertical	6	5	179
Horizontal	~15-20	~15-20	206

2.4 Summary/Impact

In summary, Aim 1 accomplished a stated goal of making the Bionode stimulation interface highly reliable, flexible, adaptable, and affordable. Virtually every aspect of the Bionode can be manufactured in the laboratory with basic lab equipment and off the shelf parts.

The Bionode stimulator can deliver the desired level and precision of stimulation needed for small animal experiments, and can be easily adjusted either during fabrication, or in many cases, during the experiments with the Dataview software interface, to meet specific experimental needs. Issues discovered in the earlier Bionode 4.1 version have been fixed for our latest Bionode version 5.0, and a relative impedance measurement system has been added to give even more insight into experiments.

Manufacturing and package improvement were made that make production of fully implantable and operational Bionodes possible in both small and large animal subjects. The Bionode has become modular in design allowing for easier troubleshooting and repair. Packaging now includes feedthrough caps that stop previously prevalent leakages from occurring, and the use of pre-formed 3D printed packages sealed with epoxy make a perfect platform for developmental designs that could be upgraded to more robust packaging materials in the future.

The biological interface has also been improved with development of nerve cuffs that can be made and adapted for multiple applications, affordably and in-house.

3. AIM 2: STUDY OF ACUTE SUBDIAPHAGMATIC INFLAMMATORY RESPONSE

3.1 Motivation

One of the primary purposes of our research was to explore the biology behind VNS. We wished to explore not only physiological effects of cervical VNS, but to find the specific subdiaphragmatic branches that contribute most to it and to what effect. Our lab therefore set out to perform acute experiments in which we would stimulate specific subdiaphragmatic nerve branches. This was originally attempted by Kaitlyn Neihouser and her results were presented in her 2017 thesis titled "An Exploratory Study of How Acute Neuromodulation of the Subdiaphragmatic Branches Regulates Inflammation." While her results were interesting and gave a good indication that effects of nerve branch stimulation could be analyzed, we determined that the protocols used were insufficient to obtain a robust analysis.

I therefore set out to improve the methods used and re-do many of the subdiaphragmatic nerve branch stimulations and perform new subsets that could be better analyzed. I also discovered a large temporal variation in the time when inflammatory cytokines levels in plasma would rise that was significantly complicating the data analysis, and I resolved to develop a better methodology to handle this variation. In conjunction with Kelsey Wasilczuk, I produced the work that follows in this chapter.

Material in sections 3.1.1 – 3.5 come directly from my paper titled "Characterization of cytokine response to intraperitoneally administered LPS & subdiaphragmatic branch vagus nerve stimulation in rat model," and its supplemental data, co-authored by Kelsey Wasilczuk, to be submitted to the Journal of Neural Engineering in 2018. Formatting changes and updates have been made as appropriate.

3.1.1 Acute subdiaphragmatic stimulation study introduction

Central to many inflammation studies is the use of an inflammatory challenge, most commonly using lipopolysaccharide (LPS) endotoxin, to induce an acute inflammatory response that can

then be treated by a given drug or therapy. However, the LPS injection method, dosage, and timing can vary greatly between studies, and the results of said experiments may indeed depend in part on these variables. LPS administered through intraperitoneal (IP) and intravenous (IV) injection are generally thought to produce similar inflammatory responses [64-66], but show some differences likely due to distinct mechanisms in the delivery and creation of cytokines.

Steven et al [67] recently made a strong case for better methods characterization and standardization by illustrating differences between LPS challenges in mice and rats. In addition, the dosage of LPS shows different cytokine creation and timing in their responses [68]. We submit that one important and under-characterized aspect in inflammatory research is that of LPS administration method. In VNS research related to inflammation, we most commonly find IV injections used on rat subjects [15, 19, 69, 70], while IP injection methods are reserved for studies on mice [6, 71], presumably due to the technical difficulty of IV insertion into the smaller blood vessels. Studies by Lenczowski et al. [72, 73] demonstrated high variability in response to IP LPS usage in rats, and in discussion with other researches in this area, we found such variability to be the main motivation to administer LPS IV in this animal model. We assert, however, that IP administration presents a more physiologically relevant inflammatory simulation. Whereas IP application represents a foreign infection that must be responded to by the body in a more systematic way, IV delivery artificially adds LPS to the blood stream. Therefore, developing methods to better utilize IP LPS injections and a better understanding of the expected responses will benefit a large community of researchers.

In addition to pursuing a better understanding of the effects of the methods we use in inflammation research, we must continue working to narrow in on physiological mechanisms that can be manipulated to treat specific inflammatory responses. Prior work has postulated that there exists an inflammatory reflex by which the nervous system regulates immune function. By stimulating the efferent fibers of the vagus nerve, splenic macrophage release could be controlled, thus regulating cytokine release. In this way, the inflammatory reflex could be modified to produce an anti-inflammatory response [3]. However, direct innervation of the spleen by the vagus nerve has been met with uncertainty as early as 1993 [74]. More recent research has proposed that vagal innervation of the celiac ganglia is the first in a two part relay,

in which vagal action potentials regulate T cell production, thus controlling the production of the neurotransmitter acetylcholine [6]. A subsequent study showed that VNS inhibited splenic nerve activity but produced no response when the nerve was severed cranial to the stimulation site. This implies that the link between the vagus and spleen is an indirect connection through the central nervous system (CNS) rather than a direct pathway [70].

We, along with others, suggest that the GI vagal innervation proposed by Berthoud et al. in 1991 [75] modulates the release of acetylcholine synthesizing T-lymphocytes in the blood. By stimulating the vagus, distal gastrointestinal fibers stimulate lymphoid tissue into releasing cells such as these acetylcholine-synthesizing T-lymphocytes. When taken up by the spleen, these lymphocytes cause splenic macrophages to decrease their production of inflammatory cytokines, leading to the desired therapeutic effect [76].

As the left cervical vagus nerve passes through the diaphragm of the body, it becomes the anterior vagal trunk and splits into multiple branches [2]. Previous work by multiple groups have shown left cervical vagus stimulation to attenuate cytokine levels [15, 19, 69, 77], but none have analyzed the effects of stimulation of specific subdiaphragmatic branches. Berthoud and Powley have previously postulated that vagal celiac branches contribute the most toward innervation of the major ganglia that comprise the solar plexus, followed to a lesser extent by the gastric and hepatic branches [78, 79]. Following this rationale, we hypothesized that stimulation of different isolated subdiaphragmatic branches would mediate inflammation in unique ways. If true, then utilization of vagal branch stimulation to regulate circulating cytokines produced by splenic macrophages could allow selective symptoms of multiple inflammatory diseases to be alleviated, leading to new potential treatment options.

3.1.2 Experimental objectives

Our study had three primary objectives. 1) To develop methods to effectively analyze the cytokine cascades caused by an IP administered LPS challenge. We accomplished this by testing and utilizing a curve-fitting and alignment method on temporal cytokine profiles. 2) To use these methods to more fully characterize the time-varying effects over a 5.5-hour period of IP

administered LPS on multiple systemic cytokine levels and the relationships between those cytokines. In doing so, we were able to map the order and timing of seven cytokine responses. 3) To apply the first two objectives to explore inflammatory effects of electrical neuromodulation directly to the subdiaphragmatic anterior gastric branch (AGB), accessory celiac branch (ACB), and hepatic branch (HB) of the left vagus nerve. We tested 58 total rats for verification and analysis purposes and discovered distinct sets of modulatory effects caused by each branch.

3.2 Methods

3.2.1 Animals

The Purdue Animal Care and Use Committee (PACUC) approved all protocols in this study. We used 58 adult male Sprague-Dawley rats weighing between 175 – 265 g. Animals were housed under standard conditions with ad-libitum access to food and water, unless otherwise stated.

3.2.2 Electrical stimulation experiments

3.2.2.1 Animal groups

We performed two primary surgical groups – the first to study effects of stimulation of anterior subdiaphragmatic branches of the left vagus nerve and the second to study comparative effects of left cervical VNS. Rats undergoing subdiaphragmatic cuffing were separated into sub-groups as illustrated in Table 3.1. For each anterior branch (anterior gastric, accessory celiac, hepatic), animals received either an LPS challenge with no stimulation, LPS with electrical stimulation treatment, or LPS with electrical stimulation and an efferent vagotomy. The final group consisted of saline controls (n = 3), one animal per anterior branch, that were cuffed but received saline in lieu of LPS and no stimulation. For statistical purposes, the subdiaphragmatic non-stimulation subsets (SubD Sham) were grouped. Surgeries were randomized between sub-groups.

The cervical group was divided between animals that received an LPS challenge and a 5-minute stimulation treatment and those that received LPS but did not receive stimulation. In addition, we performed a sub-set of validation animals (n = 4) to verify our curve fitting methods.

Table 3.1. Overview of Subgroups Used for Acute Electrical Stimulation Experiment Results.

Stimulation Cuff Location	LPS & No Stimulation		LPS & Stimulation		LPS, Stimulation, & Efferent Vagotomy	
Left Cervical Vagus Nerve	CVns	n = 3	CVes	n = 5	N/A	N/A
Anterior Gastric Branch	SubD Sham	n = 8	AGBes	n = 5	AGBvx	n = 5
Accessory Celiac Branch			ACBes	n = 3	ACBvx	n = 4
Hepatic Branch			HBes	n = 4	HBvx	n = 5

3.2.2.2 Materials

We fabricated custom bi-polar stimulation cuffs (shown in Figure 3.1) using Platinum-Iridium wire and medical grade silicone tubing as done previously [80]. The cervical cuffs used in this study have been previously characterized [81]. Our cervical electrodes had a measured impedance of 1.40 – 1.62 kΩ at 1 kHz. The subdiaphragmatic cuff electrodes had a 0.02” inner diameter, but no suture, and an impedance of 2.07 – 3.45 kΩ at 1 kHz.

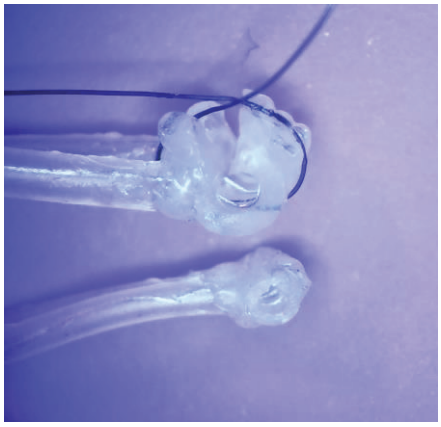

Figure 3.1 Photo of stimulation cuffs used in this study. Larger cuff for cervical vagus nerve stimulation is shown on top with built-in suture to fasten it around a nerve. Smaller cuff for subdiaphragmatic nerve branch stimulation is shown on the bottom.

An improved version of the Bionode stimulator used previously [80] was utilized for our acute stimulation experiments. The stimulator output charge-balanced, bi-phasic, square wave pulses of up to 1.1 mA constant current amplitude. To prevent stray current from permeating into the animal, we added a DC blocking capacitor in series with the stimulator and added circuitry to short the capacitor between stimulation pulses to prevent charge build-up.

3.2.2.3 Acute surgical procedures

We anesthetized rats using 4-5% isoflurane for approximately 3 minutes, then weighed, and injected the animals IP with a ketamine/xylazine cocktail consisting of a 75 mg/kg ketamine and 5 mg/kg xylazine ratio. A supplement of buprenorphine was administered subcutaneously (0.08-0.12 mg/kg). Anesthesia was maintained with IP injections of ketamine/xylazine every 30 minutes or as needed based on heart rate and toe pinch. We shaved and cleaned the incision sites and applied artificial tears to the eyes. The animal was then placed supine on a heating pad and placed under oxygen flowing at 2 L/min for the remainder of acute surgery and blood collections. We euthanized animals at experiment completion via a lethal dose of Beuthanasia-D Special (Merck; Kenilworth, NJ) (0.9 mL, IP).

Catheters for blood collection were placed before cuffing the vagus nerve branch. We followed the general procedures outline in the Bioanalytical Systems, Inc. Culex surgical manual for femoral cannulation in a rat [82]. Catheters in our experiment, however, were inserted into the femoral artery instead of the vein and remained exposed on the benchtop for connection to the Culex system versus being subcutaneously routed through the animal.

For animals in the cervical cuffing group, we made the initial incision at the midline of the jaw, moving caudally. We exposed soft tissue until the sternohyoid and sternocleidomastoid muscles, which sit on top of the carotid sheath, were visible. Via blunt dissection, we gently separated connective tissues until the carotid artery sheath could be seen. The carotid sheath was carefully dissected until the left vagus nerve was completely free from surrounding tissues. We then placed the cuff electrode under the vagus nerve, slid the nerve into the cuff, and tied the attached suture to secure the cuff in place. The area was kept moist with saline and covered with gauze for the duration of the surgery when stimulation was not being applied.

Animals in the subdiaphragmatic cuffing group were fasted for 6-12 hours before surgery to reduce stomach volume and ease access to the subdiaphragmatic nerve branches. To expose the subdiaphragmatic branches of the vagus nerve we made an incision starting at the midline above the xyphoid process and moved diagonally to the animal's left. The muscle was blunt dissected along the incision and held open using an elastic retraction system. We carefully retracted the left

liver lobule, cut the hepatoduodenal ligament, and moved the right liver lobule aside to reveal the esophagus. We then located and isolated either the anterior gastric, accessory celiac, or hepatic branch of the left vagus nerve and carefully attached a subdiaphragmatic cuff electrode. The incision site was left open through electrical stimulation therapy to ensure the cuff remained secure on the nerve. For animals receiving an efferent vagotomy, we tied off the nerve branch with 6-0 silk suture, caudal to the cuff, and cauterized the nerve fibers caudal to the suture tie. The suture physically prevented the retraction of the nerve after cauterization and kept the cuff from detaching from the nerve during stimulation.

3.2.2.4 Acute blood collection protocol

Prior to catheter placement, we primed the Culex Automatic Blood Collection System (Bioanalytical Systems, Inc.; West Lafayette, IN) [83] with heparinized saline. Once the catheter was placed in the animal, we connected it to the Culex for tending during the remaining surgical procedure.

Our blood collection protocols followed those outlined in the National Institutes for Health (NIH) Guidelines for Survival Bleeding of Mice and Rats. We programmed the Culex system to automatically collect 12 separate 115 μL blood samples, spaced 30 minutes apart after the second collection, over a period of six-hours as outlined in Figure 3.2. An initial baseline collection was done 30 minutes prior to LPS injection. In doing so, we did not exceed the maximum allowed 10% of circulating blood volume. Blood was collected into vials containing K_3EDTA (1.75 mg/ml) and centrifuged at 2000x g for eight minutes after every two collections. We then extracted the plasma, aliquoted it into 20 μL samples, and stored them at -20˚C until they could be processed.

Validation animals were performed in a similar fashion. Blood collections were doubled in number (24 samples) but halved in volume to compensate. Saline was given periodically throughout the procedure to replenish fluids lost with increased rate of blood collection.

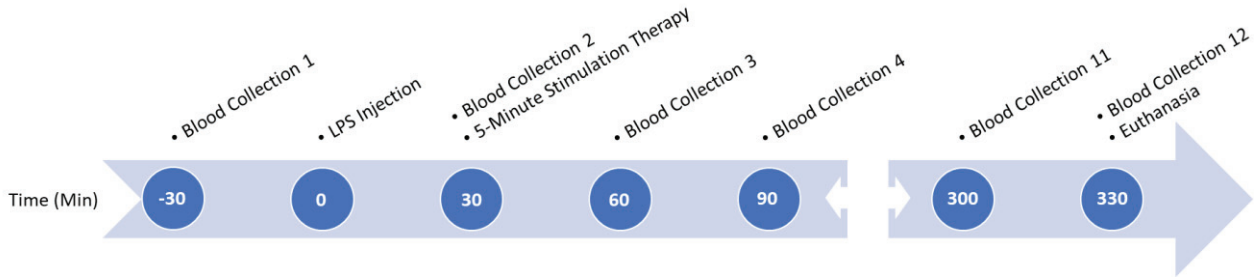

Figure 3.2 Time flow diagram outlines the process of blood collection, LPS administration, and stimulation treatments (if applicable). Time points are based in relation to the acute LPS challenge to the animal.

3.2.2.5 LPS preparation/administration

To ensure proper dosing (5 mg/kg) we prepared all LPS (Sigma-Aldrich, serotype O111:B4) solutions for acute animals in advance. We systematically added 20 mL of sterile saline (0.9% sodium chloride), mixed with a new 100 mg bottle of LPS lyophilized powder, and sonicated the mixture for a total of 45 minutes to ensure complete dissolution. We then aliquoted ~400 µL of solution into individual 1.5 mL Eppendorf tubes, before freezing and storing them at -20˚C until used.

Individual LPS aliquots were thawed by sonication for 30+ minutes at room-temperature 40 – 120 minutes before use. We then sonicated the aliquots for an additional 5 minutes directly before administering the IP LPS challenge to the animal at the specified time during our protocol.

3.2.2.6 Stimulation

Stimulation, when applicable, was performed 30 minutes after injecting LPS, following completion of the second blood collection. The stimulator was connected to the surgically affixed stimulation cuff, in parallel with an oscilloscope for recording pulses, and was powered on promptly before stimulation therapy.

We performed all stimulation treatments for 5 minutes with balanced bi-phasic, square wave pluses, but utilized two separate sets of stimulation parameters. For the cervical vagus nerve, we used a larger amplitude profile (1 mA, 200 μs, 5 Hz) that corresponds closely to effective electrical charge used in other literature [6, 15, 19] and that showed good action potential response in our preliminary testing (not shown). The stimulation intensity was reduced for our subdiaphragmatic stimulation treatments (100 μA, 200 μs, 5 Hz), due to the reduced size and fiber makeup of the subdiaphragmatic nerve branches. This amplitude was shown to be sufficient to affect the inflammatory response to LPS in a preliminary study [84].

Prior to each stimulation treatment, we verified the stimulator for consistency and balance using a known resistive load and oscilloscope. During stimulation, we utilized the oscilloscope to verify an active stimulation and to record voltage profiles of the stimulation pulses. Cervical stimulations revealed voltage amplitudes ranging from 3.24 V – 3.93 V, resulting in relative interface impedances of 3.24 kΩ – 3.93 kΩ. Alternately, subdiaphragmatic stimulations showed voltage amplitudes ranging from 0.83 V – 1.40 V, with relative interface impedances of 8.3 kΩ – 14.0 kΩ.

3.2.2.7 Plasma processing

We analyzed plasma samples using a LEGENDplex™ Rat Th Cytokine Panel (13-plex) (Biolegend, San Diego, CA), which allowed simultaneous analysis of 13 cytokines: Interleukin (IL)-2, IL-4, IL-5, IL-6, IL-9, IL-10, IL-13, IL-17A, IL-17F, IL-22, Granulocyte-macrophage colony-stimulating factor (GM-CSF), Interferon (IFN)-γ and Tumor necrosis factor (TNF)-α. The cytokine kit was modified for use with 384-well plates and the samples processed, as described previously [81]. Many of our IL-6 samples showed levels far above the upper limits of our established flow cytometry methods. To compensate, we re-ran the saturated samples using a 50:1 dilution factor over that of the 13-plex plates.

3.2.3 Data processing techniques

Due to limits on amount and timing of blood collections, along with a high temporal variation in cytokine response to IP LPS injections, we pursued simple new techniques that would allow us to better characterize resulting cytokine cascades.

3.2.3.1 Curve fitting

The first method we utilized was that of a smoothing spline interpolation of the 30-minute time points. We ran our 12 recorded time samples through a piecewise polynomial smoothing spline interpolation using Matlab (R2017b, Curve Fitting Toolbox 3.5.6) with a smoothing parameter of $p = 1$ to ensure all sample values were preserved. From these interpolations, we pulled new sets of values that could be defined by minute increments and allow a better estimate of peaks, starting points, and areas under the curves. Other interpolation methods such as Gaussian and Polynomial fitting, and cubic and shape preserving interpolants were tested, but the smoothing spline provided the most accurate estimate of actual cytokine curves.

3.2.3.2 Curve alignment

The second method that we implemented was one of aligning the resulting cytokine curves to a standard point. This is non-trivial as different cytokines display distinct temporal profiles in amplitude and shape, as well as high animal to animal variation. After multiple tests, we settled on using a starting point alignment, defining the starting point for a given cytokine uptake as the point where it reaches 5% of its peak concentration value (or first peak, if there are multiple). This effectively aligned all curves to a standard point in their respective uptake, while minimizing the significance of varying temporal profiles, as can be seen in Figure 3.3. By aligning all cytokine samples to the same starting point, we are also able to better analyze temporal variances in cytokine uptake between subsets.

In the case of late rising cytokines, if a peak had not yet been reached, we utilized the last concentration recorded as the effective peak for alignment purposes.

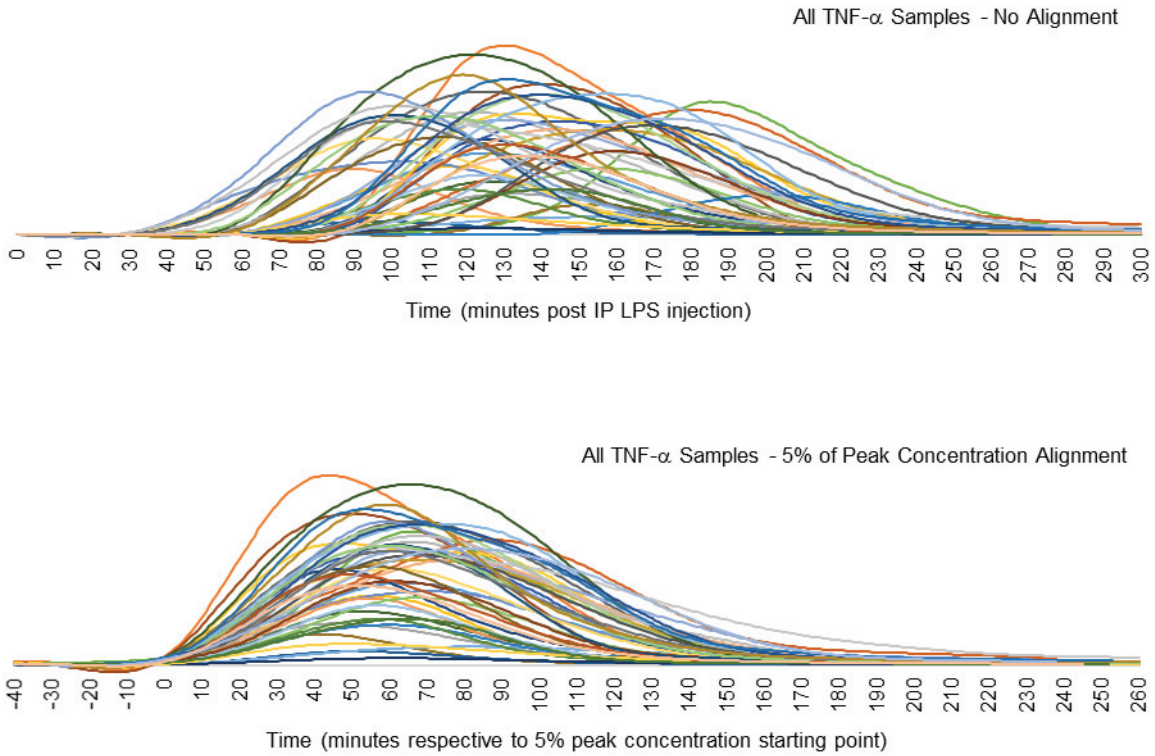

Figure 3.3 Comparison of individual TNF-α temporal profiles from all rats analyzed with LPS administered IP. Top shows unaligned plots with highly variable starting points. Bottom shows the result of aligning them utilizing our 5% of peak concentration technique as a starting point where t = 0 minutes.

3.2.3.3 Verification of curve fitting and alignment

We ran validation tests on four rats to verify that our interpolation method accurately estimated the actual cytokine cascade curves. For these tests we collected blood in 10 or 15-minute increments for a more accurate estimate of the curve, and then split them into 30-minute increment sets as we used in our study. Average variances in calculated starting point between curves were less than three minutes, and average variances in calculated areas under the curve were less than 3%. An example of this validation can be seen in Figure 3.4and quantitative results can be found in Table 3.2.

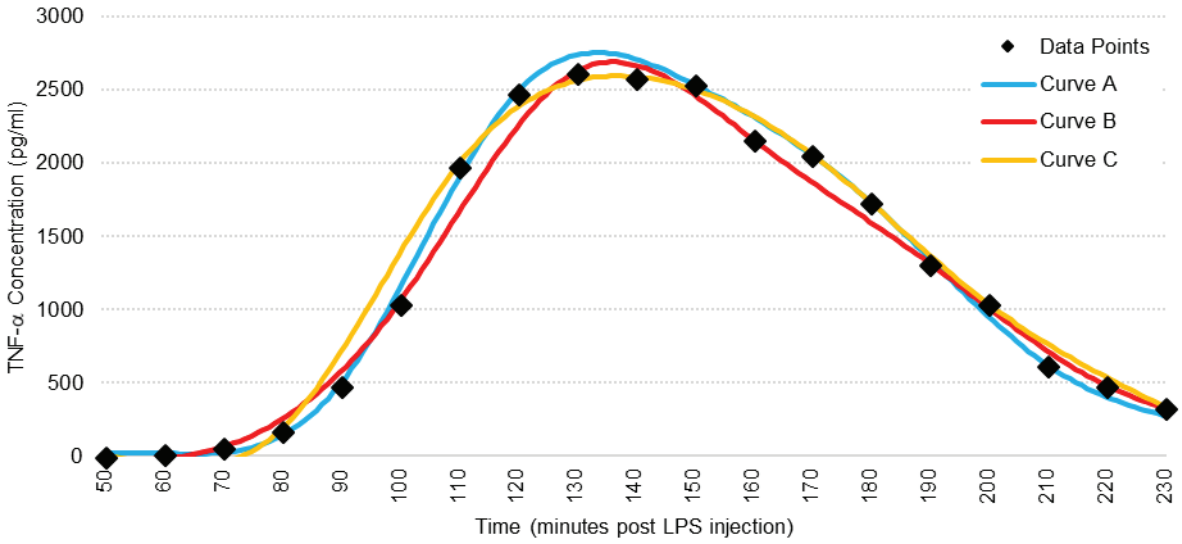

Figure 3.4 Representative figure demonstrating the effectiveness of our curve fitting method on a TNF-α cytokine cascade. Data points were taken every 10 minutes. Curve A utilized only points at 60, 90, 120, 150, 180, and 210 minutes. Curve B utilized only points at 70, 100, 130, 160, 190, and 220 minutes. Curve C utilized only points at 50, 80, 110, 140, 170, 200, and 230 minutes.

Table 3.2. Comparison of Curves Fitted With 30-minute Time Intervals vs with 10 or 15-minute Time Intervals.

	Average Difference of 5% of Max Peak Starting Points	**Average Percent Difference of Area Under Curves**
Cytokine	Minutes ± StDev	Percent Difference ± StDev
IL-10	-4.3 ± 4.1 (n = 11)	-2.6% ± 9.0% (n = 11)
TNF-α	+0.6 ± 2.3 (n = 11)	+0.5% ± 5.2% (n = 11)
GM-CSF	-3.8 ± 4.6 (n = 6)	-2.9% ± 9.7% (n = 6)
IL-17F	No elevations detected*	No elevations detected*
IL-6	-2.6 ± 3.4 (n = 11)	+2.0% ± 14.1% (n = 11)
IL-22	+3.3 ± 7.1 (n = 3)	+2.7% ± 9.7% (n = 3)
IFN-γ	+0.7 ± 2.9 (n = 3)	+1.3% ± 13.1% (n = 3)

**No validation test animals had sufficient levels of IL-17F elevation for analysis.*

3.2.4 Data and statistical analysis

Data analysis was performed after aligning each cytokine curve based on the 5% of peak concentration methods outlined prior. We detected and removed outliers based on interquartile range (IQR), or by biological and surgical anomalies, as appropriate, as outlined in Table 3.3.

Analysis of variance (ANOVA) was performed for both time and concentration data and Welch t-tests were performed to analyze statistical significance due to limited samples sizes in our subsets. We considered confidence intervals of 90% and 95% as statistically significant benchmarks, but we also noted other scientifically significant trends that did not meet these thresholds.

Table 3.3. List of Outliers Omitted from Formal Data Analysis.

Subgroup	Reason for Omission from Results
ACBes	No elevated cytokine levels after IP LPS injection
ACBes	No elevated cytokine levels after IP LPS injection
ACBvx	No cytokine elevation in 5 of 7 cytokines, statistically low outlier in remaining cytokines
HBes	No elevated cytokine levels after IP LPS injection
AGBns	Statistically high outlier in 4 of 7 cytokines, abnormally high levels in remaining cytokines
CVns	Surgical anomaly, animal showed abnormally high heart rates prior to LPS administration and throughout experiment
CVns	Surgical anomaly, animal struggled to breath throughout experiment and had to be revived twice

We considered other methods of comparing cytokine profiles between animals and subgroups such using a distance matrix with quadratic form distance or time warping distance measures, which could present more robust statistical and quantitative differences between samples (not shown). However, we found that these methods did not provide further clarity into the data over those observed when separating the time and concentration variables as we present here. Additionally, separating the variables allowed us to analyze intricacies of actual cytokine uptake profiles in the time domain.

3.3 Results

3.3.1 Temporal cytokine profiles and relationships

3.3.1.1 LPS induced cytokine cascade via IP injection

Through a combined subset analysis of recorded cytokine profiles, we detected significant increases in seven out of the 13 cytokines tested during our 330-minute sampling period post IP injection. IL-10, TNF-α, IL-6, and INF-γ had the largest and most consistent elevations, while GM-CSF, IL-22, and IL-17F showed less consistent elevations over the noise floors of our cytometry methods.

Calculated starting times of each cytokine elevation are illustrated in Figure 3.5. IL-10 is the first to rise at 49.2 (± 2.8 s.e.m, n = 44) minutes post-LPS injection, followed by TNF-α at 72.1 (± 3.5 s.e.m, n = 44) minutes. We then saw an extended delay before elevations occurred in GM-CSF at 116.6 (± 4.3 s.e.m, n = 44) minutes, IL-17F at 125.2 (± 7.0 s.e.m, n = 29) minutes, and then IL-6 at 129.6 (± 3.8 s.e.m, n = 41) minutes post-LPS. Another hour-long delay then occurred before the elevations of IL-22 at 182.6 (± 6.5 s.e.m, n = 26) minutes and IFN-γ at 186.6 (± 3.8 s.e.m, n = 44) minutes post-LPS injection. No statistical differences in recorded starting points were noted between stimulation and control subsets; therefore, all samples were combined for a more robust temporal characterization.

It is important to note that the observed temporal cascade of cytokines had a high overall variability in initial start time, as can be seen in the high standard deviations of elevation starting points in Table 2. However, we discovered that this variability was consistent through each cytokine's elevation in the cascade. For example, if IL-10 of a given rat elevated 10 minutes earlier than our noted average, then all other cytokines would also elevate ~10 minutes earlier than our presented averages.

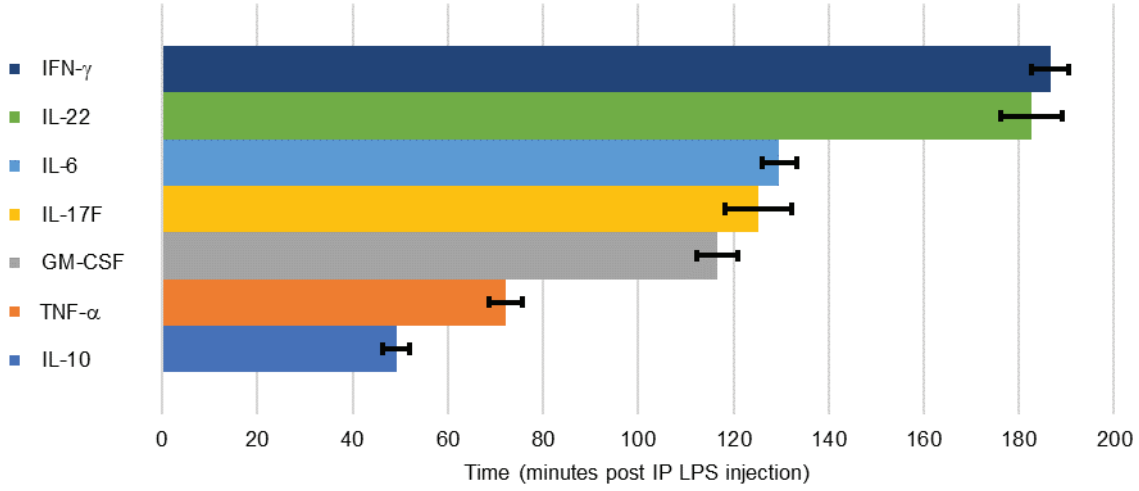

Figure 3.5 Mean starting times of cytokine elevations based on 5% of maximum elevation after IP injection of LPS (5 mg/kg). Error bars, s.e.m.

3.3.1.2 IP to IV comparisons

To compare administration methods, we utilized cytokine data obtained from our previous research, in which we performed IV injections of LPS with an identical experimental time sequence and LPS concentration [80]. In that study, however, we only extended blood collections to 150 minutes post-LPS injection and, therefore, the methods used here could only be applied to IL-10 and TNF-α. We did, however, note general elevations in GM-CFS, IL-6, and IL-22 in the chronic data. Starting point times for both IV and IP data are presented in Table 3.4.

We found there to be significant differences between temporal cytokine responses to LPS when administered IP versus IV. In general, plasma cytokine levels elevated much earlier and had significantly smaller starting point deviations in IV compared to IP. TNF-α levels showed elevations 42 minutes earlier when LPS was injected IV and showed a standard deviation almost three times smaller compared to IP administration. This disparity related to IP administration was expected and emphasizes the need for better analysis method such as those we used in this study. We noted similar earlier elevations of IL-6, GM-CSF, and IL-22 with IV injected LPS. The time of elevations and delays are consistent with those noted in previous literature [66, 68].

Interestingly, IL-10 was a glaring exception to the standard delays noted in the other cytokine elevations. Instead, we found that IL-10 had very similar elevation starting point times and standard deviations when using both IV and IP LPS injection methods. IL-10 levels began elevating at around 50-minutes post LPS injection in both methods, and, while IP LPS injections still produced a larger deviation in elevation start time, it was only 27% larger. We found it compelling to note that this changed the order of cytokine cascades from IL-10 elevating ~23 minutes before TNF-α when using IP LPS injections, to IL-10 elevating ~18 minutes after TNF-α when injecting LPS IV. This signals a distinct physiological mechanism of the body to produce IL-10 in response to LPS, separate from that of TNF-α and other cytokines, and less dependent on endotoxin administration method.

Table 3.4. Comparison of Starting Points for Cytokine Elevations Using IP Injection vs IV Injection Methods.

	Starting Point Based on 5% of Peak Method ± StDev	
Cytokine	Min After IP LPS Challenge (n = 44)	Min After IV LPS Challenge (n = 40)
IL-10	49.2 ± 18.6	48.1 ± 14.6
TNF-α	72.2 ± 22.9	30.3 ±7.9
GM-CSF	116.6 ± 28.4	60 - 90 min (n = 8)*#
IL-17F	125.2 ± 37.5 (n = 29)#	No elevations detected*
IL-6	129.6 ± 24.3 (n = 41)#	60 - 90 min (n = 40)*
IL-22	182.6 ± 33.3 (n = 26)#	90 - 120 min (n = 14)*#
IFN-γ	186.6 ± 25.2	No elevations detected*

**Due to limited time points collected in IV LPS animals (0 – 150 min post LPS injection), specific starting points could not be properly calculated for all cytokines using our methods. Instead, a range of times in which elevations were detected over our noise thresholds, if detected, in the reduced test period is given. #Had reduced number of samples showing calculable cytokine elevations.*

3.3.2 Subdiaphragmatic stimulation

The following sections outline effects on cytokine cascades seen between stimulation of separate subdiaphragmatic branches. We aligned data from each animal so that time "zero" corresponded to its 5% starting point and then plotted the cytokine cascades for the duration that included samples from all animals. We then averaged the effective areas under the curves of samples in

each subset for a quantitative measure of total cytokine concentration, used for statistical analysis. Overall qualitative results are presented in Table 3.5.

Table 3.5. Summary of Cytokine Effects of Subdiaphragmatic Branch Stimulation.

		IL-10	TNF-α	IL-6	IFN-γ	GM-CSF	IL-17F	IL-22
Accessory Celiac Branch	Intact (ACBes)	↑	◆	↓	↑	↑	↑	◆
	Vagotomy (ACBvx)	↑	◆	◆	◆	◆	↓	◆
Anterior Gastric Branch	Intact (AGBes)	↑	◆	↑	↑*	↑	↑	↑
	Vagotomy (AGBvx)	↑	◆	◆	◆	◆	◆	◆
Hepatic Branch	Intact (HBes)	↑*	◆	↓	↑*	◆	↑	↓
	Vagotomy (HBvx)	↑*	↑	↑	↑	↑	↑	↑

Increases (↑)*, decreases* (↓) *and no change* (◆) *are indicated.*
Colors are used for simplified interpretation and are not meant to signify changes as desirable or not.
**Indicates a statistically significant change in cytokine levels compared to sham group.*

3.3.2.1 IL-10 profiles

We found IL-10 concentrations to be highly affected by subdiaphragmatic stimulation of all three branches. IL-10 is primarily an anti-inflammatory cytokine, thus an increase in systemic levels is desirable. Effects can be seen in Figure 3.6 and Figure 3.7.

Stimulation of the accessory celiac branch yielded highly variable IL-10 concentration responses that averaged 146% (ACBes) and 157% (ACBvx) higher than sham controls. Concentrations on the ACBes subset showed a high initial increase in IL-10 levels that dropped at the 90-minute point. However, those with efferent vagotomies showed sustained elevations of IL-10 throughout the tested period. Stimulation of the anterior gastric branch also showed highly variable but clear elevations in IL-10 levels, with both subgroups averaging ~110% increases over sham control levels. The AGBvx subset showed a quicker average uptake with a decrease after ~60 minutes, while the AGBes subset had a much slower but extended uptake, not reaching a max level till after 100 minutes. Hepatic branch stimulation displayed the most consistent results, revealing

statistically significant IL-10 elevations of 73% (HBes) and 75% (HBvx) over that of sham controls ($p<0.05$).

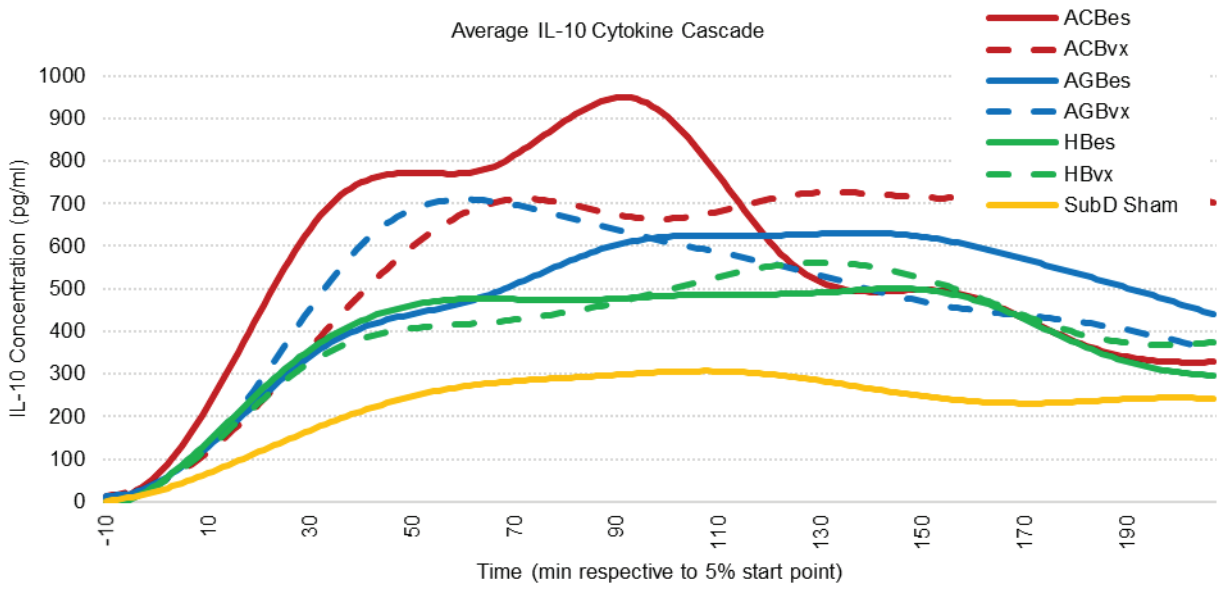

Figure 3.6 Averaged IL-10 cascade responses to IP injection of LPS (5 mg/kg). All samples were curve fitted and aligned at the time they reached 5% of peak concentration, represented as time "zero." Time axis extends to the last time point in which all samples were still recorded.

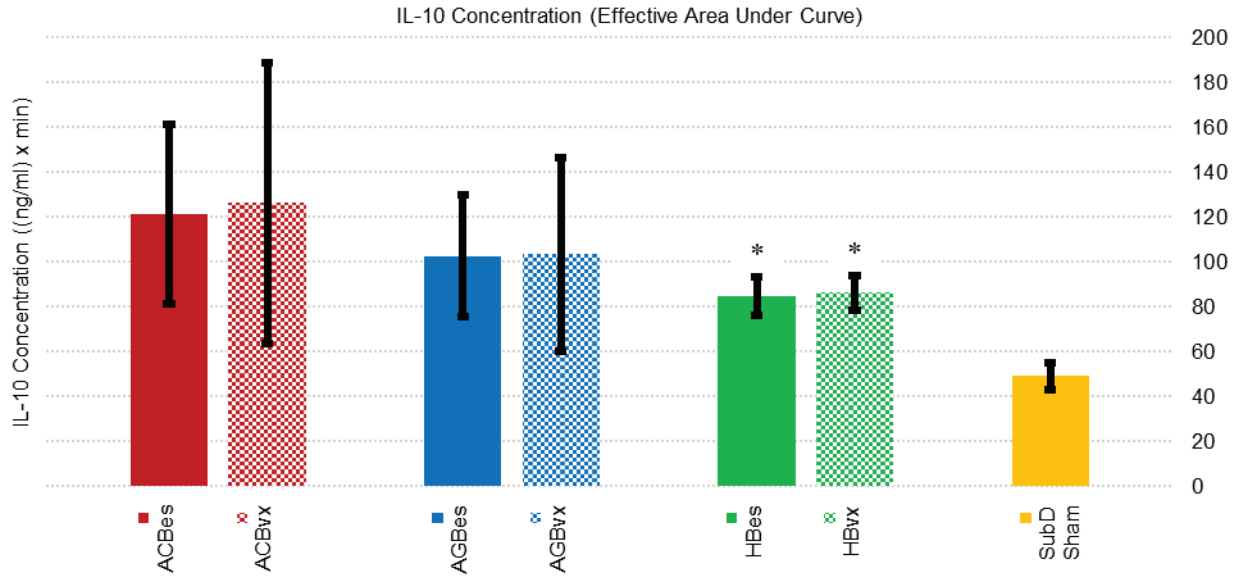

Figure 3.7 Cumulative IL-10 concentration effects of subgroup responses to IP injection of LPS (5 mg/kg). Values represent effective areas under the curve corresponding to time points illustrated in Figure 3.6. Error bars, s.e.m. *P < 0.05 compared to SubD Sham group.

The consistency in overall response between vagotomized and non-vagotomized subsets of all three branches indicated this upturn in IL-10 response to be primarily a vagal afferent effect.

3.3.2.2 IL-6 profiles

Our data showed compelling trends related to IL-6 responses to subdiaphragmatic stimulation. IL-6 is a commonly analyzed pro-inflammatory cytokine, and it is, therefore, beneficial to attenuate its levels in response to an LPS challenge. IL-6 effects can be seen in Figures 7 and 8. Stimulation of the intact accessory celiac branch produced a reduction of ~30% in overall IL-6 levels under that of sham controls while intact hepatic branch stimulation only produced an ~8% reduction. Intact anterior gastric branch stimulation, however, produced increases in IL-6 levels of 90% over sham controls. Of note is that multiple AGBes samples saturated the upper IL-6 limits of our flow cytometry methods, even when diluted. Therefore, the levels in that subgroup were likely even higher than reported here.

Effects on IL-6 changed significantly when an efferent vagotomy was performed. The increases seen from intact gastric branch stimulation were reduced, while the attenuation effects of the celiac and hepatic branch stimulation were reversed. The ACBvx subset instead resulted in increased IL-6 levels of ~18%, while the HBvx subset showed a very large initial increase in IL-6 levels that began to decrease at 80-minutes post starting point. The overall IL-6 increase of HBvx was 56% over that of sham controls.

These results indicated an anti-inflammatory effect related to stimulation of the hepatic and accessory celiac branches in which an intact efferent fiber route is present. A similar, but pro-inflammatory efferent effect was expressed by anterior gastric branch stimulation.

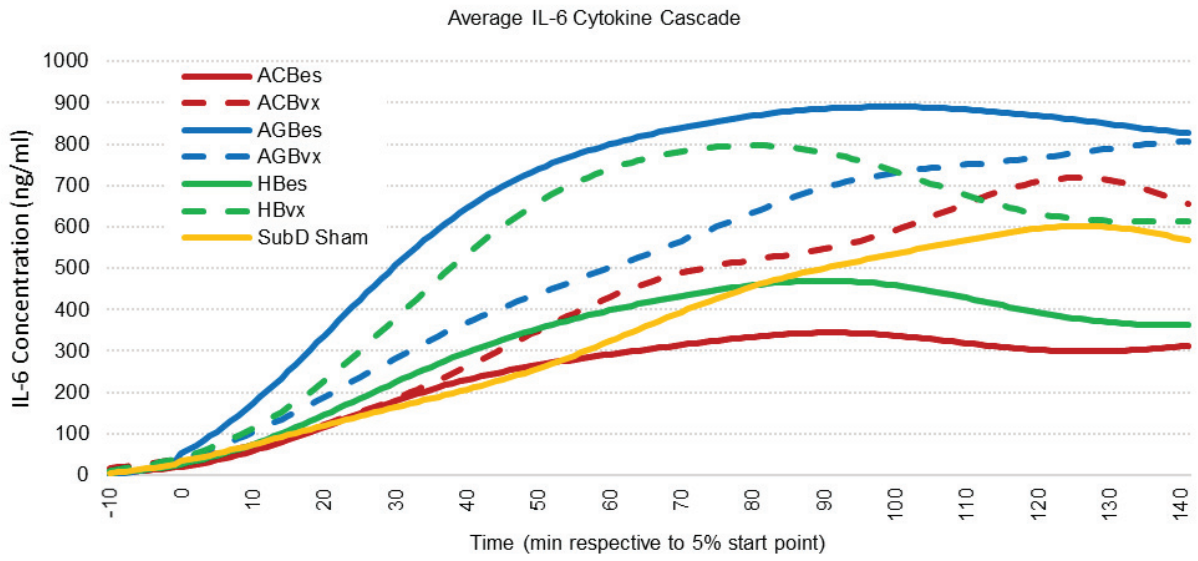

Figure 3.8 Averaged IL-6 cascade responses to IP injection of LPS (5 mg/kg). All samples were curve fitted and aligned at the time they reached 5% of peak concentration, represented as time "zero." Time axis extends to the last time point in which all samples were still recorded.

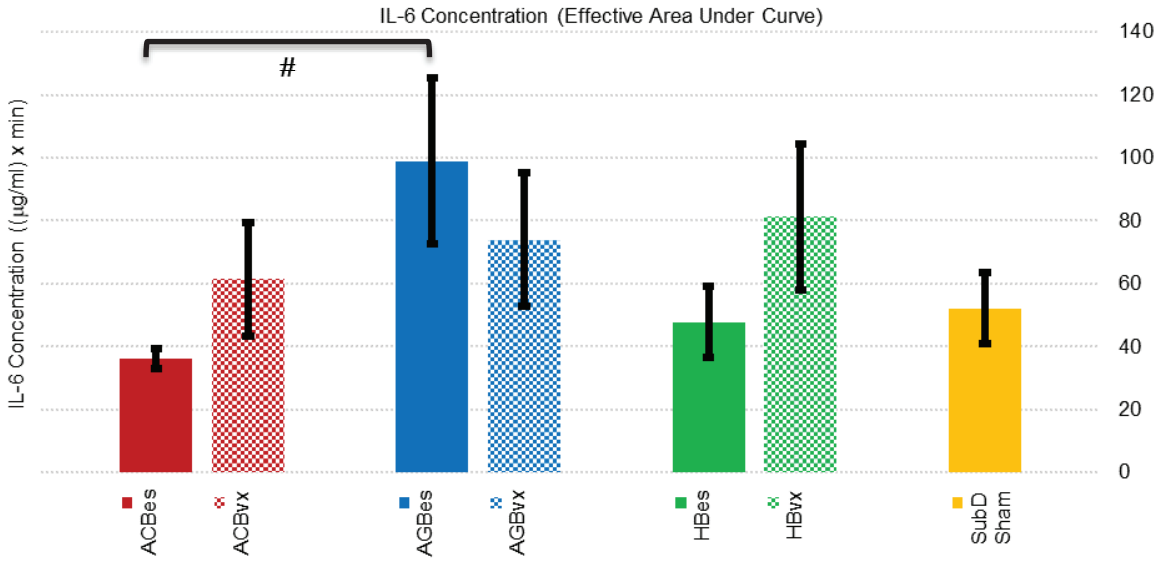

Figure 3.9 Cumulative IL-6 concentration effects of subgroup responses to IP injection of LPS (5 mg/kg). Values represent effective areas under the curve corresponding to time points illustrated in Figure 3.8. Error bars, s.e.m. $^{\#}$ $P < 0.1$ between ACBes and AGBes subgroups.

3.3.2.3 TNF-α profiles

TNF-α is the most commonly analyzed pro-inflammatory cytokine in VNS inflammation studies and attenuation of TNF-α response is desirable. While responses had high variability in all subsets that we sampled and did not show statistically significant trends, we have included it in our results to stay consistent with prior literature and further demonstrate our methods. Effects are illustrated in Figure 3.10 and Figure 3.11.

Stimulation of the intact nerve branches appeared to have little effect on the production of TNF-α. AGBes and HBes subgroups showed responses that were only 17% higher than sham control, while ACBes was nearly identical to sham. Stimulation of the accessory celiac and gastric nerve branches with efferent vagotomies exhibited virtually identical overall TNF-α responses, with the ACBvx subset appearing to have a slightly slower rate of increase. HBvx stimulation showed the largest effect on TNF-α levels, displaying a higher peak concentration and an overall average concentration 42% higher than sham controls.

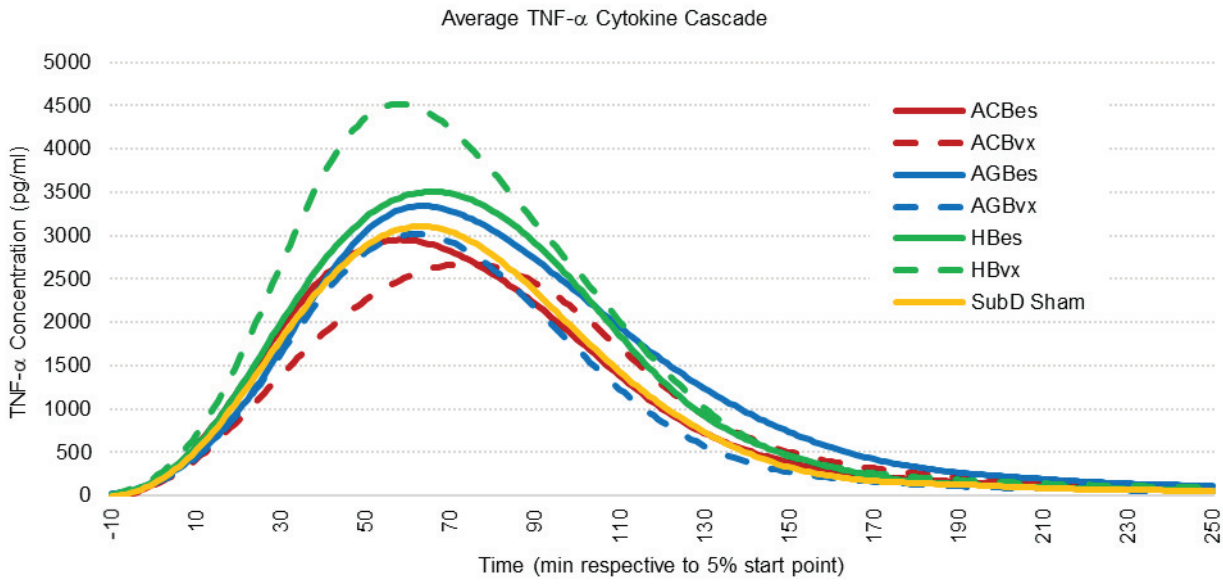

Figure 3.10 Averaged TNF-α cascade responses to IP injection of LPS (5 mg/kg). All samples were curve fitted and aligned at the time they reached 5% of peak concentration, represented as time "zero." Time axis extends to the last time point in which all samples were still recorded.

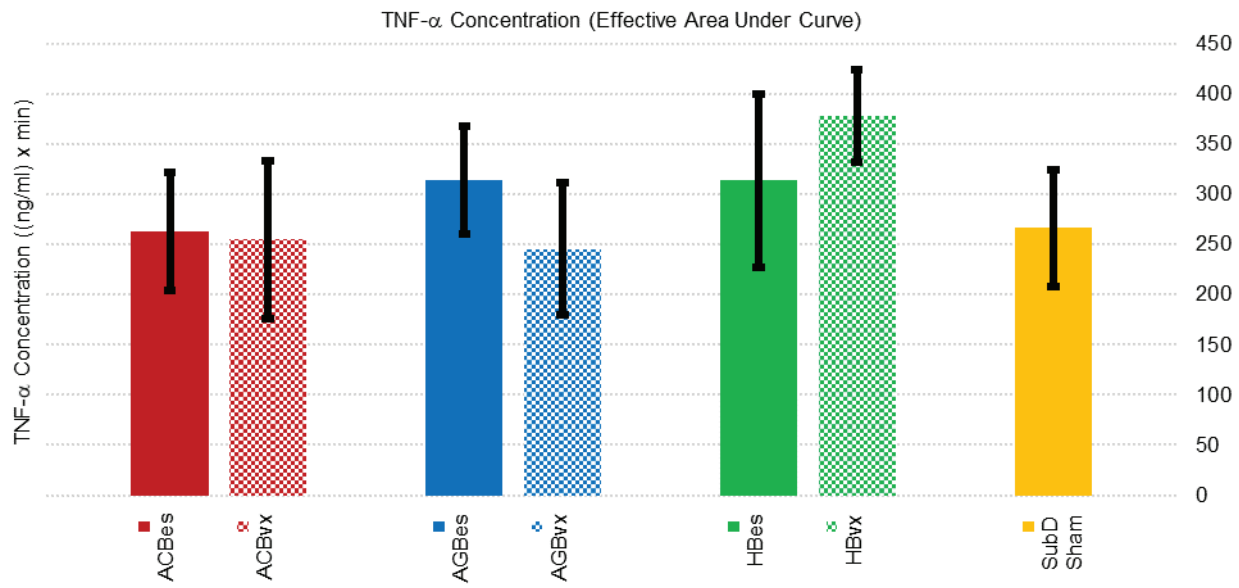

Figure 3.11 Cumulative TNF-α concentration effects of subgroup responses to IP injection of LPS (5 mg/kg). Values represent effective areas under the curve corresponding to time points illustrated in Figure 3.10. Error bars, s.e.m.

3.3.2.4 IFN-γ profiles

We observed very distinct roles of several stimulation subgroups in the proliferation of IFN-γ levels in response to IP LPS challenge. IFN-γ is a less commonly analyzed pro-inflammatory cytokine that is linked to exacerbation of numerous disorders such as rheumatoid arthritis and multiple sclerosis [85]. It has also been reported that IFN-γ increases the lethality of LPS and TNF-α in mice, and correlates to increased levels of IL-6 when combined with TNF-α [86]. Due to a lack of literature outlining VNS effects on IFN-γ levels, we believed it pertinent to present our data. Effects are illustrated in Figure 3.12 and Figure 3.13.

Though highly variable, we found that stimulation of all three intact subdiaphragmatic branches caused escalations of IFN-γ responses to the LPS over that of sham controls. The ACBes subset showed a 3.3x increase, while AGBes subset showed 3.7x increase, and the HBes had the highest increase at almost 6x the average level of sham controls. Meanwhile, we found that efferent vagotomies of the accessory celiac and gastric nerve branches prevented this increase. Only the hepatic afferent stimulation, by itself, significantly boosted systematic IFN-γ levels.

Our data points towards IFN-γ regulation being a predominantly efferent fiber effect, with hepatic afferents also playing a decided role.

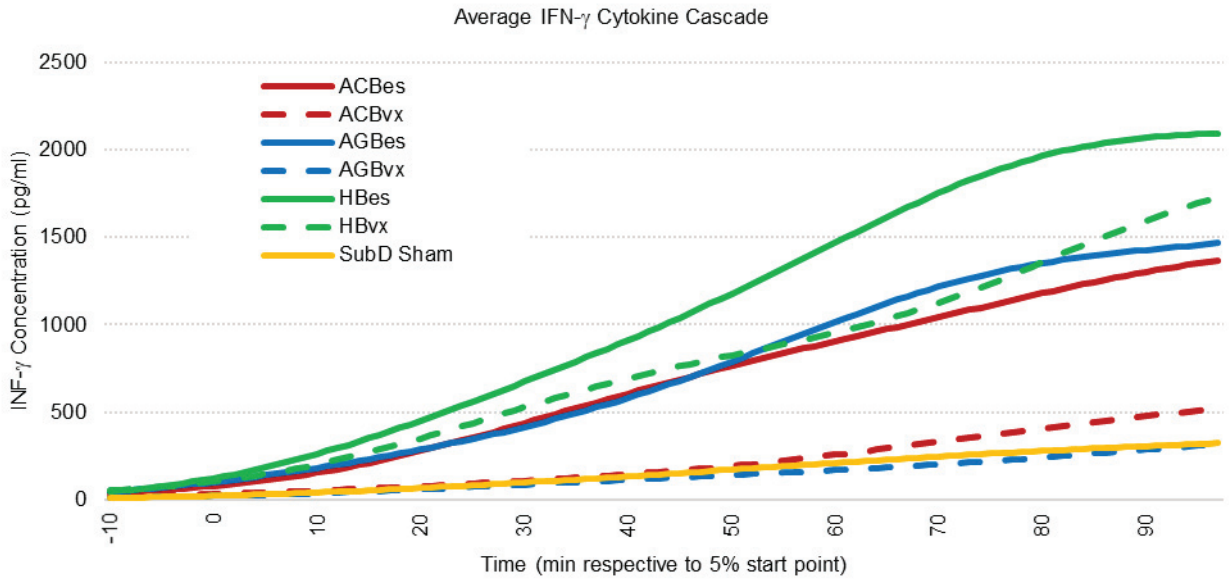

Figure 3.12 Averaged IFN-γ cascade responses to IP injection of LPS (5 mg/kg). All samples were curve fitted and aligned at the time they reached 5% of peak concentration, represented as time "zero." Time axis extends to the last time point in which all samples were still recorded.

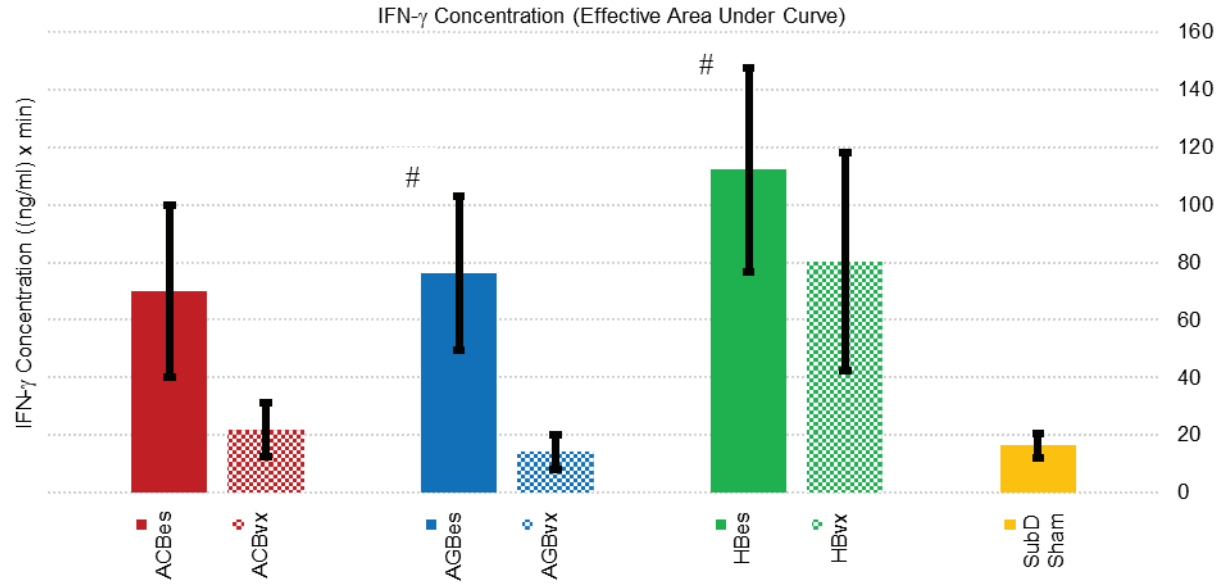

Figure 3.13 Cumulative IFN-γ concentration effects of subgroup responses to IP injection of LPS (5 mg/kg). Values represent effective areas under the curve corresponding to time points illustrated in Figure 3.12. Error bars, s.e.m. $^{\#}P < 0.1$ compared to SubD Sham group.

3.3.2.5 Remaining cytokine profiles

GM-CSF is typically linked to allergic inflammation, but presents with a wide range of pathologies [87], while IL-17F acts as a pro-inflammatory cytokine often with relation to lung inflammation [88] and IL-22 has been shown to play both a positive and negative role in different immune disorders [89]. Thereby, regulation of any or all three of these specific cytokines could yield new therapy options for inflammatory diseases.

Statistical quantitative analysis of elevations for these cytokines was unreasonable due to respectively low concentration levels and inconsistent rises. Instead, we did a simple fractional analysis of samples that rose above a nominal noise threshold for our flow cytometry methods that is shown in Table 3.6. In doing so, we found qualitative trends of note between subgroups.

Table 3.6. Fractional Analysis of Cytokine Cascades Over Given Threshold Concentrations.

Cytokine	**GM-CSF**	**IL-17F**	**IL-22**
Threshold	80 pg/ml	100 pg/ml	100 pg/ml
Subset			
ACBes	3/5	3/5	2/5
ACBvx	2/4	0/4	2/4
AGBes	3/5	3/5	3/5
AGBvx	2/4	1/4	1/4
HBes	1/4	4/4	0/4
HBvx	3/5	4/5	4/5
SubD Sham	2/8	3/8	1/8

Fractions are the number of animals that had cytokine cascade elevations above the given threshold.
Colors are used for simplified interpretation and are not meant to signify results as desirable or not. Blue cells are subsets that had over half its samples rise above threshold. Yellow cells are subsets that had half or less of its samples rise above threshold. Red cells are subsets in which none if its samples rose above threshold.

Accessory celiac branch stimulation was consistently effective at modulating both GM-CSF and IL-17F, but the consistency of elevations was reduced when the branch was given an efferent vagotomy. Simulation of the intact gastric branch also showed increased upregulation of all three cytokines, while an efferent vagotomy to the branch prevented these increases. The hepatic

branch showed the most effective regulatory ability. Stimulation of the intact hepatic branch (HBes subgroup) was effective at elevating IL-17F levels, but not GM-CSF or IL-22. However, when an efferent hepatic vagotomy (HBvx subgroup) was performed, stimulation showed increased frequency of elevations in all three cytokines.

3.3.2.6 Cervical electrical stimulation

Electrical stimulation of the left cervical vagus nerve was applied to contrast with subdiaphragmatic stimulation results. We did not, however, note any significant correlations between these subgroups and the previously analyzed subdiaphragmatic subgroups.

Cervical VNS showed variable levels of overall cytokine modulation in response to an IP LPS challenge as can be seen in Figure 3.14. There appeared to be varying attenuation effects of cervical stimulation on levels of TNF-α, IL-10, and IFN-γ in comparison to non-stimulated animals, while there were virtually no changes in IL-6 levels.

Of interesting note is that there seemed to be artificially lower levels of IL-6, IL-10, and IFN-γ in all cervical subgroups compared to the SubD Sham animals. This could indicate a local inflammatory effect of the subdiaphragmatic surgery itself.

Table 3.7 shows us very little nominal difference in the responses of GM-CSF, IL-22, and IL-17F, between CVes and CVns subsets.

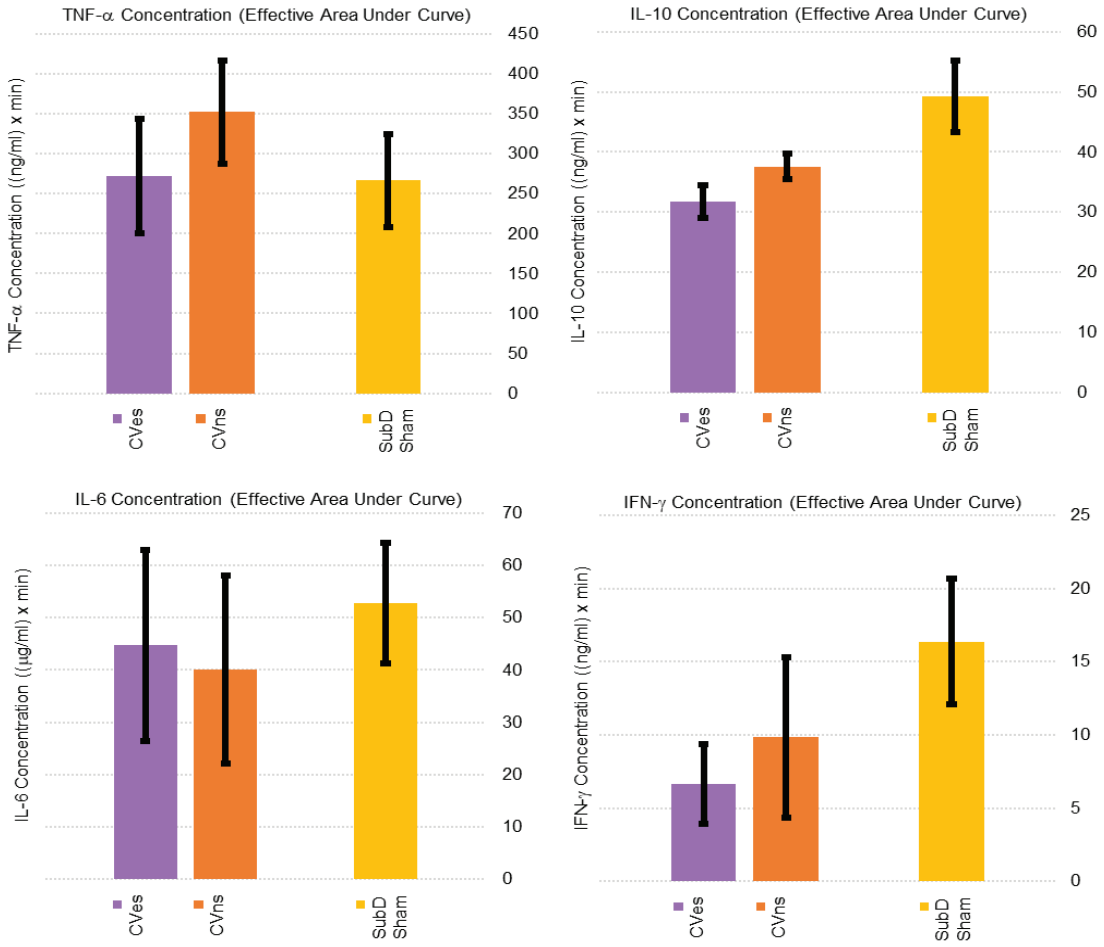

Figure 3.14 Cumulative cytokine concentration effects of cervical subgroup responses to IP injection of LPS (5 mg/kg). SubD Sham group is included for comparison.

Table 3.7. Fractional Analysis of Cytokine Cascades Over Given Threshold Concentrations for Cervical Subsets.

Cytokine	**GM-CSF**	**IL-17F**	**IL-22**
Threshold	80 pg/ml	100 pg/ml	100 pg/ml
Subset			
CVes	1/5	1/5	1/5
CVns	1/3	1/3	2/3

Fractions are the number of animals that had cytokine cascade elevations above the given threshold.

Colors are used for simplified interpretation and are not meant to signify results as desirable or not. Blue cells are subsets that had over half its samples rise above threshold. Yellow cells are subsets that had half or less of its samples rise above threshold.

3.4 Discussion

3.4.1 Temporal IP cytokine cascade interpretation

Through these studies, we determined the temporal cascade of cytokines in response to a 5 mg/kg IP injection of LPS. To our knowledge, no previous studies have taken as consistent and frequent time points, for as long a test period, or have incorporated as diverse a cytokine makeup.

For IP LPS, IL-10 is the first cytokine to surface, followed by TNF-α, GM-CSF, IL-17F, IL-6, IL-22 and finally IFN-γ. TNF-α has been characterized as one of the first cytokines to surface in several other studies [90-92] and although not believed to be the sole initiator of other cytokines, certainly affects the concentration and duration of presence of other cytokines [92]. The production of IL-10 is likely independent of the cascade initiated by TNF-α [91, 92], which could explain its early appearance as well as its similar timing in IP and IV LPS administration. Additionally, it is notable that the timing of the cytokine cascade is dependent on LPS concentration administered [68], but was unaffected by stimulation in our study. Knowing the cascade of cytokines could help to specifically target the attenuation of specific cytokines during *in vivo* studies. For example, to attenuate IFN-γ, perhaps electrical stimulation should be applied later compared to aiming for attenuation of TNF-α.

We also analyzed cross-relationships between cytokine levels. We found a rough inverse correlation between TNF-α and IL-10 levels (not shown). When IL-10 had a large spike early in the cytokine cascade, TNF-α levels were notably lower. This inverse relationship has been previously reported [93].

In addition, we compared IP to IV LPS administration, finding much greater variability with IP administration. This was expected and has been previously reported [72, 73]. Because of this variability, it was important that we collected blood at sufficient time points to understand the full curve for an individual animal and adjust the data accordingly. Our curve fitting and temporal shifting methods can be used by other researchers to account for variable IP absorption. We urge researchers to collect data at several times, rather than an individual time point,

especially when using IP administration of endotoxin. Studies that have evaluated cytokine concentrations at only one time point may continue to use IV LPS to reduce the variability in their data; however, we have also demonstrated a temporal variation in IV LPS cytokine response that is significantly smaller but still present, and we have reason to believe that the biological mechanisms are different between the two administration types.

Typically, infections are not immediately present in the bloodstream and must be identified in the intraperitoneal space first [94]. This makes IP administration a more clinically and physiologically relevant animal model. Perhaps the most difficult aspect of utilizing an IP injection of LPS is timing of treatment. With a large variability of uptake time, it becomes very hard to match a stimulation of the nerve to the exact start time of uptake. This should not dissuade researchers, however, as there is little evidence to suggest that exact timing of a therapy with relation to uptake time has had a significant impact on the effectiveness of treatment. In previous literature, we found multiple studies that have effectively used different stimulation techniques, timing, and durations (even continuous stimulation in some studies) to modulate inflammatory responses [6, 11, 69, 95, 96]. We surmise that treatment timing with relation to injection time is more important that the relation to when uptake starts. Additionally, this variability will exist clinically and serves to better model the variable state of the body when the treatment is given to a patient. We urge researchers to select the more physiologically relevant model with thought to future clinical relevance rather than selecting a less relevant model that may result in cleaner, easier to analyze data.

There is certainly a myriad of experimental aspects that could be analyzed in an inflammatory study such as treatment type, duration, and frequency, endotoxin type, injection method and location, as well as tissue or serum sample type and location. All of these have merit and could significantly influence the effectiveness of said treatment. Given limited resources, we must attempt to look at the most pertinent physiology and narrow in on those aspects and corresponding methods. Certainly, a dedicated study comparing IP to IV methods would be ideal. Notably, our IV data came from a chronic cuffing study in which the rats had no anesthesia during LPS challenge [80]. While it is very possible that variability between the set-ups could have affected cytokine response timing, we believe it to have been minimal. Our data and

analyses are supported by Kakizaki et al [66] who's IV versus IP comparison showed similar delays in TNF-α and IL-6 responses, as well as more defined average peaks utilizing IV versus IP, which would indicate a higher variability in the timing of IP responses.

3.4.2 Inflammation regulation via subdiaphragmatic stimulation

Based on our results, the most suitable nerve branch and fibers to stimulate can be deciphered based on the need to increase or decrease each of the studied cytokines. Unfortunately, the results of stimulation vary for each cytokine. For example, to increase IL-10 levels, the intact HB can be stimulated. This will also cause to varying degrees: a decrease in IL-6 and IL-22, an increase in IFN-γ and IL-17F, and no change in TNF-α or GM-CSF levels. Combining stimulation and/or vagotomies of the three branches may yield ideal results. This would allow for the individualization of therapy based on the desired cytokine results.

HB stimulation and ACB stimulation had the largest overall effect on cytokine production. While the ACB causes changes, supporting claims made in previous work upon which our theory was founded [78], the HB induces more pronounced responses in some cases. This could be due to the larger amount of sensory fibers present in the HB (73%) compared to the ACB (69%). The AGB has only 48% sensory fibers and showed the least modulatory effects, encouraging the idea that there is a correlation between increased sensory fiber activation and immunomodulation [97]. When taking these interrelations into consideration, this data suggests that there is not a singular subdiaphragmatic branch that will induce a change in all cytokine levels. These outcomes thereby allude to the likeliness that there is not a solitary mechanism of action regulating cytokines, and similar effects can be achieved by stimulating multiple combinations of nerve branches and fibers.

Afferent fibers comprise about 90% of vagal gut innervation, and a previous study by Bratton et al. implied that the connection between the vagus and spleen was indirect [70, 98], supporting our results indicating that afferent fibers had a large influence on some cytokine levels, such as IL-10. Mapping has been done that shows there is a difference in termination patterns between gastric, celiac, and hepatic afferent axons in the medulla. There are two major distribution

patterns that emerge: one due to AGB terminals and the other due to ACB and HB terminals [99]. This mapping, in conjunction with our findings, suggests that the region and density at which subdiaphragmatic afferent axon terminals occur in the medulla influences the body's inflammatory response. It is possible that there are specific areas of the area postrema (AP) that connect to the DMN of the vagus directly, or more likely, indirectly via the NTS. If these regions included hepatic or celiac branch terminals, stimulation of this branch would lead to activation of the DMN, thus the efferent vagal fibers that are initiated there [100]. More recent work has shown that these fibers pass information to the NTS, which relays signals to the DMN. Additionally, the NTS does not fire spontaneously, meaning that any of its transmitted information is due to afferent stimulation [101]. The proximity of ACB and HB axon terminals in the AP and the anti-inflammatory effects of each, lend to the idea that there is a connection between that region and an area of the DMN that activates efferent fibers.

Efferent vagal fibers could be activated due to the indirect path previously described or due to direct electrical stimulation. If fired indirectly, the various areas that the efferent fibers originate from would play a role, and, therefore, the areas of the AP and NTS that receive information from subdiaphragmatic afferents would be directly connected to the respective areas of the DMN. Thus, afferent hepatic activation would lead directly to activation of hepatic efferents in the DMN, and the areas that these efferent fibers innervate, versus that of the other branches, could be responsible for differences in modulation between branches. Anatomical mapping by Berthoud et al. has shown that while the HB innervates the liver, most of its axons supply the pylorus, antrum and pancreas. Meanwhile, the ACB innervates the celiac and superior mesentery ganglia, continuing to the pancreas, small and large intestines, and mesenteric branches [2]. These branches follow unique pathways except for their connections to the pancreas, possibly linking it as an important structure in immune function. It is also possible that these efferent fibers feed into different lymphatic areas along the intestine that regulate T cell production, thus immune function. The unique regions that the HB innervate could have different densities of T cells to regulate, explaining why the HB sometimes has the strongest effect. Further research is needed to confirm the efferent pathway of the ACB and HB, allowing for a deeper understanding of the responsibility that these branches play.

Of important note in our study is that four out of 55 rats showed little or no response in any cytokine levels after IP LPS administration. While we thought it most likely that this was a biological anomaly in these animals similar to those experienced by Lenczowski et al [72, 73], it is interesting to note that our rate of unresponsive animals was significantly less than that experienced by them. It is curious that their last data point collected was at 90 minutes post IP LPS injection, a time point in which ~20% of our animals had yet to show significant elevations of IL-6, the cytokine of interest in the Lenczowski studies. We hypothesize that had they collected samples at a later time-point, that they would have seen IL-6 elevations in a larger number of their animals. It is also interesting to note that none of our nonresponsive animals were in sham subgroups and all four were in stimulation subgroups that showed significant amounts of cytokine modulation in responsive rats (two ACBes, one ACBvx, and one HBes). Therefore, while the attenuation effect was dramatic in these four animals and we considered them outliers for statistical purposes, it is possible that the stimulation applied to these animals did indeed play some part in the absence of inflammatory response.

With regards to our lacking effects of subdiaphragmatic stimulation on TNF-α levels in any subset, we believe there to be two probable explanations. First, in successful studies in which TNF-α was attenuated with cervical stimulation, it was done so by performing an afferent vagotomy before stimulation or applying a virtual vagotomy using electrical stimulation to block afferent fibers, thereby specifically stimulating only the efferent fibers [15, 19, 69, 70]. When afferent fibers were still present, their results were variable and did not show significant reductions. Thereby, it is possible we saw the same effect in the subdiaphragmatic branches. While stimulating efferent fibers, we were also stimulating the more predominant afferent fibers of the branches and created an offsetting parasympathetic effect that prevented reductions of TNF-α levels. It is also plausible that our 100 uA pulses produced suboptimal stimulation and were only able to successfully stimulate afferent fibers in those nerve branches. It is possible that a larger stimulation profile would have produced better attenuation by effectively stimulating the efferent fibers. The scope of this study did not allow for multiple stimulation parameters to be tested, but such a study would be very beneficial to the VNS community in the future.

Selective cervical efferent stimulation used in previous studies is also a challenge to implement clinically. Surgical vagotomy causes vitamin deficiencies [102] and virtual vagotomy has not been proven in a chronic animal model or clinically to the best of our knowledge. In addition, these solutions do not account for the vagus nerve's innervation of a vast number of organs, causing potential inherent side effects if stimulated at the cervical level. Stimulation of the anterior subdiaphragmatic branches of the left vagus nerve more selectively targets the organs involved in cytokine production, and thus could reduce side effects compared to cervical VNS.

Chronic cuffing of the cervical vagus nerve has caused efferent fiber damage in rats, affecting the ability for cervical VNS to attenuate the inflammatory response [80]. However, it is possible that since certain modulatory effects of the subdiaphragmatic branches that we observed are due primarily to afferent fibers, that even if the efferent fibers were damaged, some anti-inflammatory effects might still be seen. The consequences of subdiaphragmatic vagotomy should be investigated to see if it is a clinically viable option to aid in selectivity of therapy. Alternative methods could also be used to stimulate the subdiaphragmatic branches, such as focused ultrasound, which was recently used to modulate TNF-α by activating the left cervical vagus nerve [81].

3.5 Summary/Impact

We have outlined new methods for interpreting cytokine production and addressing the variability in response to IP LPS, which we argue is a more suitable animal model for inflammatory diseases than IV injections. IP and IV administration of LPS induces different timing in the cytokine cascade for all cytokines observed except IL-10, which seems to be produced and modulated independently of other cytokines.

We also presented a robust analysis of the effects of subdiaphragmatic stimulation on cytokine response to IP LPS. Hepatic and accessory celiac branch stimulation produced the greatest effects on cytokine production following the administration of IP LPS. With the possibility of combining stimulation of various subdiaphragmatic branches and more selectively stimulating structures involved in the inflammatory reflex, use of the subdiaphragmatic branches of the left

vagus nerve shows promise in the regulation of cytokines as well as further defining the inflammatory reflex. Further studies should be performed to characterize the interactions between the AGB, ACB, and HB of the vagus nerve.

4. AIM 3: STUDY OF CHRONIC NERVE CUFFING

4.1 Motivation

The initial goal of our chronic cuffing work was to study inflammatory cytokine effects of VNS in a chronic rodent model. Similar to Aim 2, we wanted to determine stimulation protocols that could control inflammation. Rather than stimulating subdiaphragmatic branches, we were to vagotomize them instead and perform cervical VNS with different subdiaphragmatic branches left intact. A retrograde tracer analysis was part of the experiment to verify the effectiveness of subdiaphragmatic vagotomies to be performed. However, after many attempts at successful implantation, we found that the tracer was being severely suppressed in virtually all subjects from all nerve branches, indicating unexpected and more severe damage than selective vagotomies should produce.

While unexpected, this tracer suppression opened a new and perhaps more important study on the effects of chronic nerve cuffing itself. I continued with analysis in this direction and produced the work that follows.

Material in sections 4.1.1 - 4.4 come directly from my paper titled “Chronic Cuffing of Cervical Vagus Nerve Inhibits Efferent Fiber Integrity in Rat Model,” and its supplemental data, accepted by the Journal of Neural Engineering in 2017. It should be noted that this study took place prior to that in Aim 2, and thus certain parts may be repetitive of those in that study or were updated and possibly improved for that study. This study also used techniques and equipment developed in Aim 1 and therefore there may be some repetition in material from there as well. Updates to data have been made as appropriate and are marked as such throughout this section.

Section 4.5 has been added to outline a small follow up study performed by Kelsey Wasilczuk, supported by myself, to look at related effects of chronically cuffing a subdiaphragmatic nerve branch.

4.1.1 Chronic cuffing study introduction

In this study, we utilized novel combinations of verification techniques on 53 rats to analyze multiple dynamic effects of VNS on the physiology of the nerve. These included retrograde tracer analysis using Fluorogold (FG), electrophysiological responses to stimulation, visual and histological analyses of nerve samples, and plasma analysis of cytokine levels (animal names and results can be found in Appendix A). As a result, we discovered complete suppression of FG transport to the DMN of the medulla in animals that had vagus nerves cuffed for periods ranging from 13-71 days in length, and found insignificant modulation of inflammatory cytokines when applying VNS therapy, as compared to corresponding acute subjects [103]. In addition, we performed gastric emptying tests using MRI on six chronically implanted rats (details in Appendix B) to compare with equivalent acute testing in a parallel study. Results revealed attenuated effects on gastric emptying rates when the vagus nerve was chronically cuffed.

Our resulting hypothesis, that the rat model may be unsuited for chronic nerve stimulation studies, is compelling and pertinent to the entire VNS community. We revealed evident flaws related to chronic cuffing of the vagus nerve in a rat model, as it creates previously unstudied physiological effects that suppress the fluorogold transport mechanism, and ostensibly, act to suppress the anti-inflammatory and other effects of VNS. This hypothesis stands despite the outward appearance and functionality of a healthy nerve using traditional methods of integrity verification (visual, histological, electrophysiological).

Given the scarcity of related literature to verify or disprove our findings, we feel that while our results do not invalidate the findings of past chronic studies in rats due to differences in methods used, they do call into question the integrity of facets of some data. If indeed some undetected aspect of the efferent (and possibly afferent) fiber physiological operation was affected by cuffing of the peripheral nerve, then the resulting biological effects of the subject matter could also have been attenuated or completely altered by the compromised nerve fibers.

4.1.2 Comparative review of chronic cuff VNS studies in rats

A comparative literature review of 17 recent studies (details in Appendix C and D) employing chronic methods of VNS varied widely in application but revealed few common methods to contrast our experiment.

Most of the chronic VNS studies reviewed centered on biological effects related primarily to brain activity, such as seizures (epilepsy), depression, and memory, and primarily due to stimulation of afferent fibers of the vagus nerve [17, 104-111]. While there are likely secondary and indirect effects to the overall autonomic peripheral nervous system response due to efferent fiber activation from VNS, evidence suggests that VNS affects the brain primarily through afferent fiber activation and not through indirect efferent effects [13]. Studies that focused on primarily efferent targets of VNS were rare, with four groups specifically studying cardiac effects [96, 112-114]. Only Meregnani et al [95] centered on the topic of inflammation in the gastric region of the body as we sought to.

None of the reviewed literature implemented our retrograde tracer (Fluorogold) analysis into their studies of chronic nerve stimulation. We argue this to be a definitive and critical evaluative measure of nerve functionality. To our knowledge, we are the first to use it in a VNS study.

Merely two of the reviewed papers included a mechanism to directly record compound nerve action potentials (CNAPs) from the nerve [16, 115]. Other groups relied instead on physiological indicators such as changes in measured heart rate [96, 111, 112] to verify that VNS was operating as intended or having an effect.

While histological analysis is common in developmental studies of new cuff designs [116-118], none of the reviewed studies published a histological analysis of the effect of their cuffs on the nerve during implantation. With such a dependence on the cuff/nerve interface for VNS studies and the multiple variables involved in a chronic cuff implantation including materials used, surgical techniques, and animal variances just to name a few, we felt this was a necessary analysis to include.

Three groups performed histochemical analyses of inflammatory cytokines. Chunchai et al [108] measured TNF-α levels in brain and plasma samples, while Chapleau et al [96] measured multiple cytokines in serum only and Meregnani et al [95] measured various cytokine levels directly from colon tissue samples. In comparison, we tested blood (plasma) samples on 13 different cytokine variants.

4.2 Methods

4.2.1 Experimental timing

The order and timing of multiple procedures involved in this chronic study are outlined in Figure 4.1. All parts of this experiment were organized and run to minimize unplanned variations to timing and techniques.

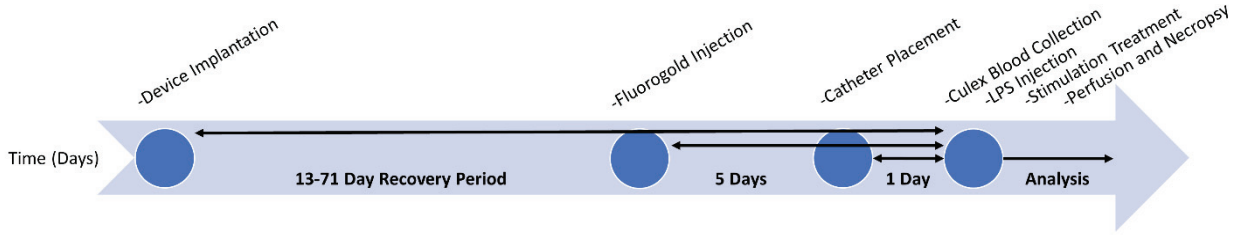

Figure 4.1 Time flow diagram of our chronic experimental design. Chart outlines the overall long-term flow of our experiment over the course of weeks, beginning with surgical implantation and flowing though data analysis.

4.2.2 Materials

4.2.2.1 Nerve cuffs

Our standard cuff electrodes were custom made from 1x7x0.001” (75 μm outer diameter) braided Platinum Iridium (Pt/Ir) wire (Fort Wayne Metals; Fort Wayne, IN) threaded into a medical grade silicone tubing substrate (0.03” inner diameter; A-M Systems; Carlsborg, WA). A single strand of the wire was threaded through the inside of the cuff, following its contour, to create an electrode that would surround over 70% of the nerve diameter when implanted. The cranial electrode of the stimulation cuff required a larger exposed surface area due to its use as

the grounding place for our system's device electronics. To accomplish this, we threaded the Pt/Ir wire around the inner and outer contours of the cuff six times (shown in Figure 4.2) effectively increasing the electrode surface area by 15x. The lead tubing was fastened and sealed to the cuff with a fast curing silicone adhesive (Med2-4213; NuSil; Carpinteria, CA). The cuffs were 3 mm in length with Pt/Ir electrodes spaced approximately 1mm apart.

Figure 4.2 Photograph showing a standard stimulation cuff used in our studies. Threaded wire electrode was used as a grounding reference for stimulation and oriented cranially.

In addition to our standard cuff design, we attempted to use three other electrode varieties:

- CorTec tunnel cuff with PtIr electrodes. Cuff was 3 mm in length with a 0.6 mm inner diameter. Stimulation cuff only was implanted on animal eRx118. (Cat. No. 1041.2008.01; CorTec; Freiburg, Germany)
- Shape memory polymer cuff fabricated by University of Texas – Dallas as presented in Figure 2g of Ware et al[61]. Our variant had only 2 electrode traces and only the stimulation cuff was implanted on animal eRx111.
- Experimental thin film cuffs using two gold traces and pads on a 12 μm thick parylene substrate. The 4.7 mm long and 2.3 mm wide cuff electrodes were gently wrapped around the isolated vagus nerve to create ~1.5 mm diameter cuffs with separate 11 mm tabs wrapped around the

cuffed nerve and carotid artery for anchoring. Excess tab material was cut away and Kwik-Sil was used to fasten the interface in place. Record and stimulation cuffs were implanted on eRx119. The authors can be contacted for more details on this cuff design.

4.2.2.2 Devices/Headcaps

The stimulation and recording for most of our chronic rat tests were done using the Bionode; a multipurpose implantable platform designed for physiological studies [119]. For this study, the Bionode was typically implemented with a single stimulation and a single record channel, each with a cuff electrode attached. The Bionode can produce bi-phasic constant current stimulation profiles ranging from 50 μA to 1.1 mA in amplitude and 50 μs to 1 ms in pulse width through the stimulation cuff electrodes. The recording electrodes get fed through a dual stage differential amplifier. The Bionode's interface allowed real-time recording and control of stimulations to the implanted device, using a custom software platform.

Instead of using a fully implanted Bionode, we tested some of our animals with a tethered setup using a cranial headcap. This was done to vary the surgical method of some animals and verify our findings. For these animals, the headcaps were pre-built by attaching our nerve cuffs to individual pins (PlasticsOne; Roanoke, VA) and affixing those pins to head-cap pedestals (Plastics One) with dental cement. We also used headcaps with single implanted stimulation cuffs for chronic gastric emptying experiments.

4.2.3 Surgical methods

4.2.3.1 General animal preparation

All surgical methods and animal handling are approved by the Institutional Animal Care and Use Committee (IACUC). Male Sprague Dawley rats weighing between 175 – 199 g were used for data collection and housed under standard conditions. Prior to surgery, animals were given ad-libitum access to food and water. A pre-operative analgesic, butorphanol (0.5-2 mg/kg, subcutaneous) or buprenorphine (0.05-0.1 mg/kg, subcutaneous), were administered immediately prior to surgery and 4-6 doses thereafter for 48 hours post-operative. All surgical equipment was

sterilized and the animals underwent standard aseptic surgical preparation. Immediately following induction of anesthesia (isoflurane, oxygen delivered at 0.5 to 1.0 L/min, 1 to 4%), the surgical site was shaved and scrubbed with Betadine and sterile alcohol pads.

Acute surgery followed similar general surgical procedures, but a ketamine/xylazine cocktail with a 75 mg/kg ketamine and 5 mg/kg xylazine ratio was used as an alternative anesthetic to ensure proper nerve function. The dosage was determined by weight. We note that due to perceived limits to the effectiveness of this anesthetic for long periods of time, that only 90 minutes of blood collections (post LPS challenge) were collected versus the 120 minutes done with the chronic animals.

4.2.3.2 Device implantation

With the rat in the prone position, we made incisions on the side or back of the rat to facilitate the placement of the implantable device. A subcutaneous pocket was created and the device inserted into the pocket, oriented, and then sutured in place. After moving the rat to the lateral recumbent position, we created a midline incision on the neck and routed the electrodes subcutaneously to the neck. Incisions made to implant the device were next sutured closed. With the rat in the supine position we expanded the midline incision to start at the jaw line moving caudally. We reflected the skin and soft tissue to expose the underlying sternohyoid and sternocleidomastoid muscles, which sit atop the carotid sheath. Surgical retractors were carefully placed to hold open the incision site. Using a blunt dissection technique, we gently separated the soft and connective tissues until the trachea and carotid artery sheath could be seen. The cervical vagus nerve sits adjacent and runs parallel to the carotid artery above the level of the carotid bifurcation. We carefully dissected the connective tissues surrounding the vagus nerve exposing the nerve. One or two cuff electrodes were then wrapped around the exposed vagus nerve (if two, stimulation cuff rostral and recording cuff caudal to the omohyoid muscle) and cuffs were secured shut with a suture or Kwik-Sil Silicone Elastomer (World Precision Instruments, Inc.; Sarasota, FL), and any extra lead was curved into a strain relief loop and sutured to neighboring muscle tissue or skin to minimize movement of the cuff electrode. We then sutured the incision closed. During tethered procedures, no device was not implanted and electrodes were terminated

into a headcap and cemented to the skull. In some cases, we routed additional leads subcutaneously from the device to a transdermal connector port behind the shoulder blades to guarantee power fidelity while collecting blood.

Similar surgical procedures were followed for acute LPS experiments with stimulation and recording cuffs being placed around the cervical vagus nerve and then attached to an externally placed Bionode for the duration of the experiment.

4.2.4 Fluorogold injection

Analysis of retrograde tracer transport of the vagal efferent fibers to the DMN has been shown to be an effective means of verifying selective vagotomies of the five subdiaphragmatic vagal branches in the GI tract. Each of the five branches has been shown to transport to distinct areas of the DMN, with the left vagal branches (hepatic, accessory celiac, and ventral gastric) accumulating in the left side of the DMN and the right branches (dorsal celiac and dorsal gastric) to the right side of the DMN [120]. We used established methods of FG administration to verify the physiological efficacy of the left and right vagal efferent fibers [120-122].

Approximately five days prior to blood collection, stimulation, and perfusion, we gave animals an intraperitoneal injection of 1 mg/1 ml saline of FluoroGold (Fluorochrome, Inc.; Englewood, CO) that labels cell bodies of intact efferent fibers in the DMN.

4.2.5 Catheter placement and blood collection

Blood samples were obtained to track circulating levels of inflammatory cytokines. We followed procedures outlined in the NIH Guidelines for Survival Bleeding of Mice and Rats for blood sampling. The amount of blood collected did not exceed the maximum allowed 10% of the circulating blood volume. We surgically placed catheters in the rats ~24 hours prior to blood collection following femoral cannulation procedures outlined in the Bioanalytical Systems, Inc. Culex surgical manual [82] and then placed the rats into the Culex Automated In Vivo Sampling System (Bioanalytical Systems, Inc.; West Lafayette, IN) [83] while connected to the Raturn

caging system (Bioanalytical Systems, Inc.) [123]. We programmed the Culex system to automatically collect ~200 µL blood samples from each rat at predefined intervals of 30 minutes over a three-hour timeframe as outlined in Figure 4.3.

The Culex was not used for acute LPS experiments. Instead, blood was obtained by punctured leg vessels, and samples collected into K3 ETDA coated minivette tubes. Only four blood collections were taken for acute animals at times of -30, 30, 60, and 90 minutes with respect to LPS injections.

4.2.6 Testing procedures

4.2.6.1 LPS preparation/injection

LPS solution was prepared immediately prior to blood collections in the animals in a dose of 5 mg/kg. We measured LPS (Sigma-Aldrich, serotype O111:B4) into 1.5 ml Eppendorf tubes using a Mettler Toledo AB54-S/FACT digital scale and added sterile saline (0.9% sodium chloride) to the tube in a proportion of 0.2 ml saline / 1mg LPS. The solution was sonicated for 30+ minutes prior to usage. We administered LPS intravenously (chronic) or intraperitoneally (acute) at the specified time during blood collection procedures, and before stimulation treatments if applicable.

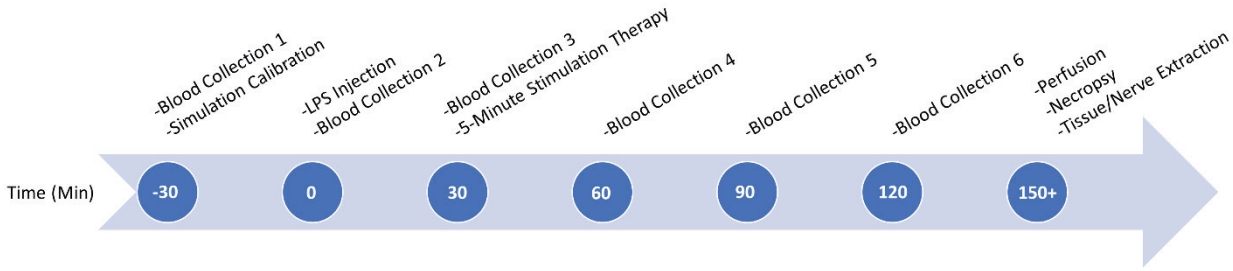

Figure 4.3 Time flow diagram outlines the process of blood collection on the last day of chronic experiments. Time points are based with relation to the acute LPS injection of the animal.

4.2.6.2 Stimulation

We performed all stimulations with balanced, bi-phasic, square wave pulses produced by either our in-house implantable BioNode system that is described in previous work [119], or equivalently by a National Instruments USB-6343 Multifunction Device (NI-DAQ; National Instruments; Austin, TX) for select animals tethered with a headcap configuration. The recording channel consisted of a differential two-stage filter/amplifier. The first stage was a low power instrumentation amplifier (INA333; Texas Instrument; Dallas, TX) configured for a gain of 20 dB, and the second stage was an inverted operational amplifier (OPA313, Texas Instrument) configuration designed for a gain of 40 dB and bandwidth from ~15 Hz - ~3 kHz. The total record channel gain was 60 dB. The stimulation was produced by a common mode voltage difference amplifier (LT6375; Linear Technology; Milpitas, CA) configured to act as a Howland Current Pump, and controlled either by the on-chip microcontroller (nRF51822; Nordic Semiconductor; Trondheim, Norway) paired with a digital-to-analog converter (DAC7551, Texas Instrument) on the BioNode or the output of the NI-DAQ.

Our system has been shown to allow fully autonomous neural control (ANC) in rats by Ward et al [42] in acute test environments, and has been used in other recent studies [124]. In our acute experiments, we attempted ANC calibrations immediately after the first blood sample, and 30 min prior to LPS injection in the animal. During calibration, we used ANC to determine a maximal activation profile for a Compound Nerve Action Potential (CNAP) response (B or C fiber) to various stimulation profiles varied in amplitude and pulse duration. Due to the highly variable environments experienced in our chronic tests however, we did not utilize the fully autonomous functions for most of our chronic animals. Instead, we manually tested different stimulation profiles in real-time to determine an optimal profile to induce a CNAP response. If successful maximal nerve activation was detected, we ran stimulation for five minutes at 5 Hz at the corresponding stimulation profile. If not, we utilized a pre-determined and default maximal activation stimulation profile (1 mA amplitude, 1 millisecond pulse duration, 5 Hz) for the five-minute stimulation. We utilized a stimulation frequency of 5 Hz which is in the range of normal nerve traffic in the vagus nerve [125].

4.2.6.3 Perfusion and brain tissue preparation

After the final blood collections, animals were deeply anesthetized with a lethal dose of Ketamine/Xylazine followed by a transcardial perfusion with 300 ml of 0.9% saline at 40˚C, followed by 400 ml of 4% paraformaldehyde at 4˚C. We then removed the medulla and cryoprotected it overnight in 15% sucrose in 4% paraformaldehyde at 4˚C. Serial 40 μm coronal sections were taken with a cryostat between the level of the facial nucleus and the pyramids. We collected sections onto gelatin-coated microscope slides, dehydrated and cleared them in alcohol and xylene, and then placed the sections under a coverslip with DPX (Sigma-Aldrich, St. Louis, MO).

4.2.7 Sample processing and analysis

4.2.7.1 Fluorogold imaging (of medulla)

FG images of the medulla were acquired using a LEICA DMRE microscope with a SPOT FLEX camera controlled using SPOT Software (V5; Diagnostic Instruments, Sterling Heights, MI). We did final post-production using Photoshop CS6 (Adobe Systems, San Jose, CA). Photoshop was used to: (1) apply text and scale bars; (2) make minor adjustments to the color, brightness, contrast, and sharpness of the images to match the appearance of the original material viewed under the microscope; and (3) to organize the final layout of the figures.

4.2.7.2 Necropsy nerve extraction and imaging

Most necropsy analysis was done post perfusion, making it difficult to locate specific nerve landmarks due to blending of tissue textures. Therefore, we visually evaluated some animals pre-perfusion to allow for improved observation and analysis.

We removed vagus nerve column (including carotid artery, superior cervical ganglia, and other surrounding tissues) samples to be analyzed for Fluorogold tracer from the animal using blunt dissection techniques, and placed them into a 4% paraformaldehyde solution.

Samples for imaging with a fluorescent microscope were dissected and positioned on clean glass slides to verify an optimal view. We then mounted them on gelatin coated (1.5% gelatin solution) Corning micro slides under a Leica M205 FA Stereomicroscope with a UV ET filter and illuminated them with a Prior Lumen 200 fluorescence illumination system. An uncoated Corning micro slide was placed on top of the nerve, and the nerve was crushed onto the gelatin coated slide by placing 4 lb weights on top of the slide for one hour. We then removed the weights and the uncoated slide from the gelatin coated slide onto which the nerve had been crushed, and let the slide dry overnight. The slides were then dehydrated in a 2-minute ascending series of alcohols (70% EtOH, 95% EtOH, 100% EtOH x 2) and xylene (6 min x 2), and then coverslipped with custom coverslips (Electron Microscopy Sciences).

Mosaic image z-stacks were collected with a Leica DFC310 FX camera connected to a Leica DM5500 microscope (D filter and HCS PL Fluotar 10x/0.30 objective), using Surveyor software. We used the mosaic image stacks to create an all-in-focus image using the Auto-Blend function in Photoshop CC.

4.2.7.3 Blood sample processing

For cytokine analysis, fresh blood was collected in EDTA (K3EDTA at 1.75 mg/ml), centrifuged at 2000x g for 10 min, and plasma extracted and either prepared immediately or aliquoted and stored at -20˚C. We analyzed plasma samples using a LEGENDplex™ Rat Th Cytokine Panel (13-plex) (Biolegend, San Diego, CA) in a V-bottom 96 well plate. This assay allowed simultaneous analysis of 13 cytokines, IL-2, IL-4, IL-5, IL-6, IL-9, IL-10, IL-13, IL-17A, IL-17F, IL-22, GM-CSF, IFN-γ and TNF-α, using a multiplexed fluorescent bead assay procedure as described. A sandwich based immunoassay was performed on 96 well plates using bead sets that had previously captured the analytes of interest. For each sample, we diluted plasma 4-fold with an assay buffer before testing it. Rat plasma samples were then distributed appropriately in duplicate on the plate and capture beads added to each well. Each analyte standard was added to a standard well, followed by serial dilutions. This established a standard curve for each plate. We incubated plates at room temperature for 2 hours while shaking at 500 rpm. We then washed the plates twice by centrifugation. After washing, 25 µl of biotinylated detection antibody was added

to each well and the plates were sealed and placed on a plate shaker (500 rpm) in the dark for 60 minutes. All wells then received 25 µl of the streptavidin with phycoerythrin (PE) and we resealed and incubated the plates at room temperature in the dark on a plate shaker (500 rpm) for 30 minutes. Plates were washed again as previously, with addition of 200 µl wash buffer and centrifuged. 150 µl of wash buffer was then added to each well and beads resuspended by trituration. We then read the plates on the flow cytometer.

4.2.7.4 Flow cytometry

We read plates on one of two instruments: a CytoFlex 13 color cytometer (Beckman Coulter, Miami, Florida) or an Attune 14 color cytometer (Thermo Fisher, Eugene, Oregon). Allophycocyanin (APC) content was used to distinguish different capture beads. Setup for each instrument was similar and required calibration using instrument calibration beads to ensure the instruments were calibrated properly. The 96 well plates were automatically read by either flow cytometer and output files generated were standard FCS files. We set the instruments to collect 4000 beads per well, ensuring approximately 250-350 beads of each cytokine per well. Prior to running plates, we ran set-up beads included in the kit on each instrument to ensure the detection probe (PE) was properly calibrated and the bead probe (APC) was set at previously determined voltages to ensure the best bead separation.

4.2.7.5 Blood data extraction

Upon completion of each plate, FCS files were analyzed by MPLEX software (Doclu LLC, West Lafayette, In). The software opened the entire 96 listmode files, and upon identification of the bead signal (APC) and the detection signal (PE), it collected a 2-parameter plot with APC on the x-axis and forward scatter on the y-axis. In this manner, the 13 populations of beads were resolved. For Legendplex bead assays, two bead sizes were discriminated by forward or side scatter and by bead intensity on the APC detection parameter. Each cytokine was then identified by its preset bead size and dye intensity level. There were six intensity levels for the smaller beads (A beads) and seven intensity levels for the larger (B beads). We identified the standard curves by their location on the 96 well plates and identified duplicates. The MPLEX software

was preset for a Legendplex assay profile which associated either A beads or B beads with the appropriate cytokine. An automated clustering algorithm was used to fit the bead populations to the predesignated beads, and the standard curves for all 13 cytokines were automatically calculated, followed by production of a CSV output file with all well data.

4.2.7.6 Blood data analysis

Raw concentration signals from cytokines attached to functional beads were compared to calibration curves calculated for each plate of samples run, and used to produce cytokine concentration data for statistical analysis and figures. We averaged two replicates per sample before analysis.

Multivariate analysis of variance (MANOVA) was first performed on raw sets of all 13 measured cytokine concentrations collected from plasma samples. Post-hoc ANOVA was also performed on raw sets of each cytokine concentration. To compensate for significant noise in the cytokine calibration curves (at low concentration levels), we converted raw data into fractions of the total cytokine signal for each sample. To then allow for Gaussian analysis to be performed, we computed angular arcsine transformations with equation (3.1) and corresponding Cohen's h effect sizes with equation (3.2):

$$= 2\arcsin\sqrt{p} \tag{3.1}$$

$$h = \left| {}_1 \quad {}_2 \right| \tag{3.2}$$

Where p is a given proportion and h is a resulting Cohen's h effect size. ANOVA was again performed on the angular transformations. $P < 0.05$ was considered statistically significant, but we did note other scientifically significant trends that did not meet this threshold.

4.2.7.7 Histology

To further verify the integrity of the chronically implanted vagus nerve, cuffed nerve samples from eight rats were fixed and then embedded. We used paraffin molds for silicone cuffs with no metal electrode and Poly-Methyl Methacrylate (PMMA) resin molds for cuffs with wire electrodes to prevent tearing of enclosed nerves. Specific details on these processes can be found in supplemental materials of the publication.

4.2.8 Gastric MRI scanning

Surgical procedures for implanting stimulation cuffs in rats used for gastric emptying testing are in line with those outlined previously for headcaps, with the exception that we used only a single stimulation cuff and no recording cuff, and we limited headcaps to only two pins to reduce potential imaging artifact. All dietary training, scanning procedures, and image processing and analysis techniques mirrored those methods established by Lu et al [126].

Stimulation was performed using our Bionode system utilizing our standard cuffs as described earlier. We stimulated throughout the period of scanning, using balanced bi-phasic pulses of 600 μA, 360 μs, at 10 Hz. The parameters were determined by earlier collaborative testing to induce the largest electromyography (EMG) response on the stomach wall. Stimulation was applied continuously throughout the 4-hour test period with trains of 20 seconds on followed by 40 seconds off. During stimulation scans, we noted that some rats showed severe signs of apnea and bradypnea resembling what was explored by Zaaimi et al [127]. These phenomena were commonly accompanied by a corresponding arrest in observed stomach motility during stimulation. It was not our goal here to explore this effect in detail, therefore, we excluded animals that exhibited this trait from our data.

4.3 Results

4.3.1 Fluorogold transport

Early in chronic VNS testing, we recognized an issue with efferent FG transport in the left (cuffed) vagus nerves of the animals. 36 of the 44 cuffed animals showed complete suppression of FG transport to the left side of the DMN in medulla samples, indicating a complete cervical vagotomy of the left vagal nerve, despite the animals receiving no surgical vagotomy. In addition, all animals demonstrated expected FG transport in the uncuffed right vagus nerve. Based on visual analysis during necropsy, it was first considered that the cause was likely due to surgical techniques, and mechanical stresses and migration of our cuff electrodes on the nerves.

A visual inspection of the left cervical vagus site was performed on 32 rats during necropsy. Early inspections revealed moderate to severe cuff migration and manipulation of the nerve in several animals. We hypothesized that these issues were causing the lack of FG transport, prompting multiple iterations of surgical technique and materials improvements. Such included: added lead lengths and strain relief loops, increased flexibility of the lead materials, altered lead anchoring techniques and locations, changed wire electrode configurations within the cuffs (including inert cuffs with no metal electrode), implanted single stimulation cuffs (versus a second recording cuff as was standard for our study), employed multiple different surgeons, and tried multiple types of cuffs (as presented in our methods).

These changes produced significant visual decreases in mechanical strain to the nerve and all later subjects showed good integrity of cuffs and leads in the surgical site (shown in Figure 4.4). Despite the adjustments and improved cuff/nerve interface integrity, FG transport results did not improve (Figure 4.5). We, therefore, hypothesized that the cuffing of the nerve itself had a dominant effect on nerve physiology regardless of other external stresses.

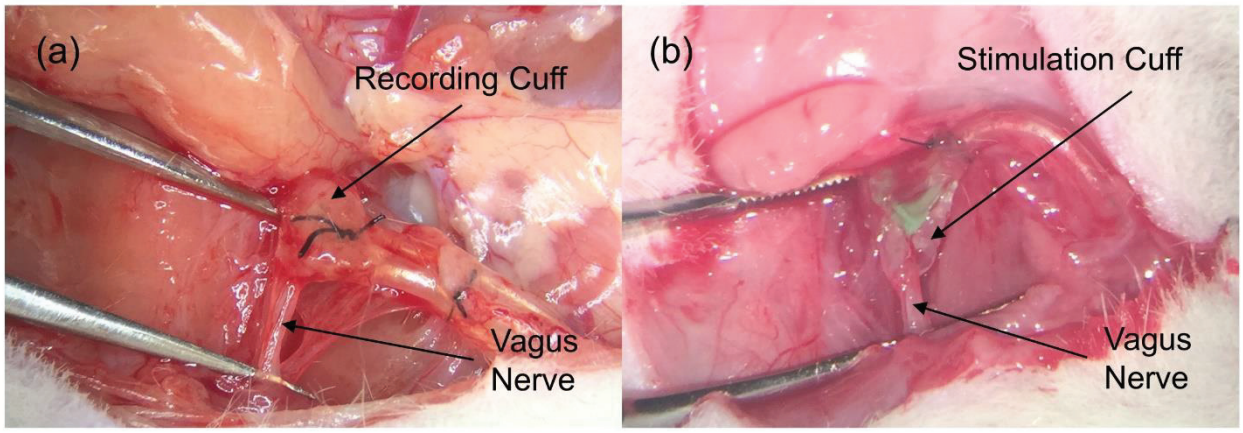

Figure 4.4 Pre-perfusion visual inspection of two animals, both showing cuffs in correct location with vagus nerve intact. (**a**) From a rat that demonstrated complete suppression of Fluorogold transport (eRx71), while (**b**) demonstrated a limited but present transport (eRx103).

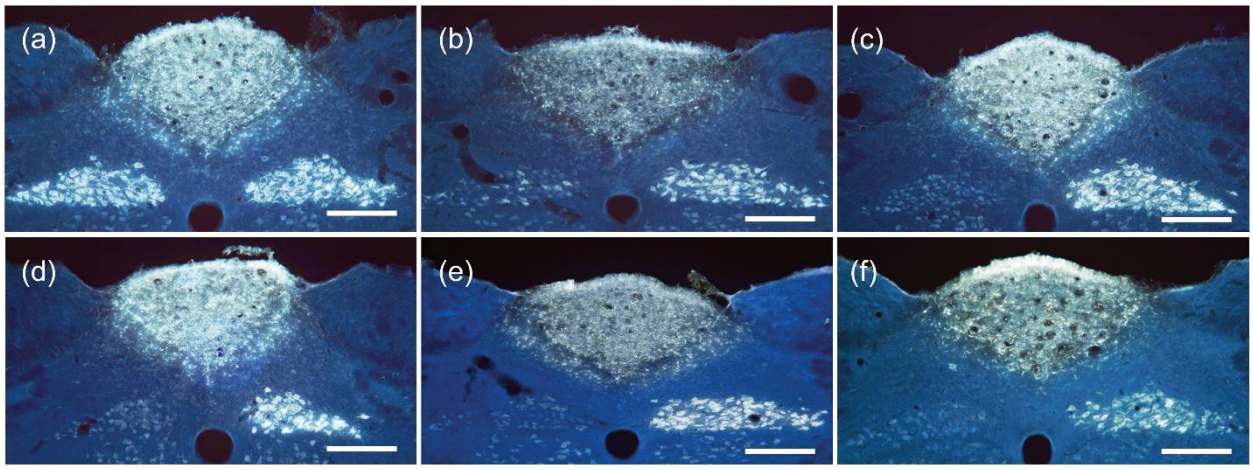

Figure 4.5 Fluorescent images of medulla samples from multiple cuffing variations of rats. (a) Cuffs placed adjacent to left vagus nerve, but not enclosing it (eRx110), produced bright efferent fiber FG transport illumination on both left and right sides of DMN. (b) Cuffed with standard record and stimulation cuffs by visiting surgeon (eRx116), showing bright FG illumination on the right side of the DNM from uncuffed right vagus nerve, but limited efferent transport from the left vagus on the left side of the DMN. (c-f) All rat medulla samples showed near-complete suppression of efferent transport on the left side. (c) Cuffed with single industry-made (CorTec; Freiburg, Germany) tunnel electrode with 0.6mm inner diameter (eRx118). (d) Cuffed with a single standard stimulation cuff (eRx113). (e) Cuffed with sham record and stimulation cuffs containing no metal electrodes (eRx132). (f) Cuffed with standard record and stimulation cuffs, but not stimulated (eRx75). Scale bars = 250 microns.

To further explore the physiological phenomena, we extracted the right and left (still cuffed) vagus nerve columns from 18 rats during post perfusion necropsy. These nerve samples were observed under a fluorescence scope for signs of FG in the nerves and nodose ganglia and were then either mounted onto a slide to be photographed or fixed for basic Hematoxylin and Eosin (H&E) histology (n = 8). Samples that were extracted with both left and right nodose ganglia still intact (n = 7) were analyzed using a fluorescence microscope (details shown in Figure 4.6). Observations showed that the ganglia of the cuffed left vagus nerves and the uncuffed right vagus nerves both contained FG illuminated cells, indicating an active FG transport in the afferent nerve fibers, despite a severe or complete suppression of efferent fibers to the medulla as demonstrated in Figure 4.7.

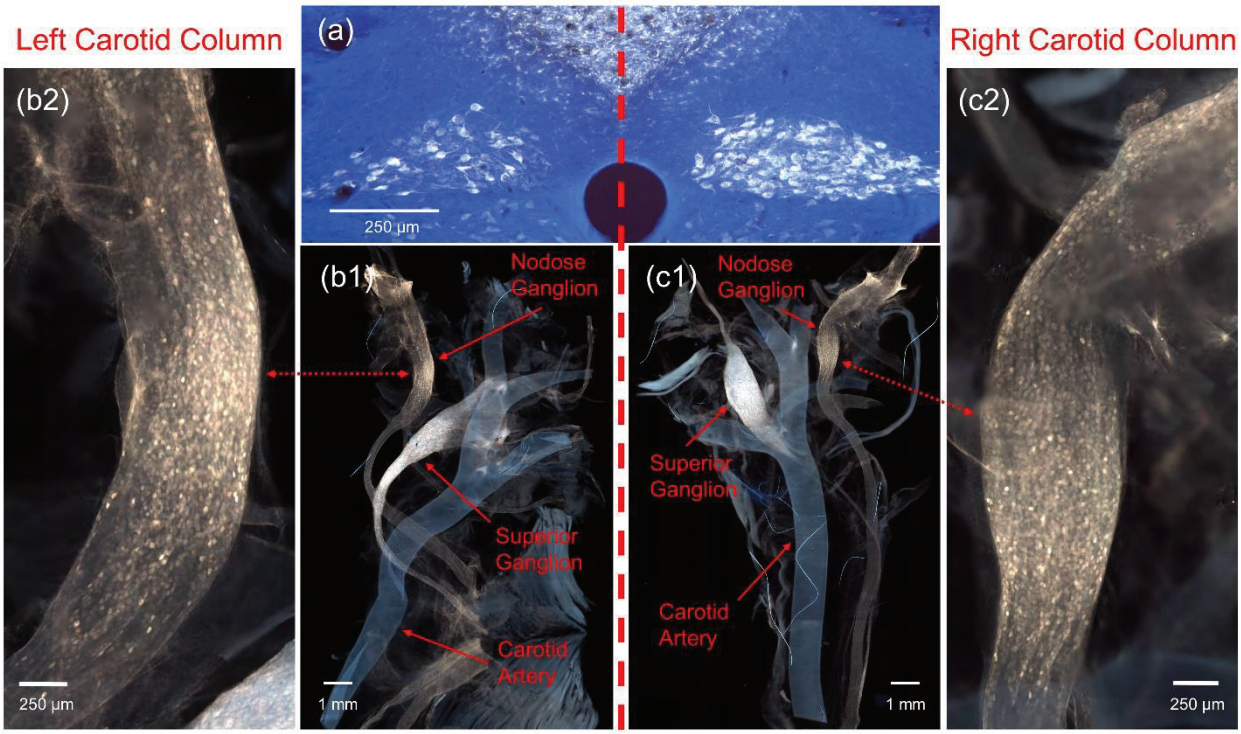

Figure 4.6 Representative fluorescence images and image mosaics of a single rat (eRx162). (**a**) medulla image showing clear efferent fiber FG transport on the right side of the dorsal motor nucleus, and significant suppression of transport on the left side. (**b1**) cervical column dissected cranial to stimulation cuff on left vagus nerve, with enhanced image of nodose ganglia (**b2**) showing FG illumination. (**c1**) cervical column of right vagus nerve and surrounding tissue, with enhanced image of nodose ganglia (**c2**) showing FG illumination. Vagus nodose ganglia from each side show similar size, shape, location, and textural illumination, indicating similar active afferent fiber transport in both despite a suppression of efferent fiber transport in the cuffed left vagus.

It is important to note that FG brightness varied between animals as is common due to biological, surgical, and tissue extraction and processing variances. Despite this inconsistency, the trends noted above were present in all samples and there was no consistent difference observed in density of FG illumination between nodose samples from cuffed left vagus versus un-cuffed right vagus nerves.

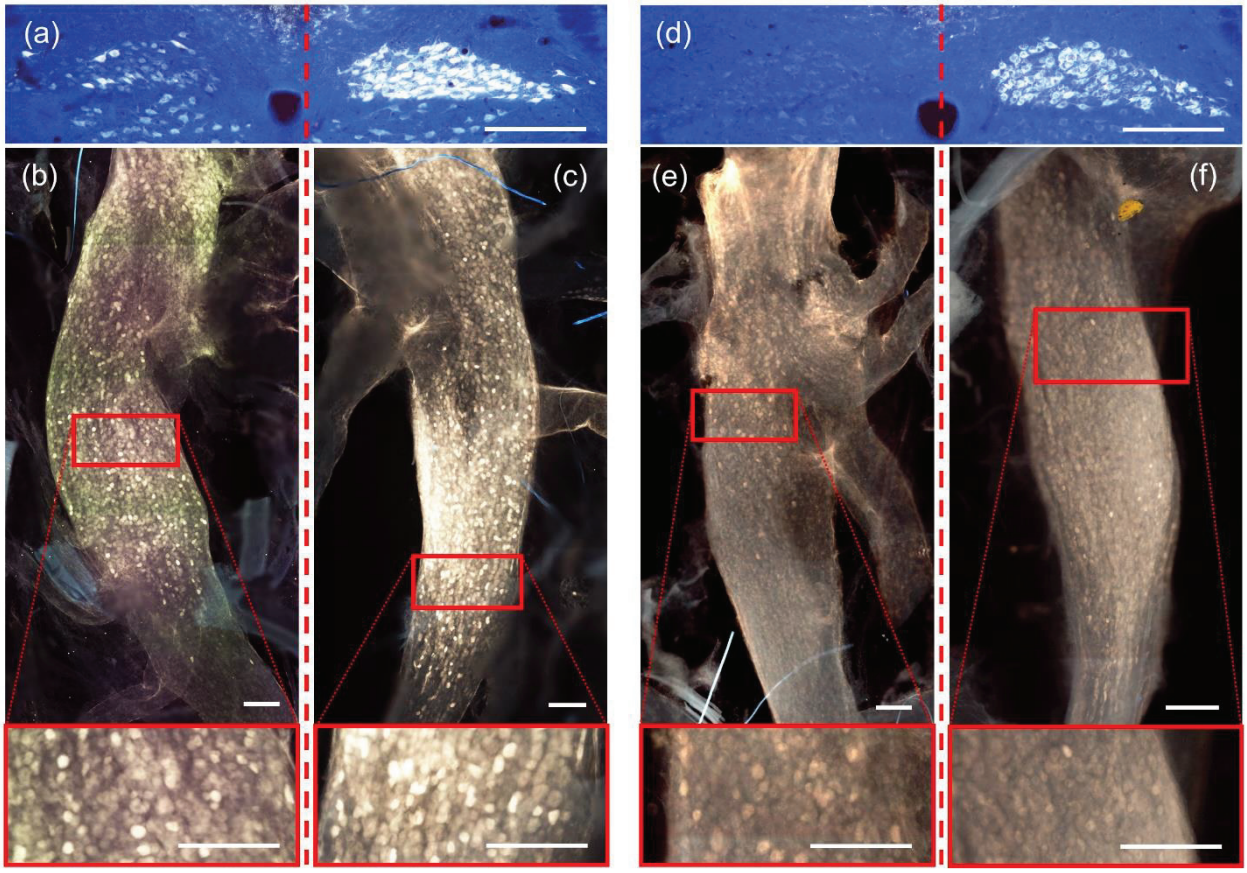

Figure 4.7 Comparative fluorescence images of two separate rats demonstrating healthy FG transport through efferent fibers to the DMN and afferent fibers to the nodose in uncuffed right vagus nerves, but only through afferent fibers in cuffed left vagus nerves. (a) medulla image (from eRx159) showing clear efferent fiber FG illumination on the right side of the dorsal motor nucleus, and severe suppression of FG on the left side. (b & c) corresponding fluorescence nodose images of the cuffed left and uncuffed right (respectively) vagus nerves (from eRx159), with enhanced images (red boxes) highlighting FG illuminated cells on both sides. (d) medulla image (from eRx163) also showing strong efferent fiber FG illumination on the right side of the dorsal motor nucleus, and complete suppression of FG on the left side. (e & f) corresponding fluorescence nodose images of the cuffed left and uncuffed right (respectively) vagus nerves (from eRx163), with enhanced images highlighting FG illuminated cells on both sides. Red dashed lines separate the left vagal effects from right vagal effects. Scale bars = 250 microns.

4.3.2 Compound nerve action potential (CNAP) detection

A complex, but telling, measure to test the integrity of a peripheral nerve during VNS is to record the responsive action potentials of the nerve to a prior electrical stimulation. CNAP recordings can provide a direct indication of the variety and extent of nerve fibers being activated by a given stimulation.

Recording CNAP responses in real time, however, is challenging due to multiple factors including noise in the stimulation or recording channels, and overlap of artifact in the signal due to the electrical stimulation and laryngeal [115, 128] and other muscle artifacts. This difficulty is compounded by factors related to the chronic test environment. As mentioned, most reviewed studies used pre-determined stimulation parameters and concentrated only on analyzing the resulting biological data [96, 111, 112], or recorded the signal during testing and post-processed the data afterwards to determine the fiber response [16, 115].

In our study, we employed two nerve cuffs (one stimulation and one recording) that allowed simultaneous stimulation and recording in a closed-loop system [42]. Testing fiber responses resulting from stimulation is paramount due to frequent changes in the biology of an animal during recovery from implantation and due to foreign body response to the nerve cuffs. Literature has shown that impedances and the resulting nerve response to electrical stimulation can fluctuate for weeks and even months before stabilizing [129]. This was confirmed in our own testing by fluctuations in CNAP responses seen when tested on multiple days during recovery as seen in Figure 4.8. It is important to note that stimulation parameters shown in Figure 4.8 are significantly lower than those utilized during functional stimulation treatments. Functional stimulation in our LPS experiments utilized amplitudes of 1 mA or higher that were more likely to have recruited significant C-fiber activations.

For this animal we also saw larger potentials on day 36 (with rat freely moving) than on days 23 and 27 (rat anesthetized with isoflurane). Differences could be contributed in part to effects of being anesthetized and to peripheral stimulation effects such as laryngeal muscle and movement artifacts. Due to practical restraints such as limited surgical space near the vagus, we did not perform any formal testing for such artifacts in this study.

We did not endeavor here to make conclusions based on the labeled fiber types of CNAP responses presented in Figure 4.8, but strictly to demonstrate that diverse CNAP responses can still be recorded over time in absence of healthy FG transport to the medulla. Using our methodology, we successfully detected varied CNAP responses in 13 of our stimulated animals prior to LPS administration and stimulation treatment. Despite this sign of nerve functionality in those animals, only two of the rats showing CNAP response showed indication of efferent FG transport, both attenuated, through the nerve. The resulting CNAPs could have strictly been the result of remaining healthy afferent fibers, or could have included remaining intact efferent fibers. We believe this to be a topic worthy of further exploration.

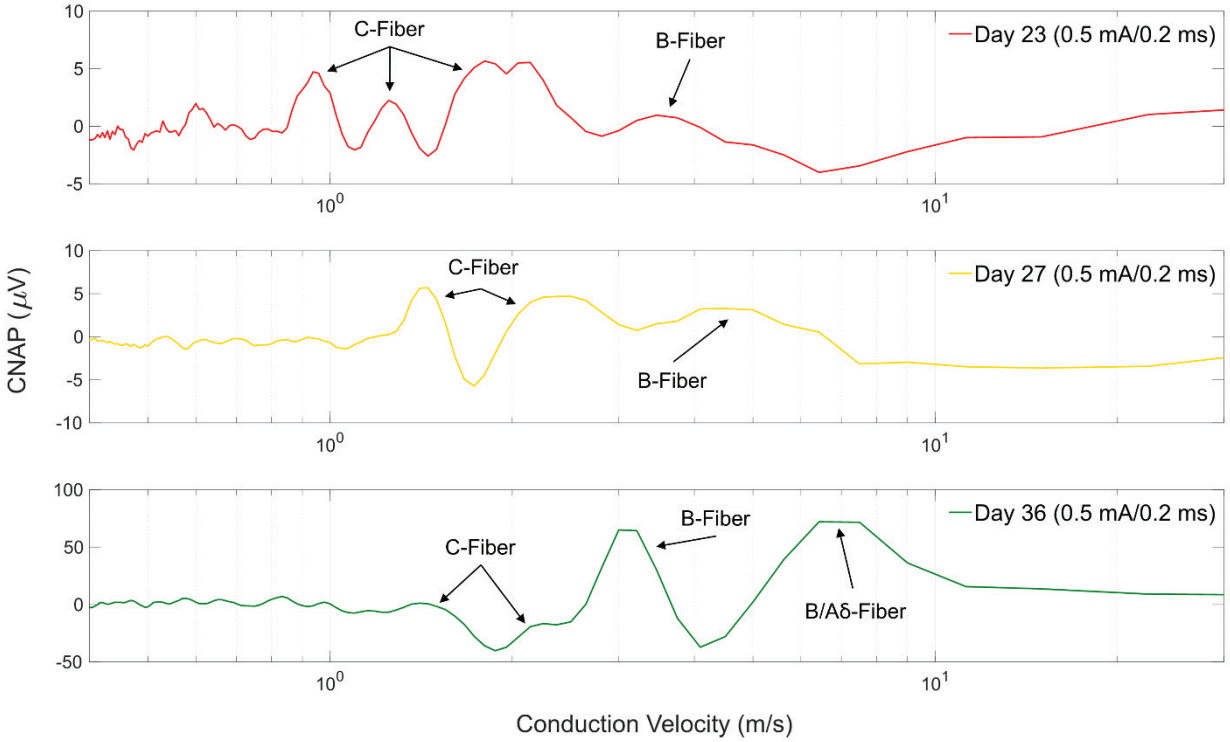

Figure 4.8 Representative CNAP responses of the left cervical vagus nerve in a rat subject (eRx144) show variance in fiber responses to similar stimulation over multiple days after three weeks of recovery. Similar CNAP responses were seen in multiple animals despite having suppressed FG transport. Fiber labels were calculated using conduction velocities based on measured distance between stimulation and recording cuff at time of chronic implantation. No measurements were made during necropsy to verify original cuff distances.

4.3.3 Hematoxylin and eosin (H&E) histology

Samples were sectioned either longitudinally to analyze the length of the nerve (Figure 4.9 a-d) or transversely across the diameter of the cuff to analyze the cross section of the nerve (Figure 4.9 e-f). Industry standard H&E staining was performed on all samples using standard protocols. We did not apply myelination specific stains to the nerve samples in this study.

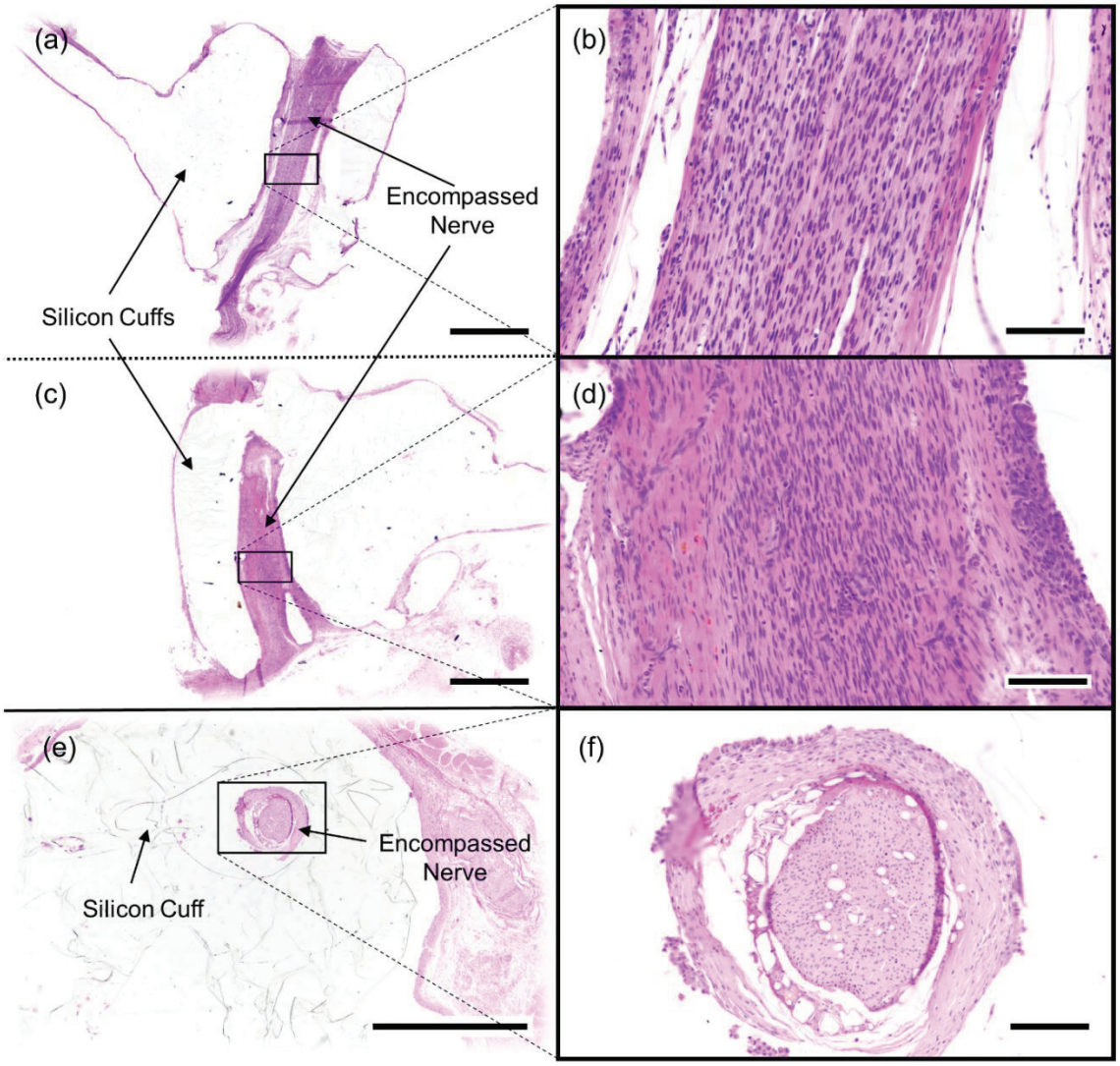

Figure 4.9 Representative photomicrographs of cuffed vagus nerves stained with hematoxylin and eosin (HE). Images (a-d) are from the same nerve (eRx143). Images (e-f) are of a separate nerve (eRx132). (a) Longitudinally sectioned nerve encompassed by a stimulation cuff, (b) higher magnification of (a). (c) Longitudinally sectioned nerve encompassed by a caudally positioned recording cuff, (d) higher magnification of (c). (e) Example of a nerve cuffed with an inert cuff with no metal electrodes sectioned in the transverse plane, (f) higher magnification of (e). Scale bars = 1000 microns (a, c, & e) or 100 microns (b, d, & f).

Cuffed vagus nerves were histologically normal. The cuff was surrounded by fibrous connective tissue, epithelioid macrophages, and multinucleated giant cells; consistent with a granulomatous foreign body inflammatory reaction. Similar inflammatory cells were identified surrounding the epineurium (connective tissue surrounding the nerves), but not infiltrating the nerve. Such findings suggest a perineuritis, or inflammation surrounding the nerve, but not penetrating it. Such inflammation is commonly analyzed during cuff design and well documented in literature [129-131].

4.3.4 Cytokine measurement from blood (plasma) samples

We used plasma cytokine concentrations to analyze the effects of VNS on modulation of inflammatory cytokine levels in both chronic and acute environments. Only the pro-inflammatory cytokines IL-6 and TNF-α, and anti-inflammatory cytokine IL-10 were significantly elevated over time after injection of LPS, consistent with prior literature [66, 132, 133].

Due to a high level of variability in cytokine concentrations from sample to sample, and noise in the cytokine calibration curves in our raw data, we performed statistical analyses using angular transformations of proportional compositions of each cytokine compared to the overall content in the samples and utilized Cohen's h analysis for effect sizes. Samples collected at 90 minutes post-LPS injection demonstrated important distinctions between effects of stimulation with chronically and acutely cuffed vagus nerves (Figure 4.10).

Pro-inflammatory TNF-α levels in acutely cuffed rats displayed higher proportions than in chronically cuffed animals, and acutely stimulated animals showed distinctly lower proportions than the acute controls ($h = 0.44$). This indicated a modulatory effect of stimulation on acutely cuffed subjects due to VNS. Chronically cuffed rats, however, showed virtually no impact on TNF-α due to stimulation.

The second pro-inflammatory cytokine, IL-6, showed much higher proportions in chronically cuffed animals at 90-minutes post-LPS challenge, than in their acute counterparts ($h > 0.8$). Both

chronic and acute samples showed slightly lower proportions in stimulated animals versus controls, but neither were significant.

Anti-inflammatory IL-10 cytokine proportions again revealed no difference between stimulation and control groups in chronically cuffed rats. It did, however, show a small but statistically significant increase (h = 0.22) in proportions due to stimulation in acutely cuffed animals over the acute controls.

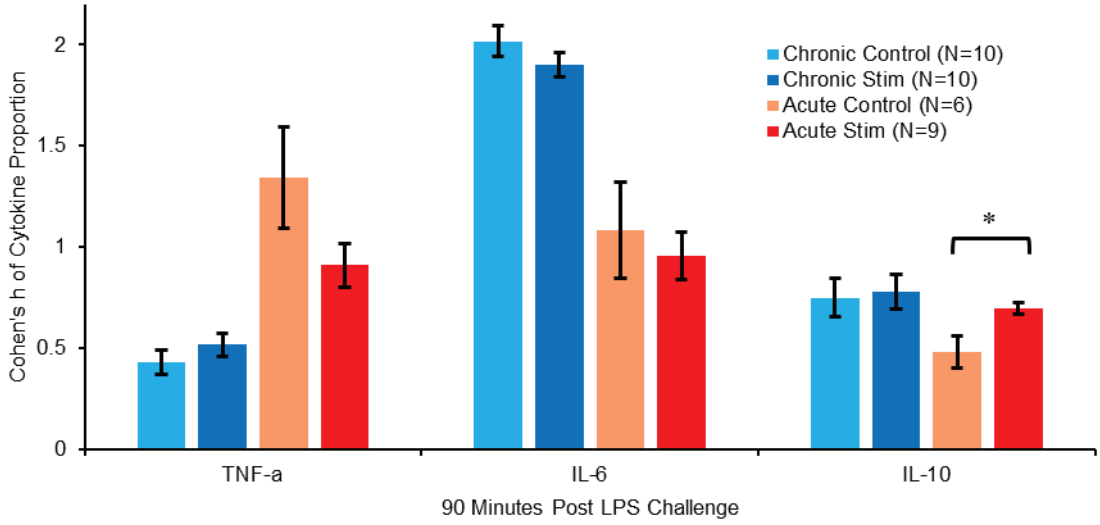

Figure 4.10 Plot shows compositional analysis with angular (arcsin) transformations of proportional make-up in specific cytokine levels at 90 minutes post-LPS injection. Acute subjects showed a decrease in TNF-α proportion ($h > 0.4$) and a small ($h < 0.25$) but significant increase in IL-10 proportion due to stimulation, indicating strong inflammatory modulation due to stimulation. Chronic subjects showed no significant modulation in proportion levels due to stimulation in any of the three cytokines, consistent with compromised vagus function after chronic cervical cuffing. Error bars, s.e.m. *$P < 0.05$.

A decrease in TNF-α proportion and increase in IL-10 in our acutely cuffed rats were both convincing indications of inflammatory modulation using our Bionode system, consistent with similar work by multiple groups mentioned earlier presenting repeatable cytokine modulation in acute environments. Chronically cuffing the vagus nerve resulted in distinctly different cytokine proportion trends from those of our established acute baselines. Importantly, it appeared to stunt all ability to modulate plasma cytokine levels with stimulation. Having already established a

critical physiological lapse in the vagus nerve's ability to transport FG in a rat when cuffed, we hypothesized, accordingly, that chronic vagal nerve cuffing also compromises the vagus nerve's ability to modulate inflammation.

4.3.5 Gastric emptying

Note: This section has been updated to reflect data from a more recent publication [134]. Gastric functions have been shown to be primarily modulated with vagal sensory and motor signals as was investigated by Travagli et al [135], and alterations in those vagal signals can result in altered gastric functions [136]. Accordingly, gastric physiology such as emptying rates is a good measure to determine an altered state of vagal nerve operation. Utilizing MRI to determine gastric functions in humans has been well documented [137-139], and a similar approach was taken in collaborative research efforts to test gastric functions in an acute rat model [126, 134].

To further verify our chronic cuffing hypothesis, six rats were outfitted with a single stimulation cuff on the left vagus nerve and recovered. These rats were scanned using MRI to determine stomach emptying rates first as non-stimulated controls, and a second time after a recovery and re-training period, with stimulation. Those animals that produced reliable data according to our methods were used for comparison (Figure 4.11).

Control scans with no stimulation applied revealed a similar overall emptying effect to those that received VNS. Both groups resulted in a stomach volume reduction of ~25% from their starting volumes after 225 minutes. This is also in line with an acute control group that showed an average volume decrease of 25% over the same time period [134]. While the stimulation sample size used is small due to discarded samplings, it nevertheless showed a negligible overall variation between stimulation and control. The chronic stimulation samples do show an increased emptying rate from the 30 – 90-minute time points which could be a result of remaining intact efferent nerve fibers given that neither animal used for this data set showed a complete suppression of efferent FG transport. The increased rate however slows after the 90-minute point. This lacking overall effect of stimulation on stomach emptying rate of chronically

cuffed rats contrasted with significant and continued increases in emptying rates seen between acutely cuffed and stimulated rats that showed ~41% stomach volume reductions in the same time period [134], and indicated a compromise of vagus nerve function likely due to chronic cuffing.

In addition, we noted a delayed emptying period, with a slight increase in stomach volume, in half of our chronic controls from the 30 – 75-minute time points. This increase is also a strong indicator of an altered gastric function due to the chronic cuffing of the left vagus nerve given that it was not observed in acute controls [126, 134].

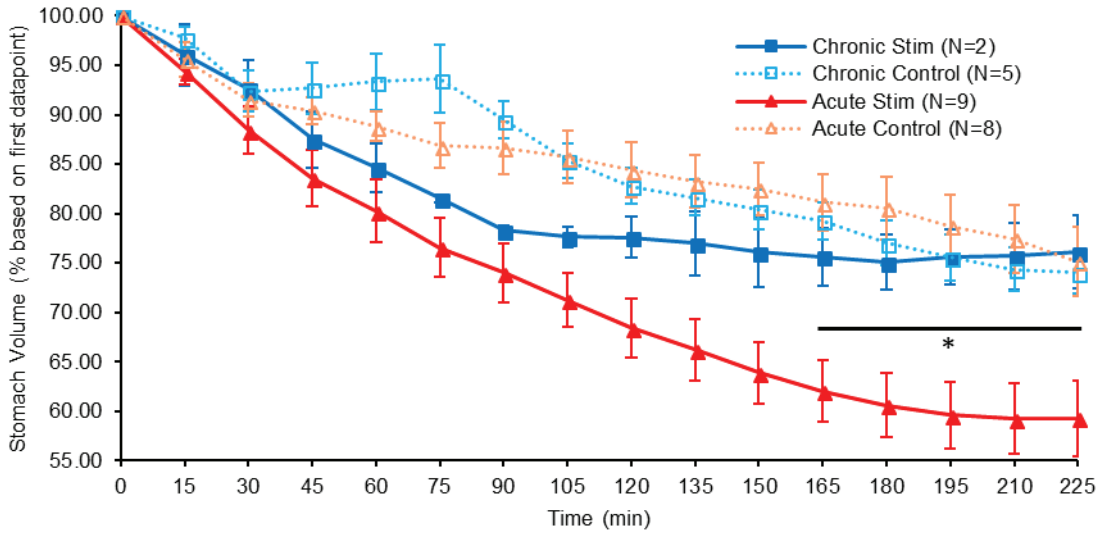

Figure 4.11 Gastric (stomach) emptying rates of rats with chronically implanted vagus cuff electrodes versus acute sample sets. Overall emptying with stimulation (solid lines) in a chronically implanted animal is indistinguishable from control (dashed line) after four hours, unlike acute stimulation, consistent with compromised vagus function after chronic cervical cuffing. Acute stim and control sets come from collaborative publication [134]. Error bars, s.e.m. *P < 0.05 between chronic and acute stimulation sets.

4.4 Discussion

The prominent finding in our study is that chronic cuffing of the vagus nerve in a rat creates an unreliable model for VNS studies. To date, cuffing the nerve caused still unexplored physiological effects, that suppressed efferent retrograde tracer transport mechanisms, affected

the vagal anti-inflammatory response to an LPS challenge, and degraded the response of gastric emptying rates to VNS. These adverse effects persisted despite a healthy outward appearance through visual and histological observation, and a full functionality of the nerve to create a CNAP response in the caudal direction from the stimulation cuff.

A shortcoming in this study was our decision not to implement a myelin specific stain such as Luxol fast blue and utilize electron microscopy to monitor potential demyelination effects that would be undetectable with basic H&E staining. It is therefore possible that while we did not observe any gross nerve alteration, local demyelination could have been present that would help explain attenuated effects of VNS in our study. Still, even observed morphological changes cannot always be linked directly to functional deficits with respect to electrical stimulation [131].

It followed that cuffing the nerve produced inflammatory foreign body response around the material of the cuff, creating a fibrotic layer of inflammatory cells between the nerve and inner cuff. Thil et al [130] showed that this process most commonly resulted in a stabilized interface after about 30 days, but also presented evidence that this foreign body response can penetrate into the epineurium, and that even small manipulations and deformations can cause effects in the nerve anatomy. This is supported by Tyler et al [140] whose flat interface nerve electrodes showed that larger manipulations of the nerve caused increased breakdowns and demyelination of nerve tissue.

Furthermore, Rydevic et al [141] demonstrated that applied pressures as small as 20 mmHg could introduce interference with intraneural blood flow to peripheral nerves. Theoretical pressure calculations of a split-ring cuff such as ours were presented by Naples et al [142] and experimentally verified by Cuoco et al [143]. Using their computations and accounting for a full 133% nerve swelling effect, our cuffs could be utilized on a nerve diameter greater than 600 μm (almost double the diameter of some cervical vagus nerves we measured) and not pass the 20 mmHg pressure threshold. We accordingly believe our cuffs had sufficient diameter to cuff the cervical vagus nerve in a rat safely.

Even a loosely fitting cuff though, can exert minor manipulations to the outer edges of the enclosed nerve tissue. Evidence from a study by Evans et al [144] suggested that motor fibers of the vagus nerve of a rabbit were commonly found grouped toward the edges of the nerve. Following this logic, it is possible that the efferent fibers in the vagus nerve of a rat would be similarly located in the lateral part of the nerve and be most susceptible to cuffing manipulations and related physiological effects. There is very little literature to support this claim in rats, however.

The possibility remains that efferent nerve fiber functionality may be severely attenuated while afferent fibers remain intact. Indeed, Phillips et al [122, 145], and more recently, Payne et al [146], reported on motor axons' inability to regenerate after nerve injury, while sensory axons did. While still speculative, our results support this hypothesis by noting the illumination of FG in the nodose ganglia of cuffed nerves while FG transport to the medulla is completely suppressed. If this is the case, studies concentrating on afferent effects of VNS may be minimally impaired by this cuffing effect. Moreover, if vagal efferent fibers are not working correctly, but afferent fibers are, VNS could negatively affect para-sympathetic systems, such as the inflammatory reflex, by sending afferent signals to the brain to increase inflammation, while suppressing the anti-inflammatory efferent signal. Suppression of the desired anti-inflammatory signal helps explain the lack of VNS effects in our study.

Concerning electrophysiological nerve functionality, the encapsulation process can take weeks or months to stabilize, making the cuff/nerve interface variable during the healing process. Sahyouni et al [129] explored short and long term electrical threshold changes that all eventually stabilized for stimulation purposes. Our results reflected this as the CNAP response showed to be variable during our regular four-week recovery period. Therefore, it was important to verify that a given stimulation profile was inducing a desired CNAP response before utilizing such profile to induce a biological response. A legitimate argument can be made that using a variable set of pre-stimulations, such as we did, introduced an unknown variable into our methodology. However, a number of acute studies have used pre-stimulation as a standard procedure [5, 18-20], and an initial study was done on the potential benefits of a pre-stimulation period [15], finding it not to have a noticeable effect either way on experimental results. The topic of pre-

stimulation during VNS application is worthy of further investigation in both acute and chronic settings.

No correlation, however, was found between different profiles of electrical stimulation through our cuffs with varying CNAP responses, and attenuation of FG transport in the nerve. We surmise that electrophysiological signals, while potentially affected by surgical nerve cuffing, are not alone, a conclusive indicator of potential neural damage as CNAP response can still be present in the absence of efferent FG transport.

In addition to the lack of retrograde transport integrity, we verified differences between chronically and acutely cuffed nerves in two separate measures of vagal physiological control. While noisy and variable in raw concentration levels, we nevertheless noted significant variations in plasma cytokine responses between acutely and chronically cuffed data samples when presented as percentages of an overall cytokine make-up: arguably a more robust method of analysis [103]. We discovered a complete lack of cytokine modulation through VNS when chronic cuffing was applied. Meanwhile, the influence of stimulation on gastric emptying was also revealed to be inconsequential when chronic cuffing was utilized. We did not endeavor to interpret specific physiological effects of either acute portion of these tests here, as they will be thoroughly scrutinized in separate and ongoing studies for future publication. Our primary finding was an established disparity between acutely and chronically cuffed vagus nerves, and evidence of compromised vagus nerve functionality when chronically cuffed.

An analysis of notable distinctions in the reviewed chronic VNS literature allows us to discuss potential pros and cons of prior studies. Nearly half of the reviewed studies utilized industry-made helical electrodes (Cyberonics). This helical design has shown to be mechanically advantageous in reducing mechanical stresses directly to the nerve in human subjects [147]. In rat subjects, the implantation involved wrapping the electrodes around the entire carotid sheath rather than the nerve being dissected away from the carotid artery before being independently cuffed [17, 95, 105-107, 113]. Anchoring to the artery conceivably allowed more support for the cuff and significantly reduced the mechanical manipulation to the nerve itself, but also likely resulted in less surface contact of the electrode with the nerve and, expectedly, a less-focused

stimulation to the nerve. It is unlikely that such an arrangement would be sufficient for studies wishing to selectively stimulate specific fiber types and accurately record CNAP responses in a closed-loop arrangement. It would be pertinent to explore the effect this cuffing strategy might have on retrograde tracer transport.

A second noteworthy difference in reviewed publications was in the method and length of stimulation employed. Most studies utilized a chronic stimulation strategy that stimulated the nerve for continuous stretches throughout days, weeks, and even months which is inconsistent with our singular five-minute stimulation in response to an acute LPS injection. It is possible that effects of chronic stimulation can overcome inhibition of vagal efferent fibers over the course of time with repeated application, working through separate secondary para-sympathetic pathways. It is also feasible that over the course of time parts of the nerve interface did heal and allow some function of the vagal efferent fibers [146, 148, 149]. This, however, is not supported by our results that showed no improvement of FG transport over 13-71 day recovery periods.

In summary, despite the body of previously performed studies utilizing chronic nerve cuffing for VNS trials, we believe we are the first to employ our novel combination of integrity checks of the nerve. To our knowledge, there was only one previous chronic VNS study that centered on inflammatory effects in the gastric region of rats [95]. While their results are compelling, the significance of cytokine modulation they reported is in contrast with our findings. Variations in cuff designs, surgical techniques, or stimulation strategies they utilized could account for this, but without further study on the integrity of nerves prepared with theirs' and others' methods, we can only speculate. We have, however, presented evidence of physiological degradation of vagus nerve functionality when utilizing our methods of chronic cuffing for VNS therapy in rats in the form of suppressed efferent FG transport, and altered effects on inflammatory cytokine modulation and gastric emptying. To confidently and reliably continue advancement in the science of chronic VNS, such effects should be seriously considered and further investigated by the VNS community as a whole.

4.5 Chronic Cuffing of Anterior Gastric Subdiaphragmatic Nerve Branch

4.5.1 Protocols

In addition to the chronic cuffing experiments outlined above, we also performed a small subset of seven rats with chronically cuffed anterior gastric nerve branches. To do this, we followed similar surgical protocols to those in Aims 2 and 3. The surgical cuff placement was like that in Aim 2, but done chronically, in a sterile surgical setup, and the cuffs were anchored as in Aim 3. The cuffs were similar to those outlined in Aim 2 but were attached to a transdermal connector port behind the shoulder blades as described above in Aim 3 surgical methods.

Each rat recovered for ~13 days after implantation before LPS administration, stimulation, blood collections, and perfusions. We followed all protocols for terminal stimulation experiments done in Aim 2, as the rats were knocked out with isoflurane and anesthetized during the blood collection period with a ketamine/xylazine cocktail. The rats received FG injections as done in the chronic cervical experiments ~5 days before the terminal stimulation experiment.

4.5.2 Results and analysis

FG images of the perfused medulla samples showed a similar pattern of efferent fiber damage to those of chronic cervical cuffing experiments. In this case, the damage was more selective and tended to be isolated to the fibers related to the anterior gastric nerve branch as shown in Figure 4.12. We can see that the inward section of cells normally illuminated by efferent transport of the anterior gastric nerve fibers has been severely depressed. Meanwhile, the outer section of cells representing the uncuffed accessory celiac efferent fibers remain bright. There remains a small number of illuminated cells in the areas populated by the anterior gastric nerve. These cells could be the result of either a few unaffected efferent gastric fibers, or could be strictly due to uncuffed hepatic efferent fibers as they have been shown to transport into that area of the medulla as well [120]. Analysis of the nodose of these animals showed no noticeable difference between FG illumination of the left and right vagus nerves (not shown), complementary to those seen in the cervical study.

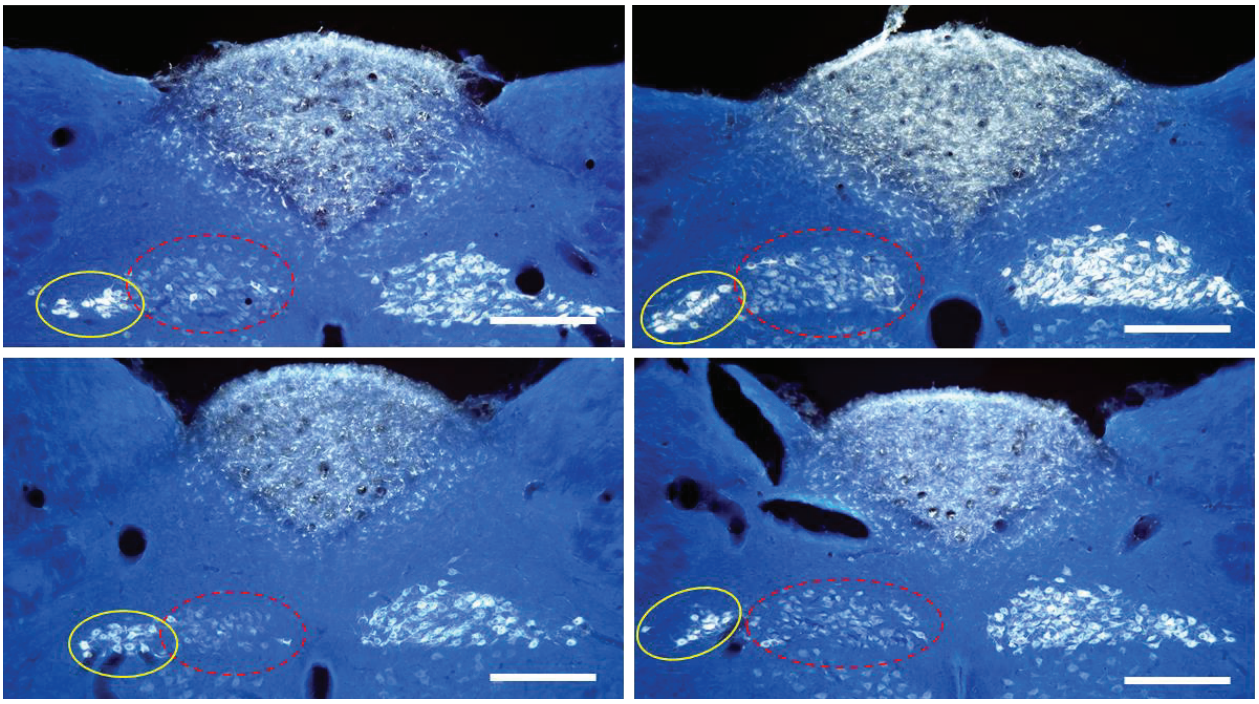

Figure 4.12 Fluorescent images of medulla samples from multiple rats with chronically cuffed anterior gastric branches of the left cervical vagus nerve. All four images show severely or completely suppressed gastric efferent FG transport to the medulla (inside red dashed ovals), while strong transport remains from accessory celiac efferent fibers (inside solid yellow ovals). Scale bars = 250 microns.

In addition to analyzing the FG images, we tested concentrations of serum cytokines as was done in Aims 2 and 3. When comparing the resulting TNF-α levels in the chronically cuffed rats versus those of the acute subgroups from Aim 2, we saw that the chronically cuffed, and presumably damaged, efferent fiber animals had an increased rise in cytokine levels 120 - 150 minutes after stimulation similar to that of the acute animals that received an anterior gastric branch efferent vagotomy. This can be seen in Figure 4.13. While the results are still quite variable with deviations outside of the standard 95% confidence interval, the pattern is further evidence to match our conclusions from Aim 3.

We therefore have hypothesized that chronic cuffing of the subdiaphragmatic vagus branches has the same damaging effect as we saw when chronically cuffing the cervical vagus nerve.

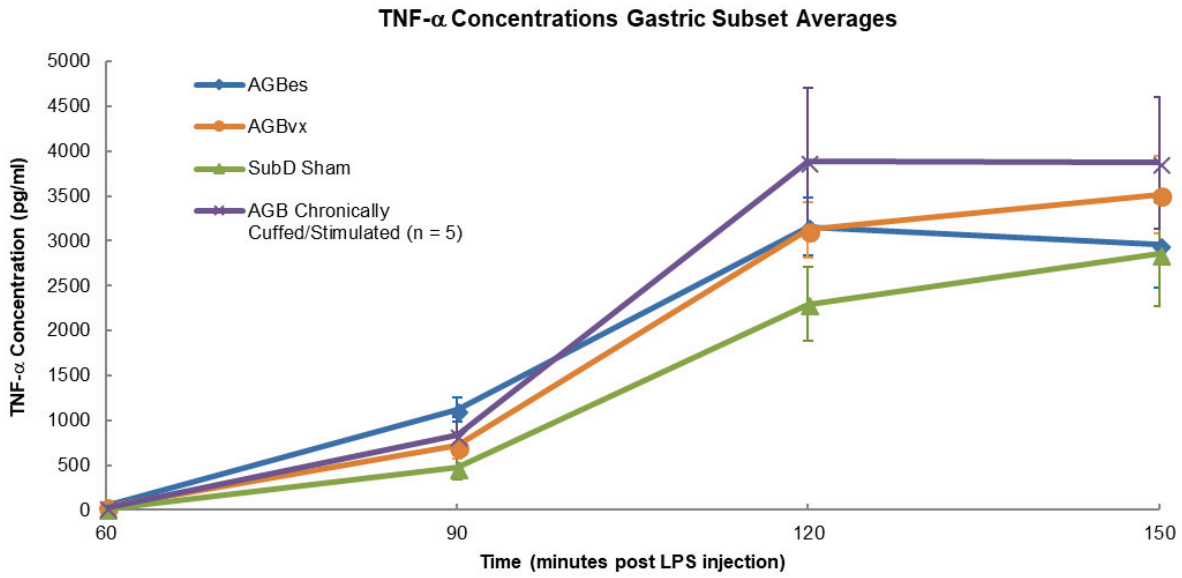

Figure 4.13 Average serum TNF-α levels of anterior gastric stimulation subsets performed acutely versus a chronically cuffed subset. Curves have been shifted to have matching starting points similar to Aim 2, but without curve interpolations. Error bars, s.e.m.

4.6 Summary/Impact

As outlined in the discussion section, this study advanced our knowledge of chronic nerve cuffing by presenting compelling evidence of previously unknown nerve damage. The lack of FG transport and attenuated physiological effects of the chronic nerve cuff implantations are a new discovery. It is very possible that if a similar analysis was done on other previous chronic nerve cuffing studies in rodents, or even larger animals, that similar results would be seen, and could call into question previously established hypotheses.

The issue of underlying and previously undetected damage by chronic electrodes has also been shown by Goss-Varley et al [150] in a study of intracortical microelectrode implantation. Along with our results presented here, functional deficits attributable to the implant itself are shown to be present. This is a potentially serious issue as we progress towards further clinical use of implanted electrode devices and deserves more attention and dedicated study by the implantable technologies community.

5. FUTURE WORK: INITIAL STUDIES

5.1 Motivation

Given the evidence of difficulty in effective chronic cuffing of rats, alternative methods need to be considered for continued animal research and clinical applications. Small animal models are limited in many respects as test subjects due to size and physiological differences between them and an actual human model. Therefore, we must think outside of the box to find replacement methods and models that will effectively aid in research aims.

As a lab, CID has already thought about some alternate methods, and has done initial work on them that show promise for continued use going forward. I have outlined a few of them in this section that I either designed or supported in my time here.

5.2 Initial VNS Study in Pigs

Aim 3 demonstrated an unintended and previously undetected issue with chronically cuffing the vagus nerve in a rat model. Many factors could contribute to this, but one major issue is undoubtedly the size of the model. It is not hard to hypothesize that the sheer size of the cuffs in relation to the nerves being cuffed create some variety of physical damage. The issue is that while researchers are continuously improving materials for better biocompatibility and smaller size, we are likely not yet to a place where we can effectively and safely cuff these small nerves without a high risk of some damage.

However, humans have been implanted with vagus stimulation cuffs for years now, and while there are inherent side-effects and the potential for undetected damage remains, it would seem that a larger nerve is better suiting to withstand the rigors of chronic cuffing.

We therefore decided that a larger animal model, in our case a pig would provide a better means of chronic testing of VNS. Literature review of the topic revealed that a good number of studies have looked at either effects of LPS administration and cytokine responses in pigs [151-155] or

VNS in pigs for multiple purposes [156-161], but to the best of my knowledge, no group had previously used LPS and VNS in a pig model to look at the inflammatory cytokine effects of the gastric region. Given the background literature, it made sense to progress forward with an initial study to explore inflammatory cytokine effects of chronic VNS in a pig model.

5.2.1 Methods

5.2.1.1 Device and materials

To successfully accomplish a chronic VNS study in a pig model, a significant effort to make multiple changes to the Bionode device, its packaging, and the cuff electrodes was required. A brief overview of the changes made are outlined here.

5.2.1.1.1 Pig stimulation and recording cuffs

Stimulation and recording cuffs were significantly increased in size. By measuring actual cervical vagus nerves from pig subjects, we determined a cuff of ~3 mm inner diameter was required for our planned testing on a 30 kg pig. This is beneficial as this is also a common size for human VNS cuffs (http://eu.cyberonics.com/en/vns-therapy-for-epilepsy/healthcare-professionals/vns-therapy/about-products). Given the larger size of the cuff, we determined that a horizontally threaded design such as that used in the rat cuffs would be the best option. It allowed a pattern of PtIr wire that could encompass most of the inner circumference of the cuff while also keeping it tightly threaded to the cuff material to prevent loose wires, and it still allowed the cuff to be flexible and durable during implantation. Horizonal thread loops were ~1 mm in length (20 – 40 loops per cuff electrode), and the threading loops were placed ~1 cm apart from each other (center to center). The outer wire loops were covered with fast curing silicon adhesive (Med2-4213; NuSil; Carpinteria, CA) to isolate them and prevent shunting of current outside of the cuffs. Cuffs used for chronic pig implantation can be seen in Figure 5.1.

I tested new cuff materials such as polyurethane but found them to be both too rigid, and susceptible to deformation when curing silicone adhesive to the cuff during fabrication.

Tying the cuffs shut with suture was discouraged by our surgeon so I instead left a length of tubing on each end of the cuff and cut a spiral shape into it that would allow the edges of the cuff to be wrapped around the nerve for added stability. This is similar to how human VNS cuffs are designed and implanted [14].

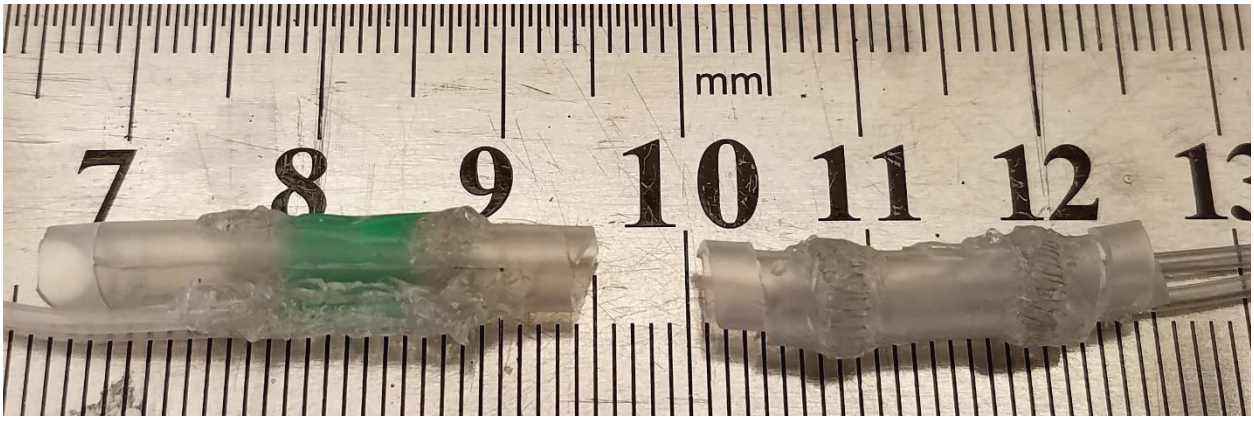

Figure 5.1 Stimulation and recording cuffs for cervical vagus nerve of pig. Cuffs each featured two electrodes made of horizontally threaded PtIr wire surrounding the inner cuff circumference. Edges of cuffs were cut in a spiral to improve stability on the vagus nerve.

Electrochemical performance of our pig cuffs proved to be excellent. We tested multiple cuffs for implantation, and comparatively tested a human Cyberonics VNS cuff. The Cyberonics cuff produced an EIS impedance measure of ~400 Ω at 1 kHz while our pig cuffs showed impedances of 200 - 300 Ω in most cases.

5.2.1.1.2 Stimulator changes

Upon multiple literature reviews, we determined that a stimulation amplitude of 1 mA (the max that our default stimulator implementation would supply) may not be enough to effectively stimulate at needed levels for a larger animal. The stimulator limits of human VNS devices can reach 3.5 mA in charge [25]. I therefore decided to use this as our benchmark.

The change was fairly simple. We needed to replace the reference resistance of the HCS on the Bionode from 800 Ω to 250 Ω, which changed our max current to 3.6 V. We were, of course,

still limited by the voltage headroom of the device, but since our stimulation electrodes showed such small impedances, this was a minimal concern.

5.2.1.1.3 Powering changes

Powering of the device was a major issue for the experiment. The Bionode had previously been designed for wireless powering in a very specific cavity for rodent use or to be powered with a powering coil wand with a matched network to that of the Bionode coils. A pig would not fit in the cavity, nor was it realistic to build one of the size needed to house a pig. We had previously utilized tethered powering in rat subjects but decided against that option as the pigs could easily damage a tethered port on the surface of their skin, and it would add significant complexity to the chronic surgery.

The decided solution was two parts: a battery powered Bionode, and an adjusted coil to turn on and re-charge said battery. We decided to use a rechargeable CR1620 Lithium cell battery due to size and capacity. The required circuitry (power management integrated circuit (PMIC) and turn-off switch) were added to integrate the battery into the Bionode circuity and a control was added to the Dataview interface that allowed us to turn the battery off when not in use.

The battery could be turned on (and recharged) by use of an inductively coupled coil wand. An issue however was noted after the first device was implanted. The device could not effectively be turned on inside of the pig with the standard coils and wands due to the tissue thickness of the pig, so we had to use a larger transmit and receive coil to get better coupling at a further distance. Because the transmit coil was larger, the inductance was larger. Further, because our impedance matching network is an L-match network using only capacitors, we physically could not realize a capacitive only L-match between the large inductance and the load at 340 MHz (the Bionode's default powering frequency). We had to use a matching network using inductors. However, inductors are very low Q for any size larger than a nano-Henry at 340MHz, which would result in losses across the matching network and low power transfer efficiency. As a result, we needed to lower the frequency of operation so that we could realize proper capacitive L-matches for the impedance matching network for the increased inductance. We picked 13.56 MHz because it's a

popular medical device ISM band as per the FCC and is a legal operating frequency for our devices.

Once the Bionode devices and powering wands were tuned to operate at 13.5 – 13.9 MHz, I was able to turn on and recharge devices at a distance of five inches or more and was able to turn the implanted devices on inside of the pig. Recharging the device while in the pig was still a challenge and was only minimally effective. This coil set-up is demonstrated in Figure 5.2.

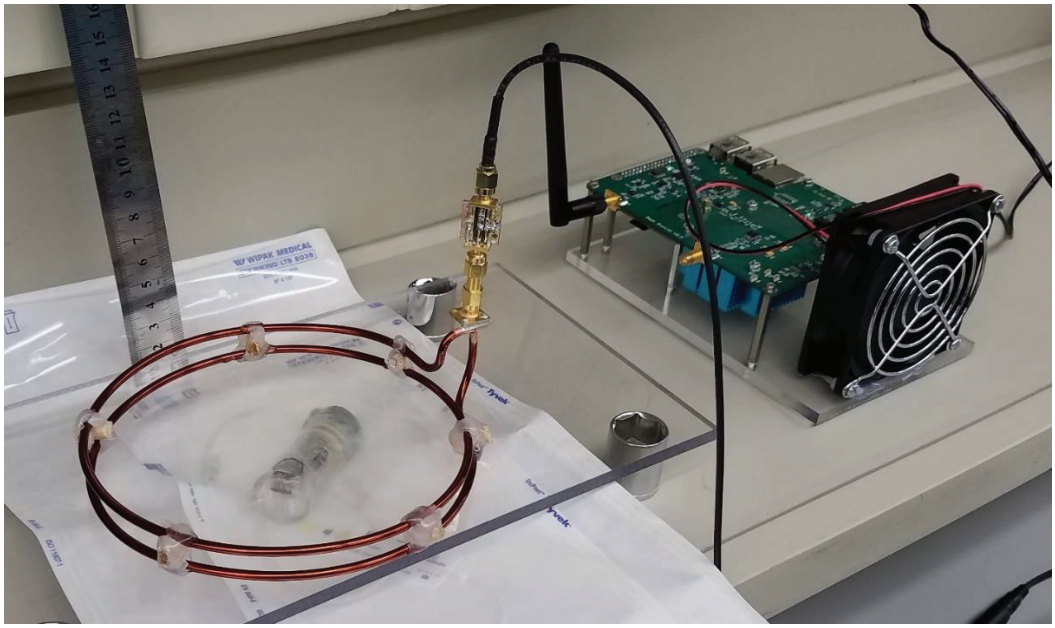

Figure 5.2 Pig Bionode re-charging set-up. Large charging coil wand is connected to base station for powering and is transmitting charge at ~13.5 MHz to the sealed bionode device below.

5.2.1.1.4 Packaging changes

Packaging of the Bionode remained very similar to that of previous versions, but a battery needed to be added. The battery could not be inserted into the bottom of the package due to its interference with the powering coils. Therefore, we added the battery to the top of the package, as can be seen in Figure 5.3. This added significant complexity to the packaging as the battery

also had to be connected through the feedthrough cap along with the recording and stimulation leads, while also being fastened in a flat position above the connected leads.

Insulation and sealing with the fast curing silicon adhesive and medical grade epoxy became a hinderance due to the tight space created between leads and limited access to these spaces. The fast curing silicon adhesive was inserted into the feedthrough cap well from the side and once cured, the entire device went through multiple rounds of hand applied coats of epoxy to seal it. This proved to be a very in-efficient and imprecise method that led to leakages in some devices. It also led to many design improvements that have been made for the new Bionode 5.0.

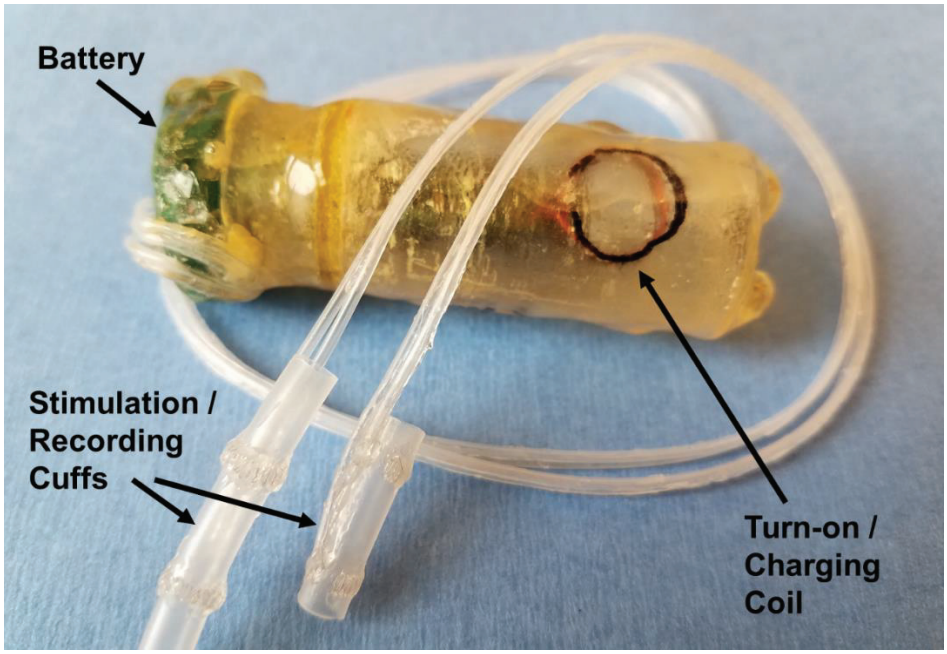

Figure 5.3 Packaged Pig Bionode for chronic implantation. Device dimensions were ~60 mm long and ~22 mm in cylindrical diameter.

5.2.1.2 Experimental protocol

Protocols for chronic pig experiments mirrored closely those for the chronic rats in Aim 3. Surgically, a sterile environment was kept for all procedures. The left cervical vagus nerve was exposed first, then a pocket for the Bionode implant was formed above and behind the left shoulder blade of the pig. We tunneled the stimulation and recording cuffs and leads to the

cervical vagus using a trocar system. The stimulation (rostral) and recording (caudal) cuffs were then carefully wrapped around the left vagus nerve at a maximal distance from each other (17 – 25 mm apart, center to center of cuffs). Once the cuffs were in place on the nerve, we closed and sutured the cervical surgical site, and then pushed the device into place in the pocket behind the shoulder blade and sealed that incision site.

Before moving the pigs for recovery, we turned the Bionode on using the 13.5 MHz powering wand and tested for functionality. The animals were then moved and given 13 – 21 days to recover.

An important lesson that we noted during these surgeries was that the shape of the Bionode package should be adjusted for future possible pig implantations. The cylindrical shape of the pig Bionodes proved to be an issue due to the difficulty we encountered trying to suture the packages in place, and their resulting tendency to rotate during the surgical implantation. As a result, the receiving coil in the Bionode package could shift from the planned parallel position to the skin's surface and cause issues with turning on and charging the devices once implanted.
In the future, a flatter and wider package would be beneficial to prevent these issues.

The day before terminal experimentation, we anesthetized the animals and tested again to ensure that the devices would turn on and attempt to charge the batteries. Once verified, the pigs were outfitted with catheters for LPS injection and blood collection, and then placed in Pigturn caging facilities (BASi; West Lafayette, IN) and connected to Culex Automated Blood Sampling systems (BASi; West Lafayette, IN) cages. The Pigturn and Culex setup and Bionode interface used can be seen in Figure 5.4.

On the day of the terminal experimentation, we followed procedures that again mirror the rat experiments in Aim 3. We collected blood samples 30 minutes before injecting LPS and every 30 minutes after LPS injection for 180 minutes. LPS was mixed with sterile saline and sonicated for 30 minutes prior to administration at a concentration of 7 μg/kg. We determined this to be a sufficient dosage based on prior literature [151] and our own prior acute tests. A 5-minute stimulation treatment was applied 30 minutes after LPS administration using 250 μs square bi-

phasic stimulation pulses at 5 Hz frequency. We determined the amplitude to use based on prior CNAP responses recorded at the time of implantation. After the final blood collections, the pigs were euthanized, and the devices were explanted for post-experimental analysis.

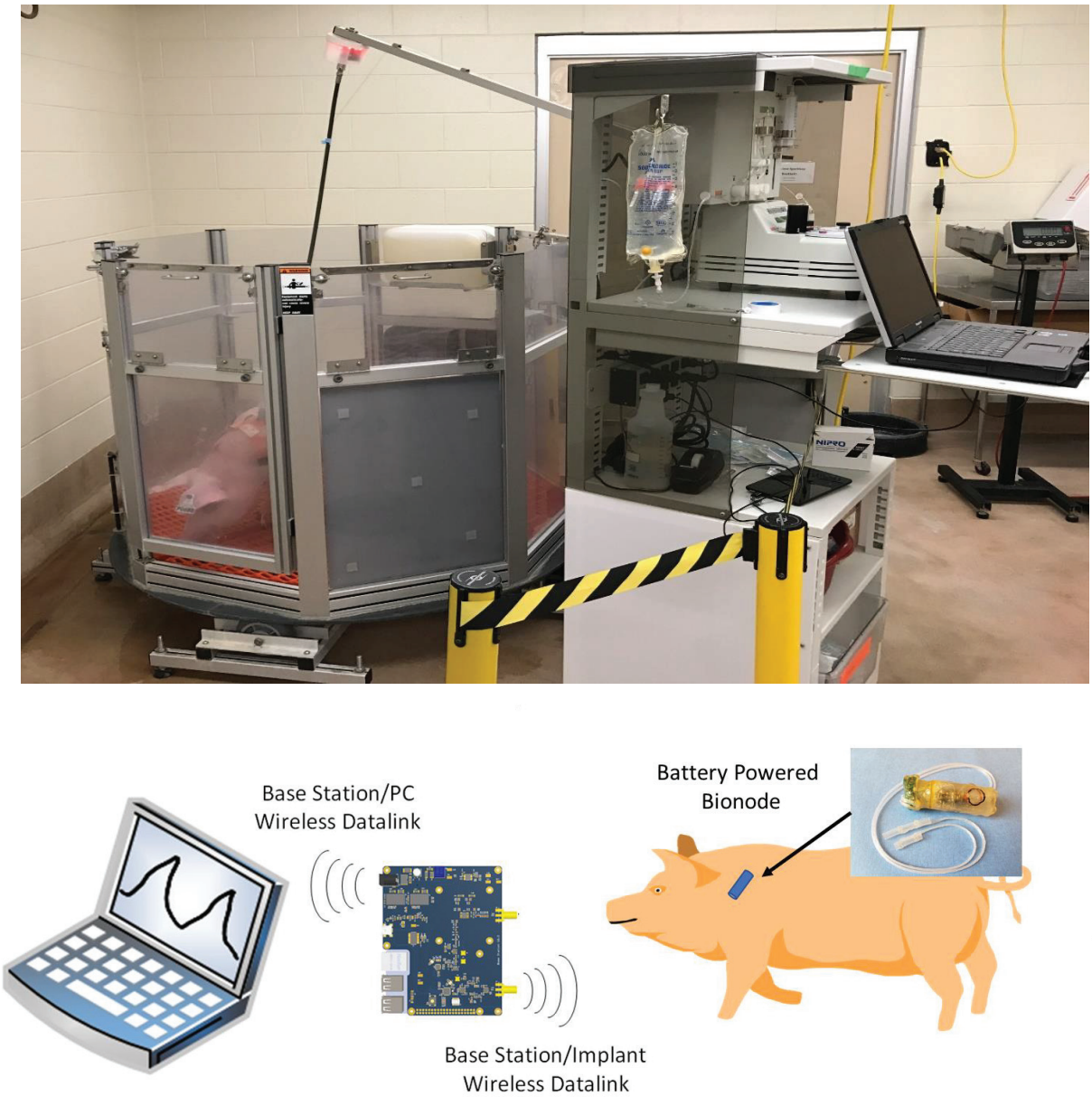

Figure 5.4 Image (top) showing the Pig-Turn Culex system for chronic blood collection in moving animals. Bionode System illustration (bottom) showing the stimulation and recording system includes implanted Bionode with cuff electrodes; base station; and computer terminal with GUI.

5.2.2 Results

We unfortunately only successfully performed three chronic surgeries during this initial experiment phase. Four animals were implanted with devices, but one suffered an infection and had to be euthanized early. Of the remaining three, one was implanted with a dummy device, while the other two were successfully implanted and tested on the day of implant. We, however, discovered on the day before terminal experimentation that one of the implanted devices had failed to hold its charge and could not be recharged. We attempted to power it manually on the day-of the experiment with the powering wand coils, but that proved unreasonable with a freely moving pig subject. Therefore, only one of the three animals received the planned stimulation treatment.

Fortunately, the small sample size did reveal some encouraging results to look at. In the successfully simulated animal we were able to consistently record CNAP responses both on the day of implantation and on the day of experimentation (see Figure 5.5). The CNAP responses also showed to be very similar at similar stimulation amplitudes. This indicated that the cuffs were successfully implanted and did not significantly shift or degrade during recovery. It was also a good indication that our cuffs and device were sufficient to stimulate the required levels for neuromodulation (though we did not formally test for maximal CNAP response).

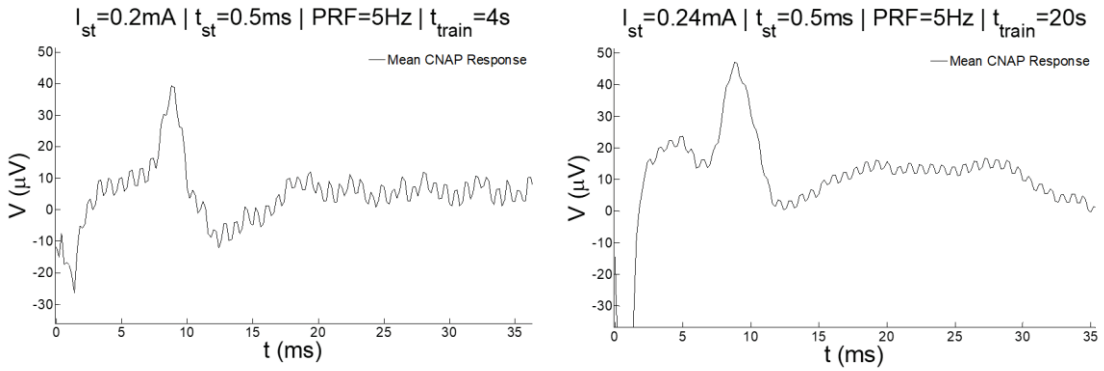

Figure 5.5 CNAP response from chronic stimulation in pig. Day 1 (left) shows prominent C-fiber response at 9 ms. Day 13 (right) shows prominent C-fiber response at 9 ms, and less prominent B-fiber response (likely multiple responses) at around 5 ms.

In addition to CNAP response, we were able to analyze inflammatory cytokine responses from the blood (plasma) samples collected. Flow cytometry methods used for pig samples were similar to those outlined for Aims 2 and 3, but the panel included a slightly different mix of cytokines (as a pig's biology varies from that of rodents). Cytokines analyzed included IL-1 , IL-1ra, IL-4, IL-6, IL-8, IL-10, IL-12, IL-18, INF-γ, GM-CSF, and TNF-α. Of these cytokines, only four of them showed significant trends: the commonly studied TNF-a (see Figure 5.6) and IL-6 (see Figure 5.7), and the less studied IL-8 (see Figure 5.8) and IL-1 variants.

It is interesting to note that all shown cytokines displayed significantly higher levels in the simulated samples than they did in the non-stimulated samples. While it is difficult for us to make any solid conclusions based on these small samples sizes, the data does appear to indicate a pro-inflammatory effect of the stimulation. While the modulation is not in the desired direction, as we seek reductions in levels, this could in fact be due to suboptimal stimulations causing pro-inflammatory effects with afferent stimulation without activating anti-inflammatory efferent pathways. Further studies should be performed.

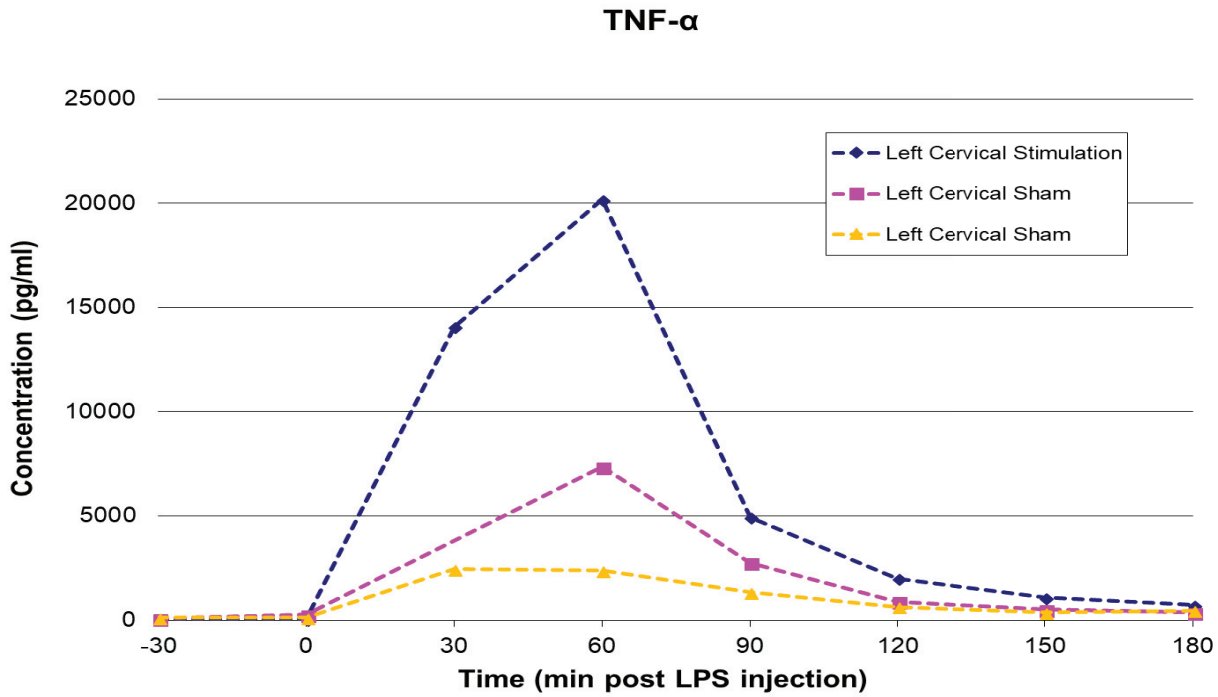

Figure 5.6 Plasma TNF-α levels after IV LPS injection into chronically cuffed pigs. Levels were significantly higher in stimulated subject than those not receiving VNS.

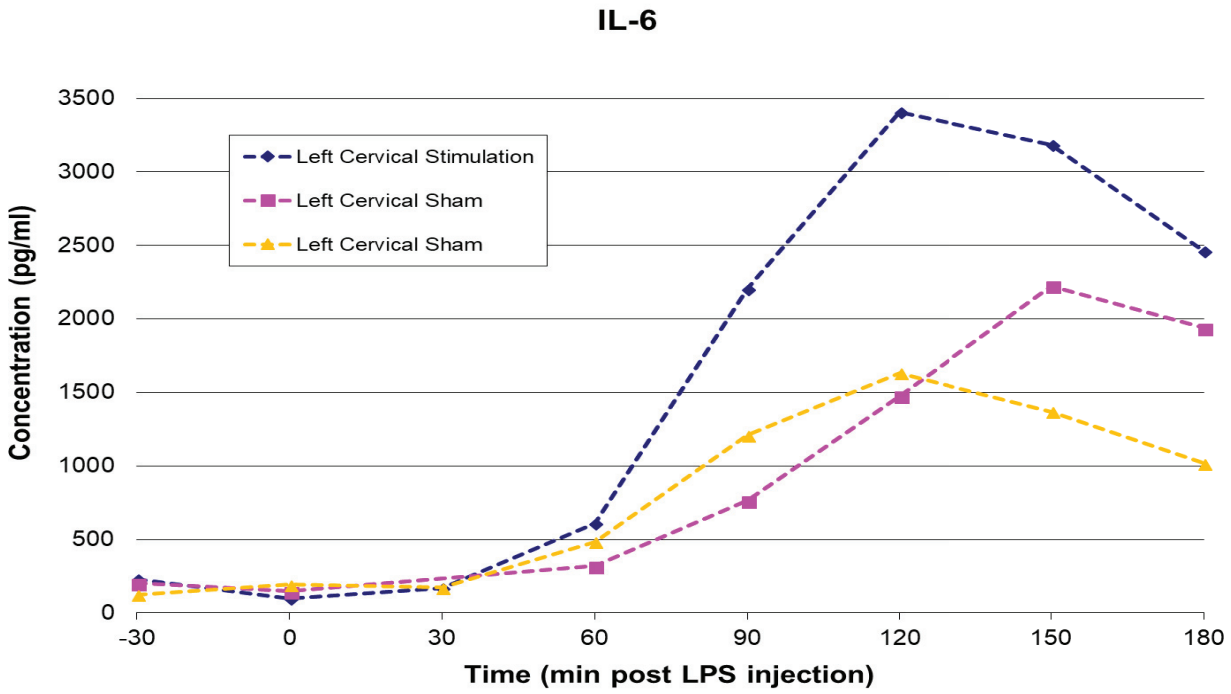

Figure 5.7 Plasma IL-6 levels after IV LPS injection into chronically cuffed pigs. Levels were significantly higher in stimulated subject than those not receiving VNS.

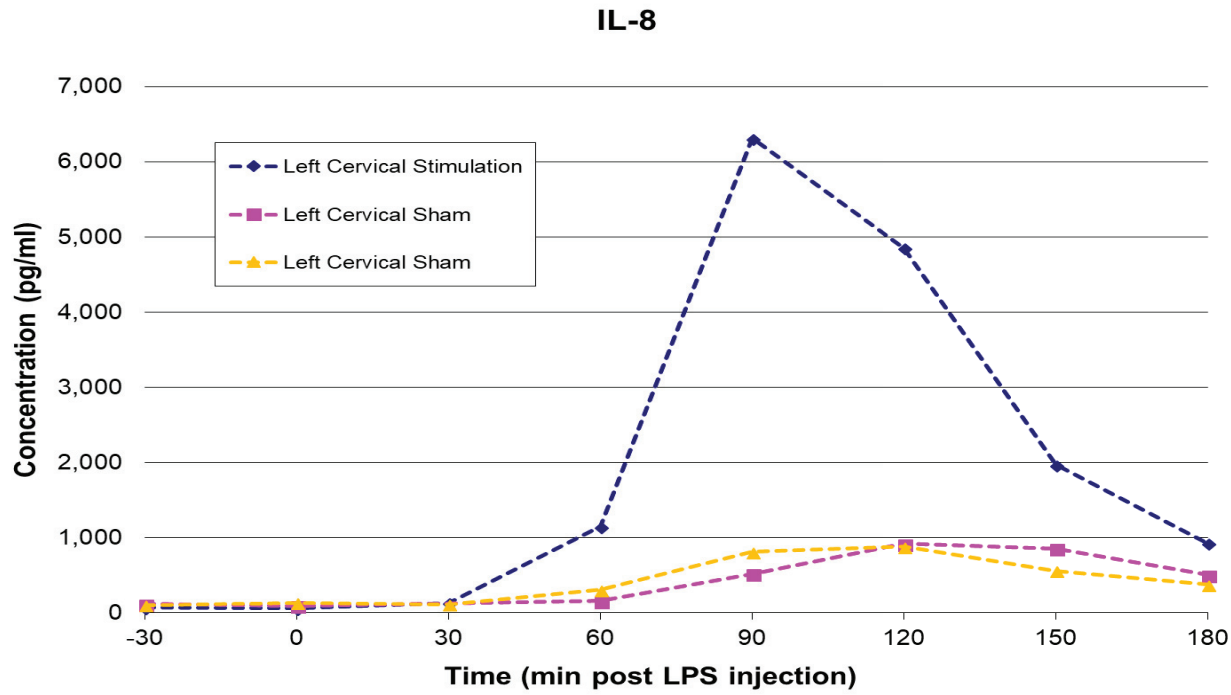

Figure 5.8 Plasma IL-8 levels after IV LPS injection into chronically cuffed pigs. Levels were significantly higher in stimulated subject than those not receiving VNS.

5.3 Initial Study of Ultrasound Stimulation

A second alternative method to physical cuffing of the nerve for VNS that we have looked at is Ultrasonic stimulation. I assisted with an initial study of this in conjunction with our Aim 2 research. The result was a paper lead-authored by Kelsey Wasilczuk and co-authored by myself titled "Modulating the inflammatory reflex in rats using low intensity focused ultrasound stimulation of the vagus nerve," that has been submitted to the journal Ultrasound in Medicine and Biology in May of 2018 [162].

The abstract from that paper reads as follows. "Tumor necrosis factor alpha (TNF-α) is linked to several chronic inflammatory diseases. Electrical vagus nerve stimulation reduces serum TNF-α levels, but may cause chronic nerve damage and requires surgery. Alternatively, we propose focused ultrasound stimulation of the vagus nerve (uVNS), which can be applied non-invasively. In this study, we induce an inflammatory response in rats using LPS and collect blood to analyze the effects of uVNS on cytokine concentrations. We applied one or three 5-minute pulsed focused ultrasound stimulation treatments to the vagus nerve (250 kHz, ISPPA= 3 W/cm2). Animals receiving a single ultrasound application had an average reduction in TNF-α levels by 19%, similar to the 16% reduction observed in electrically stimulated animals. With multiple applications, uVNS therapy statistically reduced serum TNF-α levels by 73% compared to control animals without any observed damage to the nerve. These findings suggest that uVNS serves as a suitable way to attenuate TNF-α levels."

The reported TNF-α reductions can be seen in Figure 5.9, and led us to deduce the following in the submitted paper. "With the ability to attenuate serum TNF-α levels in the blood, we see uVNS as a promising alternative therapy for chronic inflammatory diseases. With the single application of uVNS showing similar reductions to electrical VNS (eVNS), we believe it could be as, or even more, effective as eVNS. Also, since critically ill or elderly patients are not good candidates for surgery, uVNS could provide an alternative way to relieve symptoms [163]. Finally, the non-invasive nature of focused ultrasound therapy will reduce risks and costs associated with traditional eVNS therapy. This therapy could provide people the opportunity to choose a non-invasive, non-pharmaceutical treatment option."

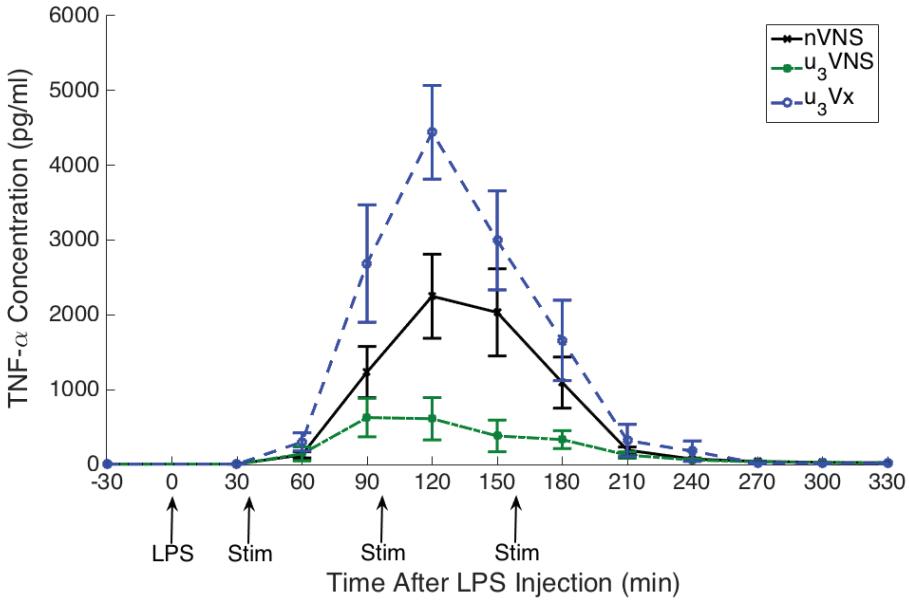

Figure 5.9 TNF-α Response to Triple Stimulation: Plot shows average serum TNF-α levels for each animal group. Animals with a cervical efferent vagotomy that were given three ultrasound stimulation treatments (u3Vx) (n=4) have statistically significant higher levels at t=120 from both those given three ultrasound stimulation treatments with no vagotomy (u3VNS) and those given no stimulation (nVNS) ($p<0.05$). u3VNS group has a statistically lower level of TNF-α at t=120 ($p=0.04$). Error bars, s.e.m. [162].

5.4 Wireless ANC

ANC, as presented in Aim 3 has the potential to revolutionize stimulation treatments by providing real-time feedback of CNAP responses to electrical stimulations, and calibrate the stimulation using the recorded CNAP responses to a specific percentage of the optimal nerve response. Originally developed to be used by a benchtop DAC and current source controlled by a Matlab algorithm, our lab attempted to make ANC wireless by conforming the software algorithm to work with the Bionode and its Dataview interface through Matlab. Jui-Wei Tsai integrated the Matlab algorithm to communicate with the Bionode software, and I, with the assistance of Matthew Ward, made it work wirelessly on an acute benchtop setup as shown in Figure 5.10. This accomplishment was presented by myself at the 2016 International Conference of the IEEE Engineering in Medicine and Biology Society in Orlando, Florida [164].

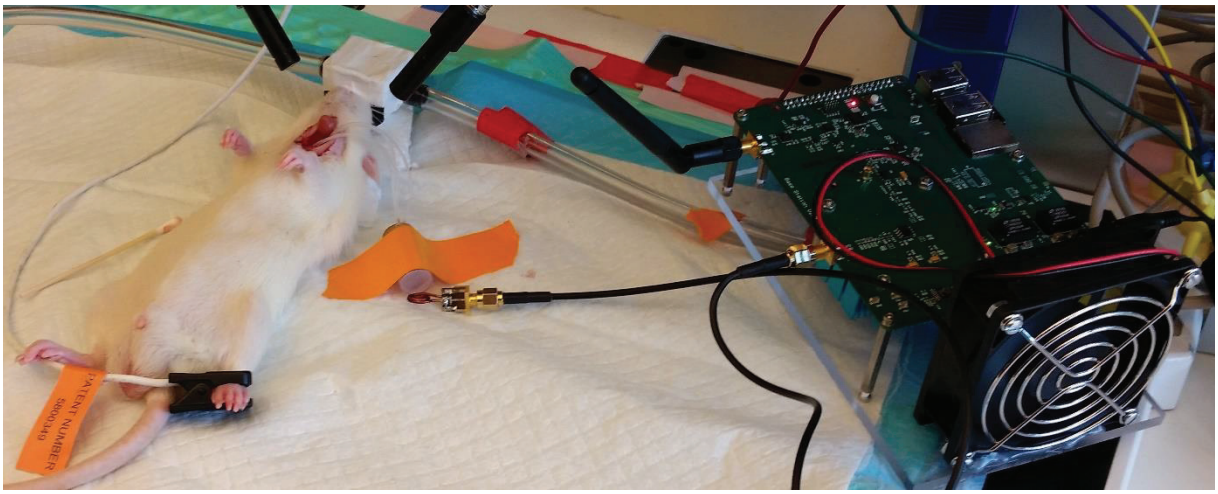

Figure 5.10 Experimental wireless ANC setup. Standalone bionode is placed near the rat with attached stimulation and recording electrodes attached to the left vagus nerve of the rat. Device is being powered with inductively coupled coil wand run from the base station.

The ANC mathematical model running on the Bionode will extract fiber-type specific activation information as a percent of maximal activation for that fiber type in that nerve and patient [42]. This introduces constant-activation stimulation and preferential fiber-type recruitment for maximal therapy with minimal side effects. This implementation represented a dramatic advancement in capabilities and utilization over a tethered ANC setup, and allowed stimulation, recording, and controls all on this singular implantable device. In Figure 5.11, we see 48 trials of B-fiber selective vagal nerve stimulation (four second durations each) in a rat. The cumulative average of the B-fiber responses tracked closely to the desired activation level in the steady state and adjusted to changes in the desired activation level using variable stimulus pulse durations. This closed-loop tracking and updating allowed for specific nerve activation, which could translate to accurate dosing of stimulation therapy in the future.

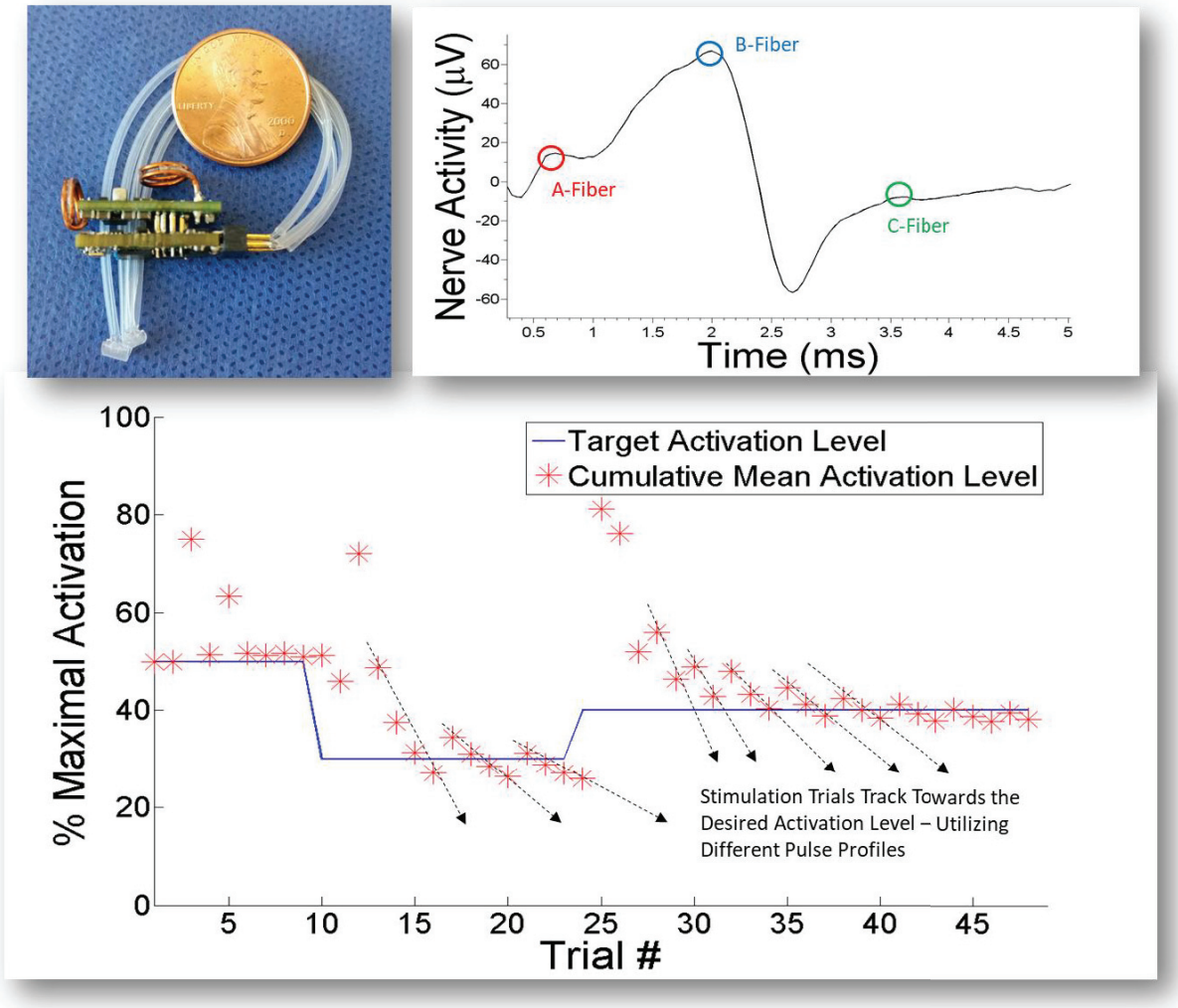

Figure 5.11 Clockwise from top left: Bionode device with vagus nerve cuffs attached, outside of package; Nerve fiber responses recorded by Binode; Nerve response prediction of B-fibers of a rat vagal nerve—arrows show the algorithm tracking to target activation level by varying stimulation amplitudes at different pulse widths [164].

This early success, however, did not translate into a consistent and usable platform. Despite many attempts by myself and Kaitlyn Neihouser during both acute and chronic experiments, we were rarely successful in making the algorithm work as intended. There were noted issues across the spectrum of software and hardware. Since ANC required a complete and uninterrupted set of calibration stimulations from a responsive nerve, there were many places where the calibration process could be interrupted.

Many of the noted issues are listed as follows:

Bionode device issues:

- Charge imbalances in stimulation profiles caused issues in stimulation artifact cancellation and CNAP detection.
- Communication latency issues due to poor antenna reception caused missed packets and data which affected CNAP detections
- Power latency issues caused stoppages in the calibration process and required a full restart.
- System noise often occurred and affected CNAP detections.
- Movement artifacts affected CNAP detections in chronic tests with un-anesthetized animals.
- Lacking grounding plane on stimulation cuff ground reference caused distorted artifact cancellations.

ANC algorithm issues:

- Algorithm could not set or account for stimulation current/voltage limits. If a maximal nerve response was not reached before the device stimulation limits, there was no default response and the algorithm would continue with false readings. Also, there was originally no way for the user to easily set a stimulation limit. Therefore, the algorithm during calibration could reach dangerously high levels of stimulation if the device allowed for it.
- Zero stimulation loops often occurred where the stimulation level would go to zero and could not increase again to calibrate, requiring the user to re-start the program.
- There were no options for a manual calibration if the automatic calibration did not work.

Given the above issues, utilizing ANC consistently was not an option in Aims 2 and 3, but with recent improvements to the Bionode stimulator, antenna, and battery circuitry, it may be worth attempting to troubleshoot the algorithm once again to make it reliable on a truly wireless and implanted Bionode device in the future.

5.5 Summary/Impact

New findings in research are only useful if they are followed up with new studies that can utilize advancements, data, and lessons learned to improve on techniques. Given our Bionode improvements in Aim 1, and our biological discoveries and new methods formulated in Aims 2 and 3, any of the three future studies presented in this section make sense to pursue going forward.

6. SUMMARY AND CONCLUSIONS

6.1 Explanation of the Problem

Inflammation remains a likely cause or contributor to many diseases, ailments, and syndromes in humans. Research of inflammation is very broad and diverse, leading to a copious variety in methods and treatment ideas. The ultimate goal remains the same though: to treat those with conditions and to improve the lives of human beings.

Among treatment options, VNS (and other electroceuticals) remains on the forefront of modern medicine. While already approved and used for those with epilepsy and drug resistant depression, VNS holds promise as a remedy for countless other inflammatory conditions, as well as many vagal-related ailments not directly associated to inflammation.

Ultimately, VNS remains a young therapeutic option in modern medicine. The complex biological mechanisms of the vagus nerve on the body, and the effects of stimulation on those mechanisms, are still not well understood and often highly debated. Variation in research methods and in turn, results, causes the research community to often backtrack looking for answers and possible mistakes before moving forward with more confidence. The study I have presented here follows along that exact mindset.

I looked at multiple aspects of VNS research including devices, interfaces, and experimental and data analysis methods.

6.2 VNS Device Development: Progress and Significance

Problem and previous status. All research is limited by the tools available to complete exploration goals. While there are significant stimulation and recording options available from commercial and laboratory equipment for VNS studies, most are made with specific uses in mind and are therefore limited in their versatility.

Our Bionode device has been developed to remedy this issue to a large extent in the small university lab setting by providing us with a modular and flexible research platform that can be made relatively cheap and easy with basic laboratory resources. Early versions of the Bionode, however, suffered from significant issues that had to be solved.

What I did. I held a critical role in resolving many of the issues plaguing the Bionode and preventing its use in chronic stimulation experiments. Among the improvements made, I helped design and test the current HCS stimulation circuit, and then did benchtop and in-vivo testing and troubleshooting of the stimulator and solved the remaining issues preventing it from being safely and consistently used in chronic experiments. In addition, I played a critical role in adding new capabilities to the device circuitry such as relative impedance measurement of the stimulation line and batter powering of the Bionode.

I also developed many of the current manufacturing and packaging techniques we are using to successfully implant the Bionode chronically in animal subjects. These methods have proven reliable for use in animal studies in the CID.

In addition, I did significant research on the design and development of stimulation and recording cuff electrodes for use in our studies. The resulting cuff electrodes have now been effectively used in rats on various nerves and in pigs for VNS.

Why we care. In my time in the CID, the Bionode has gone through multiple evolutions. It has progressed from a highly unreliable prototype with limited stimulation and recording capabilities to a device that can be customized for virtually any basic stimulation or recording need, be reliably built and tested in a quick and inexpensive manner, and confidently implanted. As such, the new Bionode 5.0 is a more useful platform than others available.

While more testing needs to be done on the Bionode 5.0, including much in-vivo testing (which has already begun), we are finally in position to move forward with further miniaturizing the device (size being one of its few downsides) with ASIC implementations.

6.3 Acute Stimulation Study: Progress and Significance

Problem and previous status. The VNS community is afflicted with inconsistencies in experimental methods. With respect to studies of inflammation, replication of results is often difficult due to these inconsistencies. One unfortunate result of this trend is that researchers pursue methods that will produce better looking results, disregarding other methods that may hold more physiological significance. This is the case with LPS usage in inflammatory studies of rats, as most groups use IV injections instead of the arguably more physiologically relevant IP method.

In addition, much work has been done to define the "inflammatory reflex" of the body and methods to control that reflex with stimulation. Most of these studies, however, limit the stimulation mechanisms to the cervical level of the vagus nerve. The subdiaphragmatic nerve branches are sometimes vagotomized for effect analysis, but never actively stimulated themselves.

***What I did*.** I performed, in conjunction with Kelsey Wasilczuk, an acute set of 58 rat experiments in which we looked at the effects of IP injection of LPS and localized subdiaphragmatic branch VNS on inflammatory cytokine levels over a 6-hour period. To analyze the highly variable (in the time domain) cytokine responses, I developed and applied new methods of curve fitting and alignment of the cytokine cascades.

Using my new methods, we determined that selective stimulation of subdiaphragmatic nerve branches does induce selective modulatory effects on the resulting cytokine levels in plasma.

***Why we care*.** We presented results that indicate evident physiological differences in inflammatory cytokine responses to IP versus IV injection methods that go beyond simple variations in temporal uptake. Therefore, selecting one method based on ease of use instead of physiological relevance could be prohibitive to future translation of results to clinical applications. Fortunately, I also produced effective new analysis methods that can be used by future researchers to utilize IP injections in their studies.

We also presented evidence that selective subdiaphragmatic nerve branch stimulation can be effectively used to produce specific modulatory effects in cytokine levels. This opens the possibility of using selective combinations of subdiaphragmatic stimulation to treat specific inflammatory ailments in the future. A localized treatment option could result in better treatment results and less side effects than are seen in cervical VNS.

6.4 Chronic Cuffing Study: Progress and Significance

Problem and previous status. Chronic VNS animal studies, specifically those on small animal subjects such as rats, present many difficulties such as device and interface integration and surgical complexity. Given the many factors involved, it is difficult for a research group to account for all possible complications. Add the inconsistencies in experimental equipment and methods covered earlier, it is easy to imagine issues going undiscovered.

Chronic implantation and use of electrodes is a prime example of where complexity and inconsistencies could be detrimental to translatable experimental results.

***What I did*.** During our chronic VNS study of 53 rats, we implemented verification methods of nerve integrity that had not been used previously in similar chronic nerve cuffing experiments. Upon discovery of an underlying issue with efferent FG transport after chronic cuffing of the cervical vagus nerve, I did a comprehensive analysis of the problem and follow-up tests to determine the severity of the issue.

I also performed a thorough literature review to determine differences in methods used of other groups that had attempted chronic VNS experiments. As expected, methods varied greatly.

***Why we care*.** My presentation of never before seen evidence of efferent fiber damage due to chronic nerve cuffing brings to light significant questions about the reliability of chronic VNS in rodent subjects and possibly even in larger animals and humans. While our methods would need to be integrated and tested on other group's cuffing materials, methods, and protocols for verification, until proven otherwise, we remain skeptical of aspects of other group's chronic

results. FG testing is a verification technique that should be implemented into future chronic rodent VNS studies.

Meanwhile, alternate methods of VNS that show potential to be less invasive and damaging should continue to be investigated. Two such options, larger animal models and focused low-intensity ultrasound stimulation, were presented in chapter 5.

APPENDIX A. OVERVIEW OF STIMULATION AND RECORDING DEVICES

Application	Recording Capability	Stimulation Capability	Impedance Measure Capability	Controls (Active vs Passive)	Powering Options	Device Size	Electronics Type	Implant Capability	Tested In-Vivo	Author
Multi	4 Channels	1 Channel, Const Current, Bipolar Pulses, 0 - 1.2 mA, 9 V max	Yes	Active stimulation and recording control	Battery, Inductive power / recharge	1.9 x 1.6 x 4.7 cm, 13.9 g	PCB, COTS	Yes, glass case / epoxy coated	Yes, rats/pigs	**Bionode (2018)**
Muscle Denervation	Not presented	1 Channel, Const Voltage, Bipolar Pulses, 0 - 11 V	No	Pre-programmed	3V Li-ion battery	5.5 x 2.4 x 1.0 cm, 19 g	PCB, COTS	Yes, epoxy coated	Yes, rats	**Dennis et al. (2003)**
Telemetry Recording	1 Channel	No	No	Passive recording	Battery	1.9 cc, 3.9 g	Commercial, Data Science International PhysioTel	Yes	Yes, mice	**Weiergraber et al. (2005)**
Nerve / Muscle Stimulation	No	1 Channel, Const Current, Bipolar Pulses, 0.2 - 30 mA, 17 V max	No	Pre-programmed	Inductive power	2.4mm dia, 16.7mm long	ASIC w/custom wirebond & die attachments	Yes, hemetic glass or ceramic package	Yes, injectable in humans	**Kane et al. (2011) BION**
Epilepsy	2 Channel	2 Channels, Const Voltage, Unipolar Pulses, 0 - 3.5V	No	Re-programmable	Battery	6.5 x 4.9 cm flat, 68 g	Commercial, Medtronic Nexframe	Yes	Yes, sheep	**Stanslaski et al. (2012)**
Deep Brain Stimulation	No	2 Channels, Const Current, Bipolar Pulses, 0.015 - 50 mA, 20 V max	No	Preset parameters	Battery	2.4 x 1.7 cm PCB, 10-14g, 1.43 cm hight	PCB, COTS	No, head or jacket mount	Not presented	**Ewing et al. (2013)**
Spinal Cord Stimulation	No	2 Channels, Const Voltage, Monophase pulses, 50 mV - 3 V, 35 mA max	No, in-vitro pre test	Re-programmable	Inductive power	2.2 x 2.3 x 0.7 cm PCB, 3.8 g; 3.8 x 6.5 x 2.5 cm external module, 20 g	PCB, COTS	Yes, epoxy coated	Yes, rats	**Xu et al. (2015)**
Seizure Detection / Stimulation	64 Channel for ECOG	64 Channel, Const Current, Biphasic pulses, 0.01 - 1 mA	No	Programmable, closed-loop feedback	Inductive power	4.8 x 3.3 mm chip, 2 x 2 cm rx coil	ASIC	No, assume tethered	Yes	**Kassiri et al. (2016)**
Intracortical Stimulation	No	8 Channel, Const current, Bipolar pulses, 2.3 - 220 uA, 20 V max	Yes	Active stimulation control	Inductive power	4.4 x 4.4 x 0.9 cm PCB stack	ASICs, multiple	No	No	**Hasanuzzaman et al (2018)**

Table illustrates other reported devices' capabilities compared to that of the Bionode as relate to our desired factors (implantable, recording and stimulating, flexible, and configurable): Blue = Bionode capabilities; Green = more capability than the Bionode; Red = lacks capabilities of the Bionode; White = similar in capability to the Bionode.

APPENDIX B. CHRONICALLY CUFFED RAT DETAILS

Experimental Results/Details of Chronically Cuffed Cervical Vagus Nerve on Rats

Animal Name	H&E Histology	Visual Inspection	CNAP Detected in Stimulation?	FG Transport to Medulla RV (not cuffed)	FG Transport to Medulla LV (cuffed)	Cytokine Analysis	Days Implanted
eRx62	Not observed	N/A (not cuffed)	N/A (control)	N/A (control)	N/A (control)	*Control (no device)*	N/A
eRx63	Not observed	N/A (not cuffed)	N/A (control)	N/A (control)	N/A (control)	Control (no device/LPS)	N/A
eRx104	Not observed	N/A (not cuffed)	N/A (dummy device)	Expected transport	Expected transport	*Control (dummy device)*	22
eRx105	Not observed	N/A (not cuffed)	N/A (dummy device)	Expected transport	Expected transport	*Control (dummy device)*	23
eRx106	Not observed	N/A (not cuffed)	N/A (dummy device)	Expected transport	Expected transport	*Control (dummy device)*	23
eRx110	Not observed	N/A (not cuffed)	N/A (dummy headcap)	Expected transport	Expected transport	*Control (dummy device)*	21
eRx114	Not observed	N/A (not cuffed)	N/A (dummy headcap)	Expected transport	Expected transport	*Control (dummy device)*	17
eRx115	Not observed	N/A (not cuffed)	N/A (dummy headcap)	Expected transport	Expected transport	Control (dummy, no LPS)	17
eRx127	Normal	Moderate migration	N/A (no metal in cuff)	Expected transport	Expected transport	NA (no blood collection)	32
eRx128	Normal	Severe migration	N/A (no metal in cuff)	Expected transport	Complete suppression	NA (no blood collection)	32
eRx132	Normal	Severe migration	N/A (no metal in cuff)	Expected transport	Complete suppression	*Control (no metal in cuff)*	38
eRx137	Normal	Moderate migration	N/A (no metal in cuff)	Expected transport	Complete suppression	*Control (no metal in cuff)*	30
eRx138	Normal	Severe migration	N/A (no metal in cuff)	Expected transport	Complete suppression	*Control (no metal in cuff)*	30
9909	Not observed	Moderate migration	N/A (not powered)	Expected transport	Complete suppression	Control (no stimulation)	71
9932	Not observed	Severe migration	N/A (not powered)	Expected transport	Complete suppression	Control (no stimulation)	42
eRx75	Not observed	Severe migration	N/A (not powered)	Expected transport	Heavy suppression	*Control (no stimulation)*	13
eRx66	Not observed	not observed	No detection / bad signal	Expected transport	Complete suppression	NA (no blood collection)	45
9915	Not observed	Severe migration	Possible CNAP / ambiguous	Expected transport	Complete suppression	Stimulated	57
eRx61	Not observed	not observed	No detection / bad signal	Expected transport	Complete suppression	Stimulated	62
eRx80	Not observed	not observed	No detection / bad signal	Expected transport	Complete suppression	Stimulated	37
eRx83	Not observed	not observed	No detection / bad signal	Expected transport	Complete suppression	*Stimulated*	29
eRx88	Not observed	not observed	No detection / bad signal	Expected transport	Complete suppression	*Stimulated*	21
eRx111	Not observed	Severe migration	No detection / no recording	Expected transport	Complete suppression	Stimulated	18
eRx113	Not observed	not observed	No detection / no recording	Expected transport	Complete suppression	*Stimulated*	18
eRx64	Not observed	not observed	Possible CNAP / ambiguous	Expected transport	Complete suppression	Stimulated	51
9937	Not observed	Moderate migration	Possible CNAP / ambiguous	Expected transport	Complete suppression	Stimulated	38
eRx53	Not observed	not observed	Possible CNAP / ambiguous	Expected transport	Complete suppression	Stimulated	48
eRx55	Not observed	not observed	Possible CNAP / ambiguous	Expected transport	Complete suppression	Stimulated	44
eRx68	Not observed	Moderate migration	No detection / bad signal	Expected transport	Complete suppression	*Stimulated*	21
eRx81	Not observed	Moderate migration	Possible CNAP / ambiguous	Expected transport	Complete suppression	Stimulated	37
eRx118	Not observed	Moderate migration	No detection / no recording	Expected transport	Complete suppression	Stimulated	14
eRx102	Not observed	not observed	Conclusive CNAP	Expected transport	Complete suppression	Stimulated	23
eRx103	Not observed	Mild or no migration	Conclusive CNAP	Expected transport	Light suppression	Control (no LPS)	22
eRx108	Not observed	not observed	Conclusive CNAP	Expected transport	Complete suppression	Stimulated	21
eRx109	Not observed	not observed	Conclusive CNAP	Expected transport	Complete suppression	Stimulated	21
eRx71	Not observed	Mild or no migration	No detection / bad signal	Expected transport	Complete suppression	Stimulated	44
eRx72	Not observed	Mild or no migration	Possible CNAP / ambiguous	Expected transport	Complete suppression	*Stimulated*	13
eRx116	Not observed	Mild or no migration	Possible CNAP / ambiguous	Expected transport	Heavy suppression	*Stimulated*	17
eRx119	Not observed	Mild or no migration	No detection / bad signal	Expected transport	Moderate suppression	Stimulated	14
eRx141	Normal	Mild or no migration	Possible CNAP / ambiguous	Expected transport	Complete suppression	*Stimulated*	27
eRx142	Normal	Mild or no migration	Conclusive CNAP	Expected transport	Complete suppression	*Stimulated*	26
eRx143	Normal	Mild or no migration	Possible CNAP / ambiguous	Expected transport	Complete suppression	*Stimulated*	26
eRx144	Not observed	Mild or no migration	Conclusive CNAP	Expected transport	Complete suppression	*Stimulated*	36
eRx147	Not observed	Mild or no migration	Conclusive CNAP	Expected transport	Complete suppression	Stimulated	36
eRx148	Not observed	Mild or no migration	Conclusive CNAP	Expected transport	Complete suppression	Stimulated	36
eRx150	Not observed	Mild or no migration	Possible CNAP / ambiguous	Expected transport	Complete suppression	Stimulated	34
eRx152	Not observed	Mild or no migration	Conclusive CNAP	Expected transport	Complete suppression	Control (no LPS)	34

Table illustrates results from chronic testing for 47 rats: Blue = a good or expected result; Red = a bad or unexpected result; Yellow = indeterminant result; White = not tested or not applicable in that animal.

* "Moderate" migration was defined as an electrode(s) that was generally in the correct location but had moved laterally ~1mm or less and/or appeared to have rotated ~30 degrees or less. The nerve still appeared to be intact and encompassed in the cuff electrode. "Severe" was be defined

as an electrode(s) that had obvious migrations of >1mm laterally, rotation of >30 degrees, and/or signs of significant pulling or tearing of the encompassed vagus nerve.

** “Heavy” suppression was quantified as having no more than 15 illuminated cells in any given medulla section. “Moderate” suppression was quantified as having more than 15 illuminated cells in any given medulla section, but still had a majority of cells suppressed. “Light” suppression was quantified as having observable cell suppression, but the majority of cells illuminated.

*** Highlighted (green) and italicized items indicate animals that were included in our cytokine analyses.

APPENDIX C. GASTRIC EMPTYING RAT DETAILS

Experimental Results/Details of Chronically Cuffed Cervical Vagus Nerve on Rats Used for Gastric Emptying Experiments

Animal Name	Control Scan	Stimulation Scan	Necropsy Nerve Inspection	FG Transport to Medulla RV (not cuffed)	FG Transport to Medulla LV (cuffed)	Medulla FG Brightness	Nodose FG Brightness	Days Implanted
eRx157	Good Results	N/A	N/A	N/A	N/A	N/A	N/A	23
eRx159	Good Results	Good Results	Mild or no migration	Expected Transport	Heavy Suppression	Bright	Bright	34
eRx160	Good Results	Total Apnia, Stopped Stim	Mild or no migration	Expected Transport	Moderate Suppression	Bright	Dull But Present	35
eRx161	Good Results	Apnia During Stim	Mild or no migration	Expected Transport	Complete Suppression	Bright	Bright	47
eRx162	Good Results	Good Results	Mild or no migration	Expected Transport	Moderate Suppression	Bright	Bright	46
eRx163	Breathing Issues	Apnia During Stim	Moderate Migration/Pulling	Expected Transport	Complete Suppression	Dull But Present	Dull But Present	48

Table illustrates results from chronic testing for 6 rats: Blue = a good or expected result; Red = a bad or unexpected result; Yellow = indeterminant result; White = not tested or not applicable in that animal.

* "Moderate" migration was defined as an electrode(s) that was generally in the correct location but had moved laterally ~1mm or less and/or appeared to have rotated ~30 degrees or less. The nerve still appeared to be intact and encompassed in the cuff electrode.

** "Heavy" suppression was quantified as having no more than 15 illuminated cells in any given medulla section. "Moderate" suppression was quantified as having more than 15 illuminated cells in any given medulla section, but still had a majority of cells suppressed.

*** eRx157 knocked its headcap off before the scheduled stimulation scan and was euthanized.

APPENDIX D. OVERVIEW OF 17 PREVIOUS STUDIES USING CHRONIC VAGUS NERVE CUFFING

Topic			Animals			Cuffs				Tests Done				Reference
Biological Topic	Fiber Target (Afferent / Efferent)	Nerve Cuffed	Breed (Rat)	Weight	Sample Size	Cuff Type	Cuff Inner Diameter	Duration Cuffed	Cuffing Technique	CNAP Recorded	Nerve Histology	Fluorogold Used	Inflammation Measured	Author
Seizure suppression	Afferent	Left	Sprague-Dawley	--	34	--	--	4 days	Nerve isolated (assumed), cuffed	No	No	No	No	Krahl et al. (2001) [104]
Anti-depression	Afferent	Left	Sprague-Dawley	275g+	5-6 per group	Cyberonics helical	1mm (assumed)	2 days + (1 hour to 90 days)	Cuffs wrapped around nerve & carotid; leads suture to muscle	No	No	No	No	Dorr et al. (2006) [105]
Tremor suppression	Afferent	Left	Long-Evans	300-350g	7	Cyberonics helical	1mm	4+ days	Cuffs wrapped around nerve & carotid	No	No	No	No	Handforth et al. (2001) [106]
Hippocampal neuronal plasticity	Afferent	Left	Sprague-Dawley	250-300g	6 per group	Cyberonics helical	--	2 days + 1 month	Cuffs wrapped around nerve & carotid	No	No (Brain)	No	No	Biggio et al. (2009) [107]
Neuroprotective effects in brain	Afferent	Left	Wistar	Variable	24	Cyberonics helical	--	13 weeks	Cuffs wrapped around nerve (carotid unspecified)	No	No (Brain)	No	Yes (Plasma, brain)	Chunchai et al. (2016) [108]
Brain biomarkers / anti-depression	Afferent	Left	Sprague-Dawley	250-350g	29	Cyberonics helical	--	4 weeks	References Dorr et al.	No	No	No	No	Cunningham et al. (2008) [17]
Anti-depression	Afferent	Left	Sprague-Dawley	250-300g	45	Self-sizing spiral cuff	1mm	8 weeks	Nerve isolated; wrapped with cuff	No	No (Brain)	No	No	Grimonprez et al. (2015) [109]
Body weight / fat mass	Both Possible	Left	Sprague-Dawley	250-300g	13 max per group	Cyberonics helical	--	2 days + 4 weeks	Cuffs wrapped around nerve (carotid unspecified)	No	No	No	No	Banni et al. (2012) [165]
Pain memory	Afferent	Left	Sprague-Dawley	300-350g	8 max per group	PVS sheath	1 mm	16 days	Nerve isolated; pvc around nerve; leads sutured to cleidomastoid	No	No	No	No	Zhang et al. (2013) [110]
Fear / memory conditioning	Afferent	Left	Sprague-Dawley	250-300g	40	Silicone tube	1 mm	13 days	Nerve isolated; cuffed	No	No	No	No	Pena et al. (2014) [111]
Enhanced memory	Both	Left	Long-Evans	350-450g	64	PVC sheath	1 mm	~3 days	Nerve isolated; pvc around nerve; leads sutured to cleidomastoid; bone wax inside cuff	Yes	No	No	No	Clark et al. (1998) [16]
Bowel Inflammation	Both	Left	Sprague-Dawley	--	48	Cyberonics helical	--	17 days	Cuffs wrapped around nerve & carotid	No	No (Colon)	No	Yes (Colon)	Meregnani et al. (2011) [95]
Cardiac remodeling (heart failure)	Both	Left	Sprague-Dawley	--	63	Silicone tube	0.75 mm	14 weeks	Nerve isolated; cuffed/sutured shut; strain relief cuff placed around nerve cuff and artery	No	No	No	No	Agarwal et al. (2016) [112]
Hypertension, Cardiovascular damage	Both	Right	Rat (not specified)	--	24	Wire with Kwik-Sil	wrapped wire	4-5 weeks	Nerve isolated; wire wrapped around; Kwik-Sil encapsulated	No	No	No	Yes (Serum)	Chapleau et al. (2016) [96]
Negative heart impacts	Both	Right	Sprague-Dawley	250-300g	9	Cyberonics helical	1.5 mm	10 weeks	Cuffs wrapped around nerve & carotid	No	No	No	No	Lee et al. (2016) [113]
Artery pressure / heart rate	Both	Right	Sprague-Dawley	250-350g	--	Silicone tube	0.5 mm	up to 3 months	Nerve isolated, cuffed/sutured shut	No	No	No	No	Zheng et al. (2014) [114]
Larynx action potentials	Efferent	Left	Wistar	250-350g	21 chronic	Self-sizing silicone tube	1 mm	8 weeks	Nerve isolated, cuffed	Yes	No	No	No	El Tahry et al. (2011) [115]
Inflammation / Gastric Emptying	Efferent	Left	Sprague-Dawley	190-300g	53	Silicone tube	0.75 mm	13-71 days	Nerve isolated, cuffed	Yes	Yes	Yes	Yes (Plasma)	Somann et al (2017)*

**This study included for comparison purposes.*

APPENDIX E. STIMULATION DETAILS OF 17 PREVIOUS STUDIES

Stimulation Details of 17 Previous Studies Using Chronic Vagus Nerve Cuffing.

Stimulation Parameters			Stimulation Protocols			Additional Stimulation Details		Reference
Amplitude	Pulse Width (μs)	Frequency (Hz)	Pulse Details	Stimulation Duration	Stimulation Timeline	Delivery Mechanism	Stimulation Verification	Author
1 mA	500	20	Square-wave pulses	15 minute continuous pulse train	Half stimulated after 2 days, the remainder after 4 days	-	-	Krahl et al. (2001) [104]
0.25 mA	500	20	-	30 sec on, 5 min off, continuous	1 hour, 1 day, 3 day, 2-week, 3-week, & 3-month VNS groups	Implanted Cyberonics 102 Pulse Stimulator	Lead impedance check, no functional test presented	Dorr et al. (2006) [105]
0.5 mA	500	20	Balanced biphasic	5 min continuous pulse train	4+ day recovery, then 5 consecutive 20 min treatments (5 min baseline, 5 min acute VNS, 10 min post period)	A-M Systems Model 2100 stimulator, tethered to headcap	-	Handforth et al. (2001) [106]
1.5 mA	500	30	-	30 sec on, 5 min off, continuous	2 day recovery, then 3 hour or 1 month VNS	Implanted Cyberonics stimulator	-	Biggio et al. (2009) [107]
0.5 - 0.75 mA	500	20	-	14 sec on, 48 sec off, continuous	1 week recovery, then 12 week VNS	Implanted Cyberonics Demipulse stimulator	-	Chunchai et al. (2016) [108]
0.25 mA	250	20	-	30 sec per 5 min, continuous	1 week recovery, then 2 hour or 3 week VNS	Implanted Cyberonics stimulator	-	Cunningham et al. (2008) [17]
0.25, 0.5, or 1 mA	250	30	-	7 sec on, 18 sec off, continuous	1 week recovery, 5 week baseline, then 2 week VNS	Stimulator tethered to headcap	Daily impedance test with 1mA square wave	Grimonprez et al. (2015) [109]
1.5 mA	500	30	-	30 sec on, 5 min off, continuous	2 day recovery, then 3 hour or 4 week VNS	Implanted Cyberonics Demipulse Model 103 stimulator	Dedicated test pre-implant	Banni et al. (2012) [165]
0.04 or 0.4 mA	500	1	-	30 seconds acute VNS pre or post conditioning	5 day recovery, pre-condition day, then 3 consecutive conditioning days	A-M Systems Model 2100 stimulator, tethered through neck incision	Respiration and behavioral response to VNS	Zhang et al. (2013) [110]
0.4 mA	500	30	-	30 seconds	1 week recovery, then 5 conditioning/ treatment days (acute VNS on day 4)	Tucker Davis Tech. MS4 stimulator, tethered to headcap	Respiration response to 0.2 mA, 60 Hz, 10 sec VNS	Pena et al. (2014) [111]
0.2, 0.4, or 0.8 mA	500	20	Biphasic pulses	30 seconds	2 day recovery, then condition testing with acute VNS	Undefined stimulator, tethered through neck incision	Action potentials recorded	Clark et al. (1998) [16]
1 mA	500	5	-	10 sec on, 90 sec off, continuous	12 day recovery, then 3 hour VNS per day (5 days)	Grass Technologies stimulator chain, tethered through head connector	-	Meregnani et al. (2011) [95]
0.05 - 0.25 mA	200	20	-	10 sec on, 50 sec off, continuous	7 day recovery, then 6 week VNS	Undefined pulse generator and connection.	Respiration and heart rate response	Agarwal et al. (2016) [112]
3 V	1000	5	Charge balanced	1 hour on, 1 hour off, continuous	3-4 day recovery, then 4 week VNS	Implanted Harald Stauss Scientific Model RNS stimulator	Heart rate and blood pressure response	Chapleau et al. (2016) [96]
1 mA	500	20	-	7 sec on, 66 sec off, continuous	10 week VNS	Implanted Cyberonics Demipulse Model 103 stimulator	-	Lee et al. (2016) [113]
0.1 - 1 mA	200	20	Rectangular pulses	Various, intermittent	6 weeks intermittent VNS	Implanted Unimec ISE1000SA pulse generator	Heart rate and artery pressure	Zheng et al. (2014) [114]
0.04 - 0.8 mA	500	-	Block-pulses	Various to determine dose response curves	5 days / week, for 8 weeks	Undefined stimulator tethered to headcap	Action potentials recorded	El Tahry et al. (2011) [115]
Various (1 mA typical)	Various (1 ms typical)	5	Balanced biphasic square pulses	5 - 10 min pre-calibration, 5 min treatment	13 – 71 day recovery, then pre-calibration VNS 30 min before, acute VNS 30 min after endotoxin	Bionode, fully implanted or tethered to headcap	Direct recording, separate recording cuff	Somann et al (2017)*

**This study included for comparison purpose.*

REFERENCES

[1] J. A. Clancy, S. A. Deuchars, and J. Deuchars, "The wonders of the Wanderer," *Experimental physiology,* vol. 98, no. 1, pp. 38-45, 2013.

[2] H.-R. Berthoud and W. L. Neuhuber, "Functional and chemical anatomy of the afferent vagal system," *Autonomic Neuroscience,* vol. 85, no. 1, pp. 1-17, 2000.

[3] K. Tracey, "The inflammatory reflex," in *Nature* vol. 420, ed, 2002, pp. 853-859.

[4] V. A. Pavlov, H. Wang, C. J. Czura, S. G. Friedman, and K. J. Tracey, "The cholinergic anti-inflammatory pathway: a missing link in neuroimmunomodulation," *Molecular medicine (Cambridge, Mass.),* vol. 9, no. 5-8, p. 125, 2003.

[5] M. Rosas-Ballina *et al.*, "Splenic nerve is required for cholinergic antiinflammatory pathway control of TNF in endotoxemia," *Proceedings of the National Academy of Sciences of the United States of America,* vol. 105, no. 31, p. 11008, 2008.

[6] M. Rosas-Ballina *et al.*, "Acetylcholine- Synthesizing T Cells Relay Neural Signals in a Vagus Nerve Circuit," *Science,* vol. 334, no. 6052, pp. 98-101, 2011.

[7] U. Andersson and K. J. Tracey, "Neural reflexes in inflammation and immunity," (in English), *Journal of Experimental Medicine,* Review vol. 209, no. 6, pp. 1057-1068, Jun 2012.

[8] D. Martelli, M. J. McKinley, and R. M. McAllen, "The cholinergic anti-inflammatory pathway: A critical review," *Autonomic Neuroscience-Basic & Clinical,* vol. 182, pp. 65-69, May 2014.

[9] B. Bonaz, V. Sinniger, and S. Pellissier, "Anti-inflammatory properties of the vagus nerve: potential therapeutic implications of vagus nerve stimulation," *Journal of Physiology-London,* vol. 594, no. 20, pp. 5781-5790, Oct 2016.

[10] A. Grimonprez, R. Raedt, C. Baeken, P. Boon, and K. Vonck, "The antidepressant mechanism of action of vagus nerve stimulation: Evidence from preclinical studies," *Neurosci Biobehav Rev,* vol. 56, pp. 26-34, Sep 2015.

[11] F. A. Koopman *et al.*, "Vagus nerve stimulation inhibits cytokine production and attenuates disease severity in rheumatoid arthritis," *Proceedings of the National Academy of Sciences of the United States of America,* vol. 113, no. 29, pp. 8284-8289, Jul 2016.

[12] M. S. M. George *et al.*, "Vagus nerve stimulation therapy: A research update," *Neurology,* vol. 59(6) Supplement, no. 4, pp. S56-S61, 2002.

[13] D. A. Groves and V. J. Brown, "Vagal nerve stimulation: a review of its applications and potential mechanisms that mediate its clinical effects," *Neuroscience & Biobehavioral Reviews,* vol. 29, no. 3, pp. 493-500, 2005.

[14] D. Panescu, "Vagus nerve stimulation for the treatment of depression," *Engineering in Medicine and Biology Magazine, IEEE,* vol. 24, no. 6, pp. 68-72, 2005.

[15] Y. A. Patel, T. Saxena, R. V. Bellamkonda, and R. J. Butera, "Kilohertz frequency nerve block enhances anti-inflammatory effects of vagus nerve stimulation," *Scientific Reports,* Article vol. 7, p. 39810, 01/05/online 2017.

[16] K. B. Clark, D. C. Smith, D. L. Hassert, R. A. Browning, D. K. Naritoku, and R. A. Jensen, "Posttraining Electrical Stimulation of Vagal Afferents with Concomitant Vagal Efferent Inactivation Enhances Memory Storage Processes in the Rat," *Neurobiology of Learning and Memory,* vol. 70, no. 3, pp. 364-373, 11// 1998.

[17] J. T. Cunningham, S. W. Mifflin, G. G. Gould, and A. Frazer, "Induction of c-Fos and DeltaFosB immunoreactivity in rat brain by Vagal nerve stimulation," *Neuropsychopharmacology,* vol. 33, no. 8, pp. 1884-95, Jul 2008.
[18] L. V. Borovikova, "Vagus nerve stimulation attenuates the systemic inflammatory response to endotoxin," *Nature,* vol. 405, no. 6785, pp. 458-463, 2000.
[19] J. M. Huston *et al.*, "Splenectomy inactivates the cholinergic antiinflammatory pathway during lethal endotoxemia and polymicrobial sepsis," *Journal of Experimental Medicine,* vol. 203, no. 7, pp. 1623-1628, 2006.
[20] T. R. Bernik *et al.*, "Pharmacological stimulation of the cholinergic antiinflammatory pathway," *Journal of Experimental Medicine,* vol. 195, no. 6, pp. 781-788, 2002.
[21] R. D. Sanders, T. Hussell, and M. Maze, "Sedation & immunomodulation," *Critical care clinics,* vol. 25, no. 3, pp. 551-570, 2009.
[22] C. A. Picq, D. Clarençon, V. E. Sinniger, B. L. Bonaz, and J.-F. S. Mayol, "Impact of anesthetics on immune functions in a rat model of vagus nerve stimulation," *PloS one,* vol. 8, no. 6, p. e67086, 2013.
[23] D. J. Pederson *et al.*, "The Design of the Bionode: An Implantable Wireless Electroceutical Device for Recording and Stimulating Bioelectric Events," *IEEE Trans Biomed Eng,* vol. In Revision, 2017.
[24] D.-B. S. f. P. s. D. S. Group, "Deep-brain stimulation of the subthalamic nucleus or the pars interna of the globus pallidus in Parkinson's disease," *New England Journal of Medicine,* vol. 345, no. 13, pp. 956-963, 2001.
[25] D. M. Labiner and G. L. Ahern, "Vagus nerve stimulation therapy in depression and epilepsy: therapeutic parameter settings," *Acta Neurologica Scandinavica,* vol. 115, no. 1, pp. 23-33, 2007.
[26] H. A. Sackeim *et al.*, "Vagus nerve stimulation (VNS™) for treatment-resistant depression: efficacy, side effects, and predictors of outcome," *Neuropsychopharmacology,* vol. 25, no. 5, pp. 713-728, 2001.
[27] J. Luigjes *et al.*, "Deep brain stimulation in addiction: a review of potential brain targets," *Molecular psychiatry,* vol. 17, no. 6, p. 572, 2012.
[28] F. T. Sun, M. J. Morrell, and R. E. Wharen Jr, "Responsive cortical stimulation for the treatment of epilepsy," *Neurotherapeutics,* vol. 5, no. 1, pp. 68-74, 2008.
[29] M. J. Kane, P. P. Breen, F. Quondamatteo, and G. ÓLaighin, "BION microstimulators: A case study in the engineering of an electronic implantable medical device," *Medical engineering & physics,* vol. 33, no. 1, pp. 7-16, 2011.
[30] M. Weiergräber, M. Henry, J. Hescheler, N. Smyth, and T. Schneider, "Electrocorticographic and deep intracerebral EEG recording in mice using a telemetry system," *Brain research protocols,* vol. 14, no. 3, pp. 154-164, 2005.
[31] H. Kassiri *et al.*, "Battery-less Tri-band-Radio Neuro-monitor and Responsive Neurostimulator for Diagnostics and Treatment of Neurological Disorders," *IEEE Journal of Solid-State Circuits,* vol. 51, no. 5, pp. 1274-1289, 2016.
[32] Q. Xu, D. Hu, B. Duan, and J. He, "A fully implantable stimulator with wireless power and data transmission for experimental investigation of epidural spinal cord stimulation," *IEEE Transactions on Neural Systems and Rehabilitation Engineering,* vol. 23, no. 4, pp. 683-692, 2015.

[33] R. G. Dennis, D. E. Dow, and J. A. Faulkner, "An implantable device for stimulation of denervated muscles in rats," *Medical Engineering and Physics,* vol. 25, no. 3, pp. 239-253, 2003.

[34] S. G. Ewing, W. J. Lipski, A. A. Grace, and C. Winter, "An inexpensive, charge-balanced rodent deep brain stimulation device: a step-by-step guide to its procurement and construction," *Journal of neuroscience methods,* vol. 219, no. 2, pp. 324-330, 2013.

[35] T. August, M. Harvey, P. Lightfoot, D. Kilbey, T. Papadopoulos, and P. Jepson, "Emerging technologies for biological recording," *Biological Journal of the Linnean Society,* vol. 115, no. 3, pp. 731-749, 2015.

[36] S. Nag and N. V. Thakor, "Implantable neurotechnologies: electrical stimulation and applications," *Medical & Biological Engineering & Computing,* vol. 54, no. 1, pp. 63-76, Jan 2016.

[37] A. C Thompson, P. R Stoddart, and E. D. Jansen, "Optical stimulation of neurons," *Current molecular imaging,* vol. 3, no. 2, pp. 162-177, 2014.

[38] S. T. Lee, P. A. Williams, C. E. Braine, D.-T. Lin, S. W. John, and P. P. Irazoqui, "A miniature, fiber-coupled, wireless, deep-brain optogenetic stimulator," *IEEE Transactions on Neural Systems and Rehabilitation Engineering,* vol. 23, no. 4, pp. 655-664, 2015.

[39] J. Arle, "Chapter 12 - Surgical Techniques," in *Essential Neuromodulation*San Diego: Academic Press, 2011, pp. 269-282.

[40] D. R. Merrill, M. Bikson, and J. G. Jefferys, "Electrical stimulation of excitable tissue: design of efficacious and safe protocols," *J Neurosci Methods,* vol. 141, no. 2, pp. 171-98, Feb 15 2005.

[41] T. Instruments, "AN-1515 A Comprehensive Study of the Howland Current Pump," *Application Note,* pp. 1-17, 2008.

[42] M. P. Ward, K. Y. Qing, K. J. Otto, R. M. Worth, S. W. M. John, and P. P. Irazoqui, "A Flexible Platform for Biofeedback- Driven Control and Personalization of Electrical Nerve Stimulation Therapy," *Neural Systems and Rehabilitation Engineering, IEEE Transactions on,* vol. 23, no. 3, pp. 475-484, 2015.

[43] G. Seo, "Bionode5.0: A Miniature, Wireless, Closed-Loop Biological Implant for Neuromodulation," Master of Science, Biomedical Engineering, Purdue University, 2018.

[44] G. Jiang and D. D. Zhou, "Technology advances and challenges in hermetic packaging for implantable medical devices," in *Implantable Neural Prostheses 2*: Springer, 2009, pp. 27-61.

[45] F. Boeser, J. S. Ordonez, M. Schuettler, T. Stieglitz, D. T. T. Plachta, and Ieee, "Non-hermetic encapsulation for implantable electronic devices based on epoxy," in *2015 37th Annual International Conference of the Ieee Engineering in Medicine and Biology Society*(IEEE Engineering in Medicine and Biology Society Conference Proceedings, 2015, pp. 809-812.

[46] C. K. Bjune *et al.*, "Package Architecture and Component Design for an Implanted Neural Stimulator with Closed Loop Control," in *2015 37th Annual International Conference of the Ieee Engineering in Medicine and Biology Society*(IEEE Engineering in Medicine and Biology Society Conference Proceedings, 2015, pp. 7825-7830.

[47] P. Wang *et al.*, "LONG-TERM EVALUATION OF A NON-HERMETIC MICROPACKAGE TECHNOLOGY FOR MEMS-BASED, IMPLANTABLE PRESSURE SENSORS," *2015 Transducers - 2015 18th International Conference on Solid-State Sensors, Actuators and Microsystems (Transducers),* pp. 484-487, 2015.

[48] L. Lonys *et al.*, "Silicone rubber encapsulation for an endoscopically implantable gastrostimulator," *Medical & Biological Engineering & Computing,* vol. 53, no. 4, pp. 319-329, Apr 2015.

[49] K. Stokes, "The Biocompatibility and Biostability of New Cardiovascular Materials and Devices," in *Implantable Neural Prostheses 2: Techniques and Engineering Approaches*, D. Zhou and E. Greenbaum, Eds. New York, NY: Springer New York, 2010, pp. 1-26.

[50] Q. Xu, J. Li, W. Han, and H. Zhou, "A fully implantable stimulator with wireless power and data transmission for experimental use in epidural spinal cord stimulation," in *2011 Annual International Conference of the IEEE Engineering in Medicine and Biology Society*, 2011, pp. 7230-7233: IEEE.

[51] A. Lay-Ekuakille, G. Griffo, A. Massaro, F. Spano, and G. Gigli, "Experimental characterization of an implantable neuro-packaging for EEG signal recording and measurement," *Measurement,* vol. 79, pp. 321-330, 2016.

[52] A. Kalaijakis, "Medical Device Interconnects Must Address Harsh Environments and Durability Challenges," *ECN: Electronic Component News,* vol. 55, no. 7, pp. 20-20, 2011.

[53] S. Grob, P. A. Tass, and C. Hauptmann, "Capacitive feedthroughs for medical implants," *Frontiers in Neuroscience,* vol. 10, 2016.

[54] R. A. Stevenson, "Feedthrough EMI filter with ground isolation for cardiac pacemakers and implantable cardioverter defibrillators," in *Proceedings of the 20th Annual International Conference of the Ieee Engineering in Medicine and Biology Society, Vol 20, Pts 1-6: Biomedical Engineering Towards the Year 2000 and Beyond*, vol. 20, H. K. Chang and Y. T. Zhang, Eds. (Proceedings of Annual International Conference of the Ieee Engineering in Medicine and Biology Society, 1998, pp. 3319-3323.

[55] J. R. Lachapelle *et al.*, "An implantable, designed-for-human-use peripheral nerve stimulation and recording system for advanced prosthetics," in *Engineering in Medicine and Biology Society (EMBC), 2016 IEEE 38th Annual International Conference of the*, 2016, pp. 1794-1797: IEEE.

[56] S. Stanslaski *et al.*, "Design and validation of a fully implantable, chronic, closed-loop neuromodulation device with concurrent sensing and stimulation," *IEEE Trans Neural Syst Rehabil Eng,* vol. 20, no. 4, pp. 410-21, Jul 2012.

[57] M. Hasanuzzaman, B. G. Motlagh, F. Mounaim, A. Hassan, R. Raut, and M. Sawan, "Toward an Energy-Efficient High-Voltage Compliant Visual Intracortical Multichannel Stimulator," *IEEE Transactions on Very Large Scale Integration (VLSI) Systems,* vol. 26, no. 5, pp. 878-891, 2018.

[58] A. Caravaca *et al.*, "A novel flexible cuff-like microelectrode for dual purpose, acute and chronic electrical interfacing with the mouse cervical vagus nerve," *Journal of neural engineering,* vol. 14, no. 6, p. 066005, 2017.

[59] S. F. Cogan, "Neural stimulation and recording electrodes," *Annu Rev Biomed Eng,* vol. 10, pp. 275-309, 2008.

[60] J. H. Lee, H. Kim, J. H. Kim, and S. H. Lee, "Soft implantable microelectrodes for future medicine: prosthetics, neural signal recording and neuromodulation," *Lab on a Chip,* vol. 16, no. 6, pp. 959-976, 2016.

[61] T. Ware, D. Simon, R. L. Rennaker, and W. Voit, "Smart Polymers for Neural Interfaces," *Polymer Reviews,* vol. 53, no. 1, pp. 108-129, 2013.

[62] G. A. Slipher, W. D. Hairston, J. C. Bradford, E. D. Bain, and R. A. Mrozek, "Carbon nanofiber-filled conductive silicone elastomers as soft, dry bioelectronic interfaces," *PloS one,* vol. 13, no. 2, p. e0189415, 2018.

[63] H. Q. Yu, W. J. Xiong, H. Z. Zhang, W. Wang, and Z. H. Li, "A Parylene Self-Locking Cuff Electrode for Peripheral Nerve Stimulation and Recording," (in English), *Journal of Microelectromechanical Systems,* vol. 23, no. 5, pp. 1025-1035, Oct 2014.

[64] Y. Asari, M. Majima, K. Sugimoto, M. Katori, and T. Ohwada, "Release site of TNF alpha after intravenous and intraperitoneal injection of LPS from Escherichia coli in rats," *Shock (Augusta, Ga.),* vol. 5, no. 3, pp. 208-212, 1996.

[65] M. Fleshner *et al.*, "Thermogenic and corticosterone responses to intravenous cytokines (IL-1β and TNF-α) are attenuated by subdiaphragmatic vagotomy," *Journal of neuroimmunology,* vol. 86, no. 2, pp. 134-141, 1998.

[66] Y. KAKIZAKI, H. WATANOBE, A. KOHSAKA, and T. SUDA, "Temporal Profiles of Interleukin-1β, Interleukin-6, and Tumor Necrosis Factor-α in the Plasma and Hypothalamic Paraven-tricular Nucleus after Intravenous or Intraperitoneal Administration of Lipopolysaccharide in the Rat," *Endocrine journal,* vol. 46, no. 4, pp. 487-496, 1999.

[67] S. Steven, M. Dib, S. Roohani, F. Kashani, T. Münzel, and A. Daiber, "Time Response of Oxidative/Nitrosative Stress and Inflammation in LPS-Induced Endotoxaemia—A Comparative Study of Mice and Rats," *International journal of molecular sciences,* vol. 18, no. 10, p. 2176, 2017.

[68] L. Givalois *et al.*, "Temporal cascade of plasma level surges in ACTH, corticosterone, and cytokines in endotoxin-challenged rats," *American Journal of Physiology-Regulatory, Integrative and Comparative Physiology,* vol. 267, no. 1, pp. R164-R170, 1994.

[69] L. V. Borovikova *et al.*, "Vagus nerve stimulation attenuates the systemic inflammatory response to endotoxin," *Nature,* vol. 405, no. 6785, pp. 458-462, May 2000.

[70] B. O. Bratton, D. Martelli, M. J. McKinley, D. Trevaks, C. R. Anderson, and R. M. McAllen, "Neural regulation of inflammation: no neural connection from the vagus to splenic sympathetic neurons," *Experimental Physiology,* vol. 97, no. 11, pp. 1180-1185, 2012.

[71] H. Wang *et al.*, "Nicotinic acetylcholine receptor α7 subunit is an essential regulator of inflammation," *Nature,* vol. 421, no. 6921, p. 384, 2003.

[72] M. Lenczowski, A.-M. Van Dam, S. Poole, J. Larrick, and F. Tilders, "Role of circulating endotoxin and interleukin-6 in the ACTH and corticosterone response to intraperitoneal LPS," *American Journal of Physiology-Regulatory, Integrative and Comparative Physiology,* vol. 273, no. 6, pp. R1870-R1877, 1997.

[73] M. Lenczowski, E. Schmidt, A. M. DAM, R. Gaykema, and F. Tilders, "Individual Variation in Hypothalamus-Pituitary-Adrenal Responsiveness of Rats to Endotoxin and Interleukin-1β," *Annals of the New York Academy of Sciences,* vol. 856, no. 1, pp. 139-147, 1998.

[74] D. L. Bellinger, D. Lorton, R. W. Hamill, S. Y. Felten, and D. L. Felten, "Acetylcholinesterase Staining and Choline Acetyltransferase Activity in the Young Adult Rat Spleen: Lack of Evidence for Cholinergic Innervation," *Brain Behavior and Immunity,* vol. 7, no. 3, pp. 191-204, 1993.

[75] H. R. Berthoud, N. R. Carlson, and T. L. Powley, "Topography of efferent vagal innervation of the rat gastrointestinal tract," *The American journal of physiology,* vol. 260, no. 1 Pt 2, p. R200, 1991.

[76] D. Martelli, M. J. McKinley, and R. M. McAllen, "The cholinergic anti-inflammatory pathway: A critical review," *Autonomic Neuroscience-Basic & Clinical,* vol. 182, pp. 65-69, May 2014.

[77] J. M. Huston *et al.*, "Splenectomy protects against sepsis lethality and reduces serum HMGB1 levels," *Journal of Immunology,* vol. 181, no. 5, pp. 3535-3539, 2008.

[78] H.-R. Berthoud and T. L. Powley, "Characterization of vagal innervation to the rat celiac, suprarenal and mesenteric ganglia," *Journal of the Autonomic Nervous System,* vol. 42, no. 2, pp. 153-169, 1993.

[79] H. R. Berthoud and T. L. Powley, "Interaction between parasympathetic and sympathetic nerves in prevertebral ganglia: morphological evidence for vagal efferent innervation of ganglion cells in the rat," *Microscopy research and technique,* vol. 35, no. 1, p. 80, 1996.

[80] J. P. Somann *et al.*, "Chronic cuffing of cervical vagus nerve inhibits efferent fiber integrity in rat model," *Journal of neural engineering,* 2017.

[81] K. Wasilczuk *et al.*, "Modulating the inflammatory reflex in rats using low intensity focused ultrasound stimulation of the vagus nerve," *Ultrasound in Medicine and Biology,* vol. In Submission, 2018.

[82] I. Bioanalytical Systems, "Surgical Procedures: Femoral Cannulation (Rat)," *Surgery Manual,* vol. Culex ABS, 2007.

[83] S. Peters, J. Hampsch, M. Cregor, C. Starrett, G. Gunaratna, and C. Kissinger, "Culex ABS Part I: Introduction to automated blood sampling," *Current Separations,* vol. 18, no. 4, p. 140, 2000.

[84] K. V. Jarry, *An Exploratory Study of How Acute Neuromodulation of the Subdiaphragmatic Branches Regulates Inflammation*. Ann Arbor : ProQuest Dissertations & Theses, 2017.

[85] M. D. Kraaij *et al.*, "Human monocytes produce interferon-gamma upon stimulation with LPS," *Cytokine,* vol. 67, no. 1, pp. 7-12, 2014.

[86] G. M. Doherty, J. R. Lange, H. N. Langstein, H. R. Alexander, C. M. Buresh, and J. A. Norton, "Evidence for IFN-gamma as a mediator of the lethality of endotoxin and tumor necrosis factor-alpha," *The Journal of Immunology,* vol. 149, no. 5, pp. 1666-1670, 1992.

[87] J. A. Hamilton and G. P. Anderson, "Mini ReviewGM-CSF Biology," *Growth factors,* vol. 22, no. 4, pp. 225-231, 2004.

[88] Q.-h. You, G.-y. Sun, N. Wang, J.-l. Shen, and Y. Wang, "Interleukin-17F-induced pulmonary microvascular endothelial monolayer hyperpermeability via the protein kinase C pathway," *Journal of Surgical Research,* vol. 162, no. 1, pp. 110-121, 2010.

[89] H.-F. Pan, X.-P. Li, S. G. Zheng, and D.-Q. Ye, "Emerging role of interleukin-22 in autoimmune diseases," *Cytokine & growth factor reviews,* vol. 24, no. 1, pp. 51-57, 2013.

[90] H. Redl, G. Schlag, S. Bahrami, U. Schade, M. Ceska, and P. Stutz, "Plasma Neutrophil-Activating Peptide-1/lnterleukin-8 and Neutrophil Elastase in a Primate Bacteremia Model," *Journal of Infectious Diseases,* vol. 164, no. 2, pp. 383-388, 1991.

[91] A. F. Suffredini, D. Reda, S. M. Banks, M. Tropea, J. M. Agosti, and R. Miller, "Effects of recombinant dimeric TNF receptor on human inflammatory responses following intravenous endotoxin administration," *Journal of immunology (Baltimore, Md. : 1950),* vol. 155, no. 10, pp. 5038-45, 1995.

[92] Charalambos A. Gogos, E. Drosou, Harry P. Bassaris, and A. Skoutelis, "Pro- versus Anti-inflammatory Cytokine Profile in Patients with Severe Sepsis: A Marker for Prognosis and Future Therapeutic Options," *The Journal of Infectious Diseases,* vol. 181, no. 1, pp. 176-180, 2000.

[93] T. van der Poll, J. Jansen, M. Levi, H. ten Cate, J. W. ten Cate, and S. J. van Deventer, "Regulation of interleukin 10 release by tumor necrosis factor in humans and chimpanzees," *The Journal of experimental medicine,* vol. 180, no. 5, pp. 1985-8, 1994.

[94] R. Medzhitov, "Origin and physiological roles of inflammation," *Nature,* vol. 454, no. 7203, p. 428, 2008.

[95] J. Meregnani *et al.*, "Anti-inflammatory effect of vagus nerve stimulation in a rat model of inflammatory bowel disease," *Auton Neurosci,* vol. 160, no. 1-2, pp. 82-9, Feb 24 2011.

[96] M. W. Chapleau, D. L. Rotella, J. J. Reho, K. Rahmouni, and H. M. Stauss, "Chronic vagal nerve stimulation prevents high-salt diet-induced endothelial dysfunction and aortic stiffening in stroke-prone spontaneously hypertensive rats," *Am J Physiol Heart Circ Physiol,* vol. 311, no. 1, pp. H276-85, Jul 01 2016.

[97] J. C. Prechtl and T. L. Powley, "The fiber composition of the abdominal vagus of the rat," *Anatomy and Embryology,* vol. 181, no. 2, pp. 101-115, 1990.

[98] N. L. Strominger, R. J. Demarest, and L. B. Laemle, *Noback's human nervous system: structure and function*. Springer Science & Business Media, 2012.

[99] R. Norgren and G. P. Smith, "Central distribution of subdiaphragmatic vagal branches in the rat," *Journal of Comparative Neurology,* vol. 273, no. 2, pp. 207-223, 1988.

[100] B. L. Bonaz and C. N. Bernstein, "Brain-gut interactions in inflammatory bowel disease," *Gastroenterology,* vol. 144, no. 1, pp. 36-49, 2013.

[101] R. A. Travagli and L. Anselmi, "Vagal neurocircuitry and its influence on gastric motility," *Nature Reviews Gastroenterology & Hepatology,* 2016.

[102] A. M. Streeter, B. Duraiappah, R. Boyle, B. J. O'Neill, and M. T. Pheils, "Malabsorption of vitamin B12 after vagotomy," *The American Journal of Surgery,* vol. 128, no. 3, pp. 340-343, 1974.

[103] K. Neihouser, B. Rajwa, G. O. Albors, and P. P. Irazoqui, "An Exploratory Study of How Acute Neuromodulation of the Subdiaphragmatic Branches Regulates Inflammation," *Autonomic Neuroscience: Basic and Clinical,* vol. In Review, 2017.

[104] S. E. Krahl, S. S. Senanayake, and A. Handforth, "Destruction of peripheral C-fibers does not alter subsequent vagus nerve stimulation-induced seizure suppression in rats," *Epilepsia,* vol. 42, no. 5, p. 586, 2001.

[105] A. E. Dorr and G. Debonnel, "Effect of vagus nerve stimulation on serotonergic and noradrenergic transmission," *Journal of Pharmacology and Experimental Therapeutics,* vol. 318, no. 2, pp. 890-898, 2006.

[106] A. Handforth and S. E. Krahl, "Suppression of harmaline-induced tremor in rats by vagus nerve stimulation," *Movement disorders,* vol. 16, no. 1, pp. 84-88, 2001.

[107] F. Biggio *et al.*, "Chronic vagus nerve stimulation induces neuronal plasticity in the rat hippocampus," *Int J Neuropsychopharmacol,* vol. 12, no. 9, pp. 1209-21, Oct 2009.

[108] T. Chunchai *et al.*, "Vagus Nerve Stimulation Exerts the Neuroprotective Effects in Obese-Insulin Resistant Rats, Leading to the Improvement of Cognitive Function," *Scientific Reports,* vol. 6, May 2016, Art. no. 26866.
[109] A. Grimonprez *et al.*, "Vagus nerve stimulation has antidepressant effects in the kainic acid model for temporal lobe epilepsy," *Brain stimulation,* vol. 8, no. 1, pp. 13-20, 2015.
[110] X. Zhang *et al.*, "Vagus nerve stimulation modulates visceral pain-related affective memory," *Behavioural Brain Research,* vol. 236, pp. 8-15, 1/1/ 2013.
[111] D. F. Peña, J. E. Childs, S. Willett, A. Vital, C. K. McIntyre, and S. Kroener, "Vagus nerve stimulation enhances extinction of conditioned fear and modulates plasticity in the pathway from the ventromedial prefrontal cortex to the amygdala," *Frontiers in behavioral neuroscience,* vol. 8, 2014.
[112] R. Agarwal, E. Mokelke, S. B. Ruble, and C. M. Stolen, "Vagal Nerve Stimulation Evoked Heart Rate Changes and Protection from Cardiac Remodeling," *Journal of cardiovascular translational research,* vol. 9, no. 1, pp. 67-76, 2016.
[113] S. W. Lee *et al.*, "Chronic cyclic vagus nerve stimulation has beneficial electrophysiological effects on healthy hearts in the absence of autonomic imbalance," *Physiol Rep,* vol. 4, no. 9, May 2016.
[114] C. Zheng, M. Li, T. Kawada, K. Uemura, M. Inagaki, and M. Sugimachi, "A Practical Use Method of Chronic Vagal Stimulation in Rats," *生体　工学,* vol. 52, no. Supplement, pp. O-438-O-439, 2014.
[115] R. El Tahry *et al.*, "Repeated assessment of larynx compound muscle action potentials using a self-sizing cuff electrode around the vagus nerve in experimental rats," *J Neurosci Methods,* vol. 198, no. 2, pp. 287-93, Jun 15 2011.
[116] G. E. Loeb, "Cuff electrodes for chronic stimulation and recording of peripheral nerve activity," *Journal Of Neuroscience Methods,* vol. 64, no. 1, p. 95, 1996.
[117] F. J. Rodri *et al.*, "Polyimide cuff electrodes for peripheral nerve stimulation," *Journal of neuroscience methods,* vol. 98, no. 2, pp. 105-118, 2000.
[118] Y. J. Lee, H. J. Kim, J. Y. Kang, S. H. Do, and S. H. Lee, "Biofunctionalization of Nerve Interface via Biocompatible Polymer-Roughened Pt Black on Cuff Electrode for Chronic Recording," *Advanced Healthcare Materials,* 2017.
[119] D. J. Pederson *et al.*, "The Design of the Bionode: An Implantable Wireless Electroceutical Device for Recording and Stimulating Bioelectric Events," *IEEE Trans Biomed Eng,* vol. In Review, 2017.
[120] T. L. Powley, E. A. Fox, and H. R. Berthoud, "Retrograde Tracer Technique for Assessment of Selective and Total Subdiaphragmatic Vagotomies," (in English), *American Journal of Physiology,* vol. 253, no. 2, pp. R361-R370, Aug 1987.
[121] R. J. Phillips and T. L. Powley, "Gastric volume detection after selective vagotomies in rats," *American Journal of Physiology-Regulatory, Integrative and Comparative Physiology,* vol. 274, no. 6, pp. R1626-R1638, 1998.
[122] R. J. Phillips, E. A. Baronowsky, and T. L. Powley, "Regenerating vagal afferents reinnervate gastrointestinal tract smooth muscle of the rat," *Journal of Comparative Neurology,* vol. 421, no. 3, pp. 325-346, 2000.
[123] C. Bohs, M. Cregor, G. Gunaratna, and C. Kissinger, "Culex automated blood sampler part II: Managing freely-moving animals and monitoring their activity," *Current Separations,* vol. 18, no. 4, p. 148, 2000.

[124] M. P. Ward and T. V. Nowak, "A new approach to study vagal control of stomach function.," presented at the 2017 Annual Meeting of the Biomedical Engineering Society, Phoenix, AZ, Oct 2017, 2017.
[125] R. Fogel, X. Zhang, and W. E. Renehan, "Relationships between the morphology and function of gastric and intestinal distention-sensitive neurons in the dorsal motor nucleus of the vagus," *Journal of Comparative Neurology,* vol. 364, no. 1, pp. 78-91, 1996.
[126] K. H. Lu, J. Cao, S. Oleson, T. L. Powley, and Z. Liu, "Contrast Enhanced Magnetic Resonance Imaging of Gastric Emptying and Motility in Rats," *IEEE Transactions on Biomedical Engineering,* vol. PP, no. 99, pp. 1-1, 2017.
[127] B. Zaaimi, R. Grebe, and F. Wallois, "Animal model of the short-term cardiorespiratory effects of intermittent vagus nerve stimulation," *Auton Neurosci,* vol. 143, no. 1-2, pp. 20-6, Dec 05 2008.
[128] M. Mermelstein, R. Nonweiler, and E. H. Rubinstein, "Intraoperative identification of laryngeal nerves with laryngeal electromyography," *The Laryngoscope,* vol. 106, no. 6, pp. 752-756, 1996.
[129] R. Sahyouni, D. T. Chang, O. Moshtaghi, A. Mahmoodi, H. R. Djalilian, and H. W. Lin, "Functional and Histological Effects of Chronic Neural Electrode Implantation," *Laryngoscope Investigative Otolaryngology,* 2017.
[130] M. A. Thil, D. T. Duy, I. M. Colin, and J. Delbeke, "Time course of tissue remodelling and electrophysiology in the rat sciatic nerve after spiral cuff electrode implantation," *J Neuroimmunol,* vol. 185, no. 1-2, pp. 103-14, Apr 2007.
[131] W. M. Grill and J. T. Mortimer, "Neural and connective tissue response to long-term implantation of multiple contact nerve cuff electrodes," *Journal of Biomedical Materials Research Part A,* vol. 50, no. 2, pp. 215-226, 2000.
[132] S. Flohe, E. D. Fernandez, M. Ackermann, T. Hirsch, J. Börgermann, and F. Schade, "Endotoxin tolerance in rats: expression of TNF-α, IL-6, IL-10, VCAM-1 and HSP70 in lung and liver during endotoxin shock," *Cytokine,* vol. 11, no. 10, pp. 796-804, 1999.
[133] A. Waage, "Production and clearance of tumor necrosis factor in rats exposed to endotoxin and dexamethasone," *Clinical immunology and immunopathology,* vol. 45, no. 3, pp. 348-355, 1987.
[134] K.-H. Lu, J. Cao, S. Oleson, M. P. Ward, T. L. Powley, and Z. Liu, "Vagus Nerve Stimulation Promotes Gastric Emptying by Increasing Pyloric Opening Measured with Magnetic Resonance Imaging," *bioRxiv,* p. 253674, 2018.
[135] R. A. Travagli and L. Anselmi, "Vagal neurocircuitry and its influence on gastric motility," *Nature Reviews Gastroenterology & Hepatology,* 2016.
[136] C. A. McMenamin, R. A. Travagli, and K. N. Browning, "Inhibitory neurotransmission regulates vagal efferent activity and gastric motility," *Experimental Biology and Medicine,* vol. 241, no. 12, pp. 1343-1350, 2016.
[137] W. Schwizer, A. Steingoetter, and M. Fox, "Magnetic resonance imaging for the assessment of gastrointestinal function," *Scand J Gastroenterol,* vol. 41, no. 11, pp. 1245-60, Nov 2006.
[138] L. Marciani, "Assessment of gastrointestinal motor functions by MRI: a comprehensive review," *Neurogastroenterol Motil,* vol. 23, no. 5, pp. 399-407, May 2011.
[139] I. M. de Zwart and A. de Roos, "MRI for the evaluation of gastric physiology," *European radiology,* vol. 20, no. 11, pp. 2609-2616, 2010.

[140] D. J. Tyler and D. M. Durand, "Chronic response of the rat sciatic nerve to the flat interface nerve electrode," *Annals of biomedical engineering,* vol. 31, no. 6, pp. 633-642, 2003.
[141] B. Rydevik, G. Lundborg, and U. Bagge, "Effects of graded compression on intraneural blood flow: an in vivo study on rabbit tibial nerve," *The Journal of hand surgery,* vol. 6, no. 1, pp. 3-12, 1981.
[142] G. G. Naples, "A spiral nerve cuff electrode for peripheral nerve stimulation," *IEEE Transactions On Bio-Medical Engineering,* vol. 35, no. 11, p. 905, 1988.
[143] F. A. Cuoco, Jr., "Measurement of external pressures generated by nerve cuff electrodes," *IEEE Transactions On Rehabilitation Engineering: A Publication Of The IEEE Engineering In Medicine And Biology Society,* vol. 8, no. 1, p. 35, 2000.
[144] D. Evans and J. Murray, "Histological and functional studies on the fibre composition of the vagus nerve of the rabbit," *Journal of anatomy,* vol. 88, no. Pt 3, p. 320, 1954.
[145] R. J. Phillips, E. A. Baronowsky, and T. L. Powley, "Long-term regeneration of abdominal vagus: Efferents fail while afferents succeed," *Journal of Comparative Neurology,* vol. 455, no. 2, pp. 222-237, 2003.
[146] S. C. Payne, P. J. Belleville, and J. R. Keast, "Regeneration of sensory but not motor axons following visceral nerve injury," *Experimental neurology,* vol. 266, pp. 127-142, 2015.
[147] X. Navarro, "A critical review of interfaces with the peripheral nervous system for the control of neuroprostheses and hybrid bionic systems," *Journal of the Peripheral Nervous System,* vol. 10, no. 3, pp. 229-259, 2005.
[148] L. Guth and S. Jacobson, "The rate of regeneration of the vagus nerve of the cat," *Experimental neurology,* vol. 14, no. 4, pp. 439-447, 1966.
[149] M. Kanje, "Survival and regeneration of the adult rat vagus nerve in culture," *Brain research,* vol. 550, no. 2, pp. 340-342, 1991.
[150] M. Goss-Varley *et al.*, "Microelectrode implantation in motor cortex causes fine motor deficit: Implications on potential considerations to Brain Computer Interfacing and Human Augmentation," *Scientific Reports,* vol. 7, no. 1, p. 15254, 2017.
[151] H. Wyns, E. Plessers, P. De Backer, E. Meyer, and S. Croubels, "In vivo porcine lipopolysaccharide inflammation models to study immunomodulation of drugs," *Veterinary immunology and immunopathology,* vol. 166, no. 3, pp. 58-69, 2015.
[152] M. A. Islam *et al.*, "Alveolar macrophage phagocytic activity is enhanced with LPS priming, and combined stimulation of LPS and lipoteichoic acid synergistically induce pro-inflammatory cytokines in pigs," *Innate immunity,* vol. 19, no. 6, pp. 631-643, 2013.
[153] S. L. Moya, L. Boyle, P. Lynch, and S. Arkins, "Pro-inflammatory cytokine and acute phase protein responses to low-dose lipopolysaccharide (LPS) challenge in pigs," *Animal Science,* vol. 82, no. 04, pp. 527-534, 2006.
[154] D. Webel, B. Finck, D. Baker, and R. Johnson, "Time course of increased plasma cytokines, cortisol, and urea nitrogen in pigs following intraperitoneal injection of lipopolysaccharide," *Journal of animal science,* vol. 75, no. 6, pp. 1514-1520, 1997.
[155] P. N. Williams, C. T. Collier, J. A. Carroll, T. H. Welsh, Jr., and J. C. Laurenz, "Temporal pattern and effect of sex on lipopolysaccharide-induced stress hormone and cytokine response in pigs," *Domest Anim Endocrinol,* vol. 37, no. 3, pp. 139-47, Oct 2009.

[156] A. M. Wolthuis, N. Stakenborg, A. D'Hoore, and G. E. Boeckxstaens, "The pig as preclinical model for laparoscopic vagus nerve stimulation," *International Journal of Colorectal Disease,* vol. 31, no. 2, pp. 211-215, Feb 2016.

[157] M. Tosato, K. Yoshida, E. Toft, V. Nekrasas, and J. J. Struijk, "Closed-loop control of the heart rate by electrical stimulation of the vagus nerve," *Medical and Biological Engineering and Computing,* journal article vol. 44, no. 3, pp. 161-169, 2006.

[158] P. Pečlin and J. Rozman, "Alternative paradigm of selective vagus nerve stimulation tested on an isolated porcine vagus nerve," *The Scientific World Journal,* vol. 2014, 2014.

[159] S. C. Ordelman, L. Kornet, R. Cornelussen, H. P. Buschman, and P. H. Veltink, "Selectivity for specific cardiovascular effects of vagal nerve stimulation with a multi-contact electrode cuff," *IEEE Trans Neural Syst Rehabil Eng,* vol. 21, no. 1, pp. 32-6, Jan 2013.

[160] C.-H. Malbert, E. Bobillier, C. Picq, J.-L. Divoux, D. Guiraud, and C. Henry, "Effects of chronic abdominal vagal stimulation of small-diameter neurons on brain metabolism and food intake," *Brain Stimulation,* vol. 10, no. 4, pp. 735-743, 7// 2017.

[161] I. Díaz-Güemes, F. M. Sánchez, L. Luis, F. Sun, S. Pascual, and J. Usón, "Continuous Vagus Nerve Stimulation Effects on the Gut-Brain Axis in Swine," *Neuromodulation: Technology at the Neural Interface,* vol. 10, no. 1, pp. 52-58, 2007.

[162] K. Wasilczuk *et al.*, "Modulating the inflammatory reflex in rats using low intensity focused ultrasound stimulation of the vagus nerve," *Ultrasound in Medicine and Biology,* vol. In Review, 2018.

[163] J. M. Huston *et al.*, "Transcutaneous vagus nerve stimulation reduces serum high mobility group box 1 levels and improves survival in murine sepsis," *Critical care medicine,* vol. 35, no. 12, pp. 2762-2768, 2007.

[164] J. P. Somann, M. P. Ward, J.-W. Tsai, A. A. Muhammed, and P. P. Irazoqui, "Wireless Bionode Implemenation for Treatment of Inflammation," in *38th Annual International Conference of the IEEE Engineering in Medicine and Biology Society*, Orlando, FL, 2016.

[165] S. Banni *et al.*, "Vagus nerve stimulation reduces body weight and fat mass in rats," *PLoS One,* vol. 7, no. 9, p. e44813, 2012.

VITA

Jesse Somann is currently a PhD candidate at Purdue University studying Electrical Engineering with a specialty in bio-medical applications and implantable devices. Jesse was born and raised in Wisconsin and attended Rose-Hulman Institute of Technology for his undergraduate BS degree in Electrical Engineering. He graduated and commissioned as a Second Lieutenant in the United States Air Force from the AFROTC program at Rose-Hulman in 2004. Jesse then attended the Air Force Institute of Technology at Wright-Patterson Air Force Base, OH, and earned his Electrical Engineering MS degree with specialty in digital electronics and VLSI in 2006. He has since served in the Air Force as a developmental engineer and program manager, and has served tours as an Assistant Professor of Aerospace Studies at University of Wisconsin, Madison, and as an Assistant Professor of Electrical and Computer Engineering at the United States Air Force Academy in Colorado Springs, CO.

Upon graduation from Purdue, Jesse will return to Wright-Patterson Air Force Base to work as a Primary Leads Engineer for the 711th Human Performance Wing before returning to the Air Force Academy to serve as a Senior Faculty Member in the Department of Electrical and Computer Engineering.